ANNUAL REPORT

2003

CORROSION RESEARCH

Materials Science and Engineering

Published

by

THE CORROSION RESEARCH GROUP HOKKAIDO UNIVERSITY

For additional copies and more information, please write to the group members

Prof. T. Ohtsuka; CORROSION ENGINEERING LABORATORY

Prof. M. Seo; INTERFACIAL ELECTROCHEMISTRY LABORATORY

Prof. T. Narita; DISSIMILAR MATERIALS INTERFACE ENGINEERING LABORATORY

Prof. H. Takahashi; INTERFACE MICRO-STRUCTURE ANALYSIS LABORATORY

Prof. H. Konno; LABORATORY OF ADVANCED MATERIALS CHEMISTRY

Prof. K. Kurokawa; LABORATORY OF HIGH TEMPERATURE MATERIALS, CENTER
FOR ADVANCED RESEARCH OF ENERGY CONVERSION
MATERIALS

Assoc.Prof. H. Tamura

Graduate School of Engineering, Hokkaido University Kita13, Nishi8, Kita-ku, Sapporo 060-8628, Japan

Prof. F. Watari; DENTAL MATERIALS AND ENGINEERING LABORATORY

Graduate School of Dental Medicine, Hokkaido University

Kita13, Nishi7, Kita-ku, Sapporo 060-8586, Japan

CONTENTS

CURRENT ACTIVITIES and PRESENTASIONS	ge
CORROSION ENGINEERING LABORATORY	• 3
INTERFACIAL ELECTROCHEMISTRY LABORATORY	
DISSIMILAR MATERIALS INTERFACE ENGINEERING LABORATORY	
INTERFACE MICRO-STRUCTURE ANALYSIS LABORATORY	
LABORATORY OF ADVANCED MATERIALS CHEMISTRY	37
LABORATORY FOR CHARACTERIZATION AND	
ANALYTICAL CHEMISTRY OF CARBONACEOUS RESOURCES	
DENTAL MATERIALS AND ENGINEERING LABORATORY	49
AFFILIATE MEMBERS	
Assoc. Prof. Dr. Hiroki Tamura	65
ABSTRACTS of PUBLICATIONS	
CORROSION	
Polypyrrole-Polymolybdate Composite Film for the	
Corrosion Protection of Steels ······	69
Corrosion Products and Adsorbed Water on Copper	
in Humid Air Containing SO ₂	70
In-situ Raman Spectroscopy for Initial Corrosion	
Process of Zinc-coated Steel	71
Corrosion Products of Tin in Humid Air Containing	
Sulfer Dioxide and Nitrogen Dioxide at Room Temperature	72
In-situ Raman Spectroscopy for Corrosion Products Formed on	72
Zinc in Humidified Atmosphere in the Presence of NaCl Precipitate	13
Structure of Benzotriazole Film on Metals	74

Structure of metal-benzotriazole Films on Copper and Other Metals	75
In situ IR-RAS investigation of corrosion of tin in air containing H ₂ O, NO ₂ and SO ₂ at room temperature	76
Corrosion Behavior of Titanium-clad Carbon Steel in Weakly Alkaline Solutions	77
Application of Resistometry to the Study of Metal Corrosion	78
Corrosion Behavior of Iron Thin Film in Deaerated Phosphate Solutions by an Electrochemical Quartz Crystal Microbalance	79
Initial Stage of Localized Corrosion on Zn - 5 mass% Al Alloy Coated Steels by Pulsed Photon Film Removal Technique	80
Initial Stage of Localized Corrosion of Al - 9 mass% Si Coated Steels After Removal with A Photon Rupture Method in Solutions	81
Initial Stage of Localized Corrosion on Zinc Coated Steel with Photon Rupture Method in Chloride Ions Containing Solutions	82
PASSIVATION and ANODIC OXIDE FILM Photoluminesce of Ti Oxide Film in Phosphate, Sulfate, and Chloride Solution	83
The Aging of the Anodic oxide of Titanium during Potentiostatic Condition by Ellipsometry	84
Difference between Passivation Film and Rust layer	85
Nano-Indentation in Solution to Passive Metal Surfaces	86
Effect of Hydrogen on Stresses in Anodic Oxide Film on Titanium	87
Effect of Applied Potential Steps on Stresses of Anodic Oxide Film on Nickel·····	88

Nano-mechano-electrochemical Properties of Passive Titanium Surface	
Evaluated by in-situ Nano-indentation and Nano-scratching	89
Mechanoelectrochemical Properties of Passive Iron Surfaces Evaluated by an In Situ Nanoscratching Test	90
Frictional Coefficients of the Passive Titanium Surfaces Evaluated with In-situ and Ex-situ Nano-scratching Tests	91
Potential Dependence of Frictional Coefficient Evaluated by In-situ Nano-scratching for the Passive Iron Surface	92
Passive Film Formed on Shape Memory NiTi Alloy in Sulfuric Acid	93
An EQCM Study on Passivation Process of Nickel Thin Films in Acidic and Alkaline Sulfate Solutions	94
Friction Coefficients of the Passive Single Crystal Iron Surfaces and Their Potential Dependences Evaluated by an <i>In-situ</i> Nano-Scratching	95
Nucleation and Growth of the Nanostructured Anodic Oxides on Tantalum and Niobium under the Porous Alumina film	96
Local Removal of Thick Anodic Oxide Film on Aluminum with a Photon Rupture Technique and Local Metal Deposition	97
Repairing of Oxide Films on Zn-55% Al Alloy Coated Steel after Removal with Photon Rupture in Solutions	98
Nanocrystalline Heterogeneity Responsible for Localized Corrosion	99
Initial Stages of Plasma Electrolytic Oxidation of Titanium	100
Anodic Oxidation of Ta/Fe Alloys	101

.

Influence of Current Density on Transport Numbers in Anodic	
Oxide Films on an Anodized Al-5.7at.%W Alloy	102
Influence of Oxidation Rate and Alloy Composition on Alloy	
Enrichments of Anodized Al-W Alloys	103
Impact of RF-GD-OES in Practical Surface Analysis	104
Influence of Silicon Species on the Electric Properties of Anodic Niobia	105
Radiofrequency GDOES: A Powerful Technique for Depth Profiling	
Analysis of Thin Films	106
Radiofrequency GDOES, EPMA and AES Analysis of Zinc Die Casting	
Plated with Copper, Duplex Nickel and Microporous Chromium for	
Corrosion Protection	107
Analysis of Anodic Films on Nb and NbNx by Glow Discharge Optical	
Emission Spectroscopy ·····	108
Mechanical Properties of Barrier-Type Anodic Alumina Films	
Using Nanoindentation ·····	109
Compositional Self-Organizing in the Anodic Film on a Mg-Ta Alloy	110
Oxygen Generation in Anodized Ta-Cu Alloys	111
Crystallization of Anodic Titania on Titanium and Its Alloys	112
High Resistivity Magnesium-Rich Layers and Current Instability in	
Anodizing a Mg/Ta Alloy ·····	113
Anodic Film Growth in the Al-Ta Alloy System	114

Interconversion between Rare-Earth Metal(III) Chromates(V) and Low-	
Crystalline Phases by Reduction with Methanol and Oxidation in Air	115
Formation of Barrier-Type Amorphous Anodic Films on Ti-Mo Alloys	116
Formation of Black Anodic Films on Aluminum in Acid Electrolytes	
Containing Titanium Complex Anion	117
Dielectric and Mechanical Properties of Anodic Films in the Ta-Ti System	118
Formation of N2O Gas Bubbles in Anodic Films on NbNx Alloys	119
CHARACTARIZATION of SURFACE and INTERFACE	
Adsorption of Thiourea on Gold Electrode in Perchloric Acids Studied	
by in situ Surface-Enhanced Infrared Absorption Spectroscopy	120
Application of CSLM to the Surface Morphological Study of Al 5052	
Alloy Anodized in Sulfuric Acid Solution	121
Stress Relaxation Effect of Functionally Graded Dental Post	122
Fine Particles and Bioreaction	123
Surface analysis of dental amalgams by X-ray photoelectron spectroscopy	
and X-ray diffraction	124
Cytotoxicity and bonding property of dental ceramics	125
Tissue Response to a Newly Developed Calcium Phosphate Cement	
containing Succinic Acid and Carboxymethyl-chitin	126
Discrimination between Composite Resin and Teeth using Fluorescence	
Properties	127

CLSM and SEM quantitative analysis of surface topography of human	
teeth irradiated by Nd:YAG, Er:YAG and CO ₂ lasers	128
Imaging and Non-Contact Profile Analysis of Nd:YAG Laser-Irradiated Teeth by Scanning Electron Microscopy and Confocal Laser Scanning Microscopy	129
Change of Mechanical Properties of Esthetic Orthodontic Wire with Fiber Reinforced Plastic Structure in Wet Condition	130
Static-Dynamic Friction Transition of FRP Esthetic Orthodontic Wires on Various Brackets by Suspension-Type Friction Test	131
Effects of Micro/Nano Particle Size on Cell Function and Morphology	132
Effect of Sphered Particles on the Firing Contraction of Porcelain	
Inlay Processed by Cold Isostatic Pressing	133
Influences of Structure and Composition on Growth of Anodic Oxide Films on Ti-Zr Alloys	134
Grain Orientation Effects on Copper Enrichment and Oxygen Generation	
During Anodizing of an Al-Lat.%Cu Alloy	135
Behavior of Hydrogen Impurity in Aluminum Alloys During Anodizing	136
Morphology of Enriched Alloy Layers in an Anodized Al-Cu Alloy	137
Preparation and Characterization of Layered Manganese Oxide (Birnessite) and Its Intercalation Reactions	138
A Protective Film Component among Corrosion Products on Galvanized	
Steels Estimated by Solubility Calculations	139

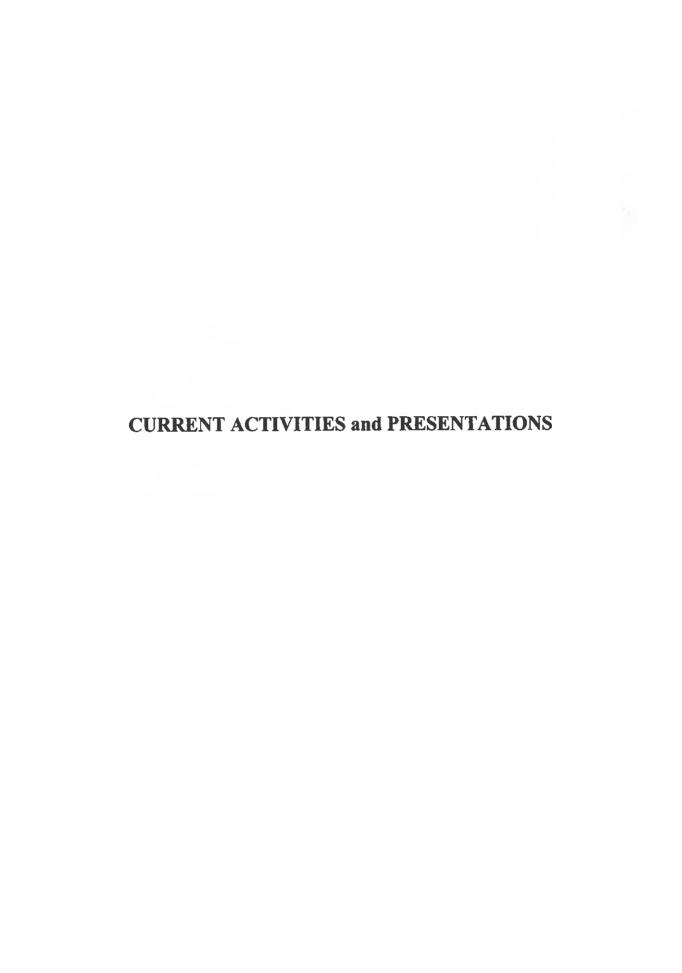
ELECTROCHEMISTRY

Construction of Photosynthetic Antena Complex Using Light-	
harvesting Polypeptide-α from Photosynthetic Bacteria, R. rubrum	
with Zinc Substituted Bacteriachlorophyll a	140
Study of Cathodic Dissolution of an Aluminum Wire Electrode	
using AC Resistometry	141
Experimental Simulation for Zincate Pretreatment of Al Pad Connected to	
LSI Circuit·····	142
Changes in Surface Stress of Platinum Electrode in Acidic and Alkaline	
Sulfate or Alkaline Fluoride Solutions	143
Study on Initiation of Localised Corrosion on Copper Thin Film Electrode	
by Combinational Use of an EQCM with a Liquid-phase Ion Gun	144
HIGH TEMPERATURE OXIDATION and SULFIDATION	
Effect of pre-oxidation on the corrosion behavior of Fe-40Al sheet	
in a N ₂ -11.2O ₂ -7.5CO ₂ -500ppmSO ₂ Atmosphere at 1273K ······	145
Corrosion Behavior of Fe-40Al Sheet in N2-11.2O2-7.5CO2 Atmospheres	
with Various SO ₂ Contents at 1273K	146
Two-Step Cr and Al Diffusion Coating on TiAl at High Temperatures	147
Effect of Coating Layer Structures and Surface Treatments on the	
Oxidation Behavior of a Ti-50at%Al Alloy	148
Isothermal Oxidation Behavior of A Sheet Alloy of Fe-40at%Al at	
Temperatures between 1073 and 1473K	149
Formation of Nickel Aluminide Coating on γ-TiAl Alloy	150

Coatings of Nb-based Alloy by Cr and/or Al Pack Cementations and Its Oxidation Behavior in Air at 1273-1473 K	151
Evaporation of Cr ₂ O ₃ in H ₂ O-Containing Atmospheres	152
TEM Observation of SiO ₂ Scales Formed on MoSi ₂	153
Structure and Oxidation Resistance of MoSi ₂ Synthesized by Spark Plasma Sintering	154
Fabrication and Oxidation Resistance of Metal Disilicides for Ultra-High Temperature Applications	155
The Sulfidation and Oxidation Behavior of Sputter-Deposited Nb-Al-Cr Alloys at High Temperatures	156
SURACE FINISHING and MICRO FABRICATION Anodic Dissolution of TiAl Surface as a Pretreatment for Al-Anodic Dissolution of TiAl Suraface as a Pretreatment for Al-Cl Electroplating	157
Direct Electroless Ni-P Plating to Sputter Deposited Al-Ni Alloy Films	158
Novel Micro-Patterning of Aluminum Surface by Anodizing and AFM-Processing	159
Fabrication of Micro-Printed Circuit Board by Aluminum Anodizing and Laser Irradiation - Influence of Thickness of Oxide Film on Formation of Pattern	160
Anodizing of Aluminum Coated with SiO ₂ by Sol-Gel Coating - Formation of New Type Anodic Oxide Film with High Voltage Sustainability-	161
Electroless Ni-P Deposition through Imperfections in Anodic Oxide Films on Aluminum and Al5052 Alloy	162

Fabrication of Nickel Micro-pattern on Insulating Board by Anodizing /	
Laser Irradiation / Electrodeposition ·····	163
Nanopatterning on Aluminum Surfaces with AFM probe	164
Purification of Carbon Nanofibers with Hydrogen Peroxide	165
Three-Dimensional Microstructure Fabrication with Aluminum Anodizing, Laser Irradiation, and Electrodeposition	166
Chromate Conversion Coatings on Aluminium: Influences of Alloying	167
Enrichment Factors for Copper in Aluminium Alloys Following Chemical and Electrochemical Surface Treatments	168
Improving the Performance of Aerospace Alloys·····	169
COLIDIFICATION	
SOLIDIFICATION Mechanical Properties and Modifying Solidification of Sn-Ag-Al Solders Alloy	170
Dissolution of Copper-plate and Growth of Reaction Layer with Lead-Free Solders	171
Phase-field Simulation of Transient Liquid Phase Bonding Process of Ni Using Ni-P Binary Filler Metal	172
Analysis of Growth Behavior of a Cellular and Dendritic Interface under a Constrained Growth Condition using a Phase-Field Model	173
Numerical Analysis of Solidification Effect on Diffusion Measurement in Liquid using the Long Capillary Method	174
Numerical Modeling of the Transient Liquid-Phase Diffusion Bonding Process of Al Using Cu Filler Metal	175

Heat Transfer Analysis for Aluminum Base and Ferrous Multi-component Alloys Using Computational Thermodynamics	176
Anoys Using Computational Thermodynamics	170
Prediction of the Solidification Structure of Casting and Heterogeneous	
Nucleation ·····	177
Macrostructure of Aluminum base Alloys during Unidirectional Solidification	178





CORROSION ENGINEERING LABORATORY

Prof. Dr. Toshiaki Ohtsuka TEL/FAX: +81-11-706-6351

E-mail: ohtsuka@elechem1-mc.eng.hokudai.ac.jp

Assoc. Prof. Dr. Takeshi Sasaki

TEL: +81-11-706-6352 FAX: +81-11-706-7813

E-mail: txsasaki@eng.hokudai.ac.jp

Lecturer Dr. Takenori Notoya

TEL/FAX: +81-11-706-6353

E mail: tnotoya@eng.hokudai.ac.jp

Res. Assoc. Dr. Mikito Ueda

TEL/FAX: +81-11-706-7813

E mail: mikito@eng.hokudai.ac.jp

Technician Dr. Shoichi Konda

TEL: +81-11-706-7236

FAX: +81-11-706-7813

E mail: konda@eng.hokudai.ac.jp

Students

H. Kigawa, T. Komatsu, M. Iida, Y. Horiguchi, Y. Sasaki, M. Matsuda, M. Ito, M. Yoshimatsu, S. Ishizuka, H. Ebe, M. Kamiya, M. Yasuda

Facilities and Capabilities

Ellipsometer: Rotating-analyzer type of automated ellipsometer with 632.8 nm wavelength of light.

Potential Modulation Reflectance: Wavelength region from 350 to 800 nm.

Raman Scattering Spectrometer: JASCO R-800T, triple type of spectrometer equipped with an Argon gas laser of 2W power.

FT-IR Spectrometer: JASCO FT/IR 550 equipped with MCT detector for in-situ measurement of corrosion layers on metals.

QCM system for in-situ gravimetry of surface layer on metals.

Electrochemical AC Impedance: NF Circuit Design 5020 FRA equipped with a specially designed potentiostat.

Spectrophotometer: JASCO V-520 in a wavelength region from 200 to 900 nm.

Electrochemistry apparatuses.

Optical Microscopy

Electrochemical Corrosion-Rate Monitor System.

Our research activities are concerned with applied electrochemistry of corrosion and corrosion prevention of metals and molten salt electrolysis.

Research programs in progress are as follows:

(1) Corrosion Resistive Coatings Consisting of Conductive Polymers

A conductive polymer coating was applied to corrosion prevention of carbon steels. A polypyrrole (PPy) film doped by hetero-polymolibdate ions was formed on the steel plate by electropolymerization from pyrrole monomers in aqueous solutions containing the poly acids. The hetero-polymolibdate may play a roll of enhancement of the formation of passive oxide film on the steel. The coated steel in which the PPy film functions as an oxidant for the substrate steel possessed the potential of the steel in the passive region during the exposure in NaCl aqueous solution for a day.

(2) Corrosion Layer on Steels Covered by Zinc and Zinc Alloys

The corrosion of steels covered by zinc and zinc alloys in a humidified atmosphere was tested. Composition of the corrosion layer was measured by in-situ Raman scattering spectroscopy. The weight gain was also measured under in situ condition. At the presence of NaCl, the absorbed water layer from the humidified air dissolves to form an aqueous NaCl layer on the steel. The following reaction sheme was assumed. During the corrosion of zinc on the top layer the aqueous layer changes to ZnCl₂ layer containing NaOH solution. When the concentration of ZnCl₂ in the aqueous surface layer increases and reaches the saturation, simonkolleite begins to precipitate.

Addition of Al and Ni into zinc coatings was found to delay the formation of ZnCl₂ layer and simonkollite.

(3) Passive Films on Stainless Steels

In order to examine the functions of the passive films on stainless steels, the potential-modulation reflectance was measured as a function of the potential, wavelength of light, and frequency of modulation. The modulation reflectance was compared with the results of AC impedance. The modulation reflectance was found to be proportional to the charge induced in the film by potential modulation. From the AC response of reflectance and charge, the distribution of potential drop and the semiconductive nature of the passive film are discussed.

(4) Functions of Rust Layer on the Weathering Steels

The rust layer which functions as a protective layer against atmospheric corrosion was studied. The conductivity of the rust layer was found to greatly depend on the water content adsorbed from the humidified air. The amount of water adsorbed was measured as a function of the relative humidity in atmosphere and compared with the conductance measured by AC technique. β -FeOOH reveals the higher conductivity under the wet condition as compared with α - and γ -FeOOH. This may be explained by presence of Cl anion in the β -FeOOH, in which Cl dissolves into the water layer absorbed. A new monitoring technique in which the corrosion productivity of the rust layer can be judged was proposed from the conductivity under wet condition.

(5) Improvement of Corrosion Resistance of TiAl Inter-metalllic Compound by Coating of Al-Cr-Ni Alloy from a Molten Salt Electrolysis

A coating layer of Al-Cr-Ni alloy was cathodically formed at 423 K on the TiAl inter-metallic compound in an AlCl₃-NaCl-KCl molten salt mixture containing CrCl₂ and NiCl₂. AlCl₃-EMIC room temperature molten salt containing CrCl₂ and NiCl₂ was also used as electrolyte for electrodeposition of the Al-Cr-Ni alloy. The relation between the alloy composition and the deposition potential was examined.

(6) Electrophoretic Deposition for Preparation of Functional Oxide Films

Sr-Co-Nb oxide powder with perovskite structure was deposited electrophoretically in organic solvent for preparation of the thin layer membrane for preferential permeation of oxygen ions. Dense oxide layer was formed on porous oxide cathode. There was a linear relation between thickness of the layer and applied electricity. By sintering of the deposited layer on the cathode at 1523K for 6h, compact thin layer was formed.

(7) Corrosion products on copper in humid air containing sulfur dioxide

Corrosion products initially formed on copper in air containing SO₂ have been investigated by in situ IR-RAS. The corrosion products were identified and the formation rates were determined by combining in situ IR-RAS and QCM measurements. The layer-thickness of the physically adsorbed water was also determined as a function of time. The growth-rates of the corrosion products were low at the initial stage for the protection by oxide films and the rates increased after the degradation of the films. The behavior of the growth-rates of the thickness of physically adsorbed water showed nearly the same as that of the corrosion products.

(8) Adsorption of 3-mercapto, 1-propane sulfonic acid on a copper electrode in

perchloric acid

Adsorption of 3-mercapto, 1-propane sulfonic acid on copper in percholric acids was investigated using in situ surface-enhanced infrared absorption spectroscopy together with an electrochemical technique. The adsorption of the molecules to copper forming mercaptide bond between S and Cu was confirmed and it was also elucidated that the adsorption inhibited hydrogen evolution reaction.

(9) Photoluminescence of Ti Oxide Film

Photoluminescence of Ti anodic oxide film by UV-light Photo-excitation was measured in phosphate, sulfate buffer solution. Maximum luminescence intensity was observed at bias potential of -0.6 V vs.Ag/AgCl, decreasing with increase of bias potential. The potential of -0.6 V corresponds to the flat-band potential of TiO₂. A peak in the luminescence spectra was observed at 420 nm wavelength in every solution. This peak corresponds to the band-gap energy of TiO₂ at 3.1eV.

Other Activities

Prof. Ohtsuka attended the Asian Pacific Corrosion Control Conf., Osaka, 16 21 Nov., 2003 and presented a paper entitled by Photoluminescence of Ti oxide film in phosphate, sulfate, and chloride solution. Associate professor T. Sasaki attended The 204th Meeting of ECS, Orlando/USA, October 12-16 and presented a paper entitled by quantitative determination of corrosion products and water on copper in humid air containing SO₂ by using IR-RAS and QCM.

Prof. Plieth (Technical University of Dresden, Germany) stayed in the laboratory under the support of JSPS visiting program from 7 to 20 Sep. He took a lecture on the title of corrosion protection by conductive polymer. He further visited many groups on electrochemical research in Hokkaido University during the stay. Visiting professor S. Gopukumar (The Central Electrochemical Research Institute, Karaikudi, India) visited the laboratory, July 24-25 and gave a lecture entitled by CECRI and designing of materials for lithium batteries.

Dr. Ueda received the 2003 Young Researcher Award of the Electrochemical Society Japan for study on aluminum recycle and new surface finishing by molten salt electrolysis.

Presentations

Effect of Dispersant on Electrophoretic Deposition of Functional La-Sr-Co Oxide Powder, M. Yoshimatsu, M. Ueda and T. Ohtsuka, The Joint Meeting of The Hokkaido Sections of ECS Jpn, Surf. Finish. Soc. Jpn, and Jpn Soc. Corros. Eng., Sapporo, Jan., 2003.

Anodic Dissolution of Oxide on TiAl in AlCl₃-NaCl-KCl Molten Salt, H. Kigawa, M. Ueda and T. Ohtsuka, Winter Meeting of Hokkaido Branch of Jpn Inst. Metals and ISIJ, Muroran Jan., 2003.

Corrosion protection of mild steel by conductive polypyroll film, T. Domyo, M. Ueda and T. Ohtsuka, Winter Meeting of Hokkaido Branch of Jpn Inst. Metals and ISIJ, Muroran, Jan., 2003.

Corrosion Protection of Mild Steel by Composite Polypyrrol Film Formed under Ultrasonic Irradiation, T. Domyo, M. Ueda and T. Ohtsuka, The 107th Annual meeting of Surface finishing soc. Jpn, Tokyo, March, 2003.

Initial Corrosion Process of Steels Coated by Zinc and Zinc Alloy Containing Ni amd Al by Using In-situ Raman Spectroscopy, M. Matsuda and T. Ohtsuka, The 145 annual meeting of ISIJ, Chiba, March, 2003.

In-situ Raman spectroscopy for study on the corrosion process of zinc, M. Matsuda and T. Ohtsuka, The 145 annual meeting of ISIJ, Chiba, March, 2003.

Electric Conductivity of Rust Layer on Weathering Steels under Wet Condition, T. Komatsu, T. Sasaki, and T. Ohtsuka, The 107th Annual meeting of Surface finishing soc. Jpn, Tokyo, March, 2003.

Aluminum Recycle and New Surface Finishing by Molten Salt Electrolysis, The 70th Annual Meeting of Electrochem. Soc. Jpn., Tokyo, April, 2003.

Anodic Dissolution of TiAl as a Pre-treatment of Electroplating in Molten Salt, M. Ueda, H. Kigawa, S. Konda, and T. Ohtsuka, The 70th Annual Meeting of Electrochem. Soc. Jpn., Tokyo, April, 2003.

Nickel Passivation Film in Acidic Sulfate Solution by Ellipsometry, S. Iida and T. Ohtsuka, The 2003 Annual meeting of Jpn Soc. Corros. Eng., Tokyo, June, 2003.

Corrosion Prevention of Steels by Conductive Polypyrrole Coating in 3.5 wt% NaCl solution, T. Domyo and T. Ohtsuka, The 2003 Annual meeting of Jpn Soc. Corros. Eng., Tokyo, June, 2003.

Electrodeposition of Al-Cr-Ni alloy from chloride molten salt containing CrCl₂ and NiCl₂, H. Kigawa, M. Ueda and T. Ohtsuka, Summer Meeting of Hokkaido Branch of Jpn Inst. Metals and ISIJ, Muroran, July, 2003.

The Role of adsorbed water in Copper Corrosion in Air Containing SO₂, Y. Horiguchi, T. Sasaki, and T. Ohtsuka, Summer Meeting of Hokkaido Branch of Jpn. Inst. Metals and ISIJ, Muroran, July, 2003.

Electric Conductivity of Ferric Oxyhydroxde under Humidified Air Conduction, T. Komatsu, T. Sasaki, and T. Ohtsuka, Summer Meeting of Hokkaido Branch of Jpn. Inst. Metals and ISIJ, Muroran, July, 2003.

Influence of Anion on Copper Corrosion in Neutral Aqueous Solutions, T. Notoya, T. Ohstuka, M. Nakayama, and T. Ohsakai, Summer Meeting of Hokkaido Branch of Jpn Inst. Metals and ISIJ, Muroran, July, 2003.

Electrodeposition potential of Al-Cr-Ni alloy from AlCl₃ molten salt containing CrCl₂and NiCl₂, H. Kigawa, M. Ueda and T. Ohtsuka, The 2003 fall meeting of Electrochem. Soc. of Jpn, Sapporo, Sep., 2003.

Film Growth and Aging of Anodic Oxide Film on Titanium, T. Ohtsuka, The 2003 fall meeting of Electrochem. Soc. of Jpn, Sapporo, Sep., 2003.

Quantitative Analysis of Corrosion Products Formed in Atmospheric Environment by in-situ IR-RAS and QCM, T. Sasaki, Y. Horiguchi, and T. Ohtsuka, The 2003 fall meeting of Electrochem. Soc. of Jpn, Sapporo, Sep., 2003.

Atomospheric Corrosion Products on Zinc-Coated Steel -QCM and Raman Spectroscopy -, M. Matsuda, M. Ueda and T. Ohtsuka, The 146th fall meeting of ISIJ, Sapporo, Oct., 2003.

Nano-level Observation of Corrosion Process, T. Ohtsuka, The Fall Meeting of Jpn. Inst. Metals, Sapporo, Oct., 2003.

Enhancement of Conductivity in Iron Rust and Ferric Oxyhyroxide by Wet Condition, T.

Komatsu, T. Sasaki, and T. Ohtsuka, The Fall Meeting of Jpn. Inst. Metals , Sapporo, Oct., 2003.

Quantitative Determination of Corrosion Products and Water on Copper in Humid Air Containing SO₂ by Using IR-RAS and QCM, T. Sasaki, Y. Horiguchi and T. Ohtsuka, The 204th Meeting of ECS, Orlando, USA, Oct. 2003.

Corrosivity of Mild Steel Covered by Conductive Polymer Film Doping Phosphate, S. Iida, M. Ueda and T. Ohtsuka, The 50th Discussion Meeting of Jpn. Corros. Eng., Okinawa, Nov., 2003.

Photoluminescence of Ti Oxide Film in Chloride Solution, M. Ueda and T. Ohtsuka, The 50th Discussion Meeting of Jpn. Corros. Eng., Okinawa, Nov., 2003.

Photoluminescence of Ti Oxide Film in Phosphate, Sulfate, and Chloride Solution, M. Ueda and T. Ohtsuka, 13th Asian Pacific Corrosion Control Conference, Suita, Nov., 2003.

Corrosion Products and Absorbded Water on Copper in Humid Air Containing SO₂.Y. Horiguchi, T. Sasaki, and T. Ohtsuka, 13th Asian-Pacific Corrosion Control Conference, Suita, Nov., 2003.

In-situ Raman Spectroscopy for Initial Corrosion Process of Zinc-Coated Steel. M. Matsuda and T. Ohtsuka, 13th Asian-Pacific Corrosion Control Conference, Suita, Nov., 2003.

Co-deposition of Al-Cr-Ni Alloy from AlCl₃ Molten Salt Containing CrCl₂ and NiCl₂, H. Kigawa, M. Ueda and T. Ohtsuka, The 35th Symposium on Molten Salt Chemistry, Kisarazu, Nov., 2003.

INTERFACIAL ELECTROCHEMISTRY LABORATORY

Prof. Dr. Masahiro Seo TEL/FAX: +81-11-706-6735

E-mail: seo@elechem1-mc.eng.hokudai.ac.jp Assoc. Prof. Dr. Kazuhisa Azumi TEL/FAX: +81-11-706-6736

E-mail: azumi@elechem1-mc.eng.hokudai.ac.jp

Res. Assoc. Dr. Koji Fushimi

TEL: +81-11-706-6737 FAX: +81-11-706-6735 E-mail: fushimi@elechem1-mc.eng.hokudai.ac.jp

Students

M. Chiba, K. Iokibe, A. Kanada, M. Yamazaki, K. Yamaya, M. Hagioi, K. Okamoto, D. Kawamata, K. Nishimura

The research activity of the laboratory still continues to be directed towards a better understanding of the interfacial properties of metal and semiconductor electrodes in relation to the interfacial electrochemistry involving adsorption, corrosion, passivation, anodic oxidation, hydrogen adsorption/ absorption, and surface finishing. Current topics on research are as follows:

(1) Potential Dependence of Normalized Friction Coefficient for the Single-Crystal Iron Surfaces Kept at Passive State in Solution

Nano-scratching tests in solution were performed to the iron single-crystal (110) and (100) surfaces kept at passive state in pH 8.4 borate solution to investigate the potential dependence of friction coefficient. The normalized friction coefficient was newly defined to avoid the dependence of friction coefficient on indenter shape. The normalized friction coefficient increased with increasing potential for passive film formation, irrespective of crystal orientation of the substrate iron. The increase in potential would provide the promotion of repassivation at the breakdown sites of passive film during nano-scratching. The potential dependence of normalized friction coefficient may be explained in terms of the increase in repassivation rate.

(2) Cathodic Reduction of the Electrodeposited Cu / Cu_2O Multilayers The Cu / Cu_2O multilayers were electrodeposited on a gold electrode at a

constant current density of $i_c = -0.5$ mA cm⁻² in pH 9.0, 0.6 M CuSO₄ + 0.2 M lactate solution. The cathodic reduction of the multilayers was performed under a constant current density of $i_c = -20~\mu\text{A}$ cm⁻² in deaerated pH 8.4 borate solution, monitoring the mass-change with EQCM. The mass-loss due to cathodic reduction was only 50% of that estimated from the electric charge for complete reduction with 100% current efficiency, suggesting that the cathodic reduction starts at the multiplayer / solution interface and water as reduction product remains in metallic copper layer. Further study still continues.

(3) Changes in Surface Stress of Au Electrode during Underpotential Deposition of Cu

The changes in surface stress of a gold electrode during underpotential deposition (UPD) of copper in perchlorate-base solutions containing 10^{-3} M SO_4^{2-1} or Cl⁻¹ were measured by a bending beam method for a better understanding of UPD process from the viewpoint of surface energetics. The maxima of surface stress during Cu-UPD appeared at a certain potential which shifted to the noble direction in the order of Cl⁻¹ $> SO_4^{2-1} > ClO_4^{-1}$ in consistent with the order in strength of specific adsorption on gold. The responses of current density and changes in surface stress by a potential step indicated that the coadsorption of anions promoted the Cu-UPD process.

(4)Nano-scratching of n-Type InP Wafer and Preparation of Porous Wires with Electrochemical Etching

A surface scratching of n-type InP (100) wafer was performed with a conical diamond indenter under a constant normal force of 1000 μ N, followed by an electrochemical etching in 0.5 M HCl to form porous wires on the surface. The porous wires could be prepared only on the scratched grooves by a potentiostatic etching at 1.1 V (SHE) for 300 s. The line width and length of the porous wires were 1 μ m and 10 μ m, respectively. The optimum conditions for preferential decomposition at the scratched area of n-type InP (100) wafer due to cathodic polarization in 0.5 M HCl were also investigated.

(5) Investigation of Initiation Process of Electroless Ni-P Plating on Al Alloys

In the initial stage of the plating process, dissolution of a Zn layer formed by double zincate pretreatment, Ni deposition due to substitution reaction with Zn dissolution and Al dissolution occur simultaneously on the surface in the plating bath. The backside of the deposition layer was observed using an SEM and AFM after chemical dissolution of Al alloy substrates in a concentrated NaOH solution. Many Ni-P deposits with tube-like forms in pits of the substrates that seem to act as

anchors to improve adhesion strength of the deposition layer to the substrate were observed. In the case of a weakly adhesive deposition layer, the substrate was mechanically peeled off from the plating layer to observe the backside of the deposition layer and the substrate surface beneath the deposition layer. The two surfaces showed complemental morphology, which had been formed by dissolution of the substrate and growth of the deposition layer into the dissolution trace of the substrate.

(6) Development of Corrosion Monitoring System of Ti in High-Temperature Aqueous Environment

Titanium is a candidate material for the container of high level radiative nuclear waste which may be stored in the deep underground environment. Corrosion monitoring system was thus developed using resistometry technique in which thin wire electrodes (0.1 mm in diameter) of Ti was immersed in high temperature (about 353 K) aqueous solution and the change in electric resistance was recorded. In the solution containing sulfuric acid and hydrochloric acid Ti could be depassivated after some induction period and showed increase in resistance due to hydride growth. After experiment Ti was broken due to hydrogen embrittlement, indicating that the depassivation of Ti caused hydrogen evolution on it and penetration of hydrogen caused degradation of Ti.

(7) Formation of Titanium Oxide Films Containing Nitrogen

Ti electrode was discharged with cathodic DC high voltage to form glow plasma in the nitrogen gas. As a result oxide film was formed on Ti surface. The thickness of the films was in the order of ten nm and the composition of the films was mainly TiO₂ containing small amount of nitrogen, estimated from ellipsometry and XPS measurements. Light absorption edge of the oxide films was extended toward visible light direction from a value of ca. 3.1 eV for typical TiO₂ oxide film which does not include nitrogen. The photo-catalytic activity of these films for visible light is currently under evaluation.

(8) Electropolishing of Shape Memory Ni-Ti Alloy

Electropolishing of shape memory Ni-Ti alloy was surveyed. Anodic polarization of Ni-Ti to 8 V in methanolic 3 mol dm⁻³ H_2SO_4 at 263 K gave a limiting current and produced a smooth surface. It showed the best results for 0.1 mol dm⁻³ $\leq C_{H2SO4} \leq 7$ mol dm⁻³. Electro-dissolution kinetics was investigated with electrochemical impedance spectroscopy.

Its kinetic control was modeled with the compact salt-film model which was applied to that for electro-dissolution of pure titanium or pure tantalum in concentrated H₂SO₄.

Other Activities

In June, Prof. M. Seo received the 2003 Japan Society of Corrosion Engineering Award for the Study on Passive Metal Surfaces by In-situ Analyses on Nano-levels. In July, Prof. M. Seo and Mr. M. Chiba (Ph.D. student) participated in International Symposium on Corrosion Science in the 21st. Century at UMIST, U. K. to present two oral papers. On July 30th, Dr. K. Fushimi, who conducted a postdoctoral work for 14 months supervision of Prof. M. Stratmann. returned Max-Planck-Institut für Eisenforschung, Düsseldorf, Germany. In October, Prof. M. Seo participated in the 204th Meeting of The Electrochemical Society held in Orlando, Florida, USA to present one oral paper. In November, Prof. M. Seo, Dr. K. Fushimi, and Mr. M. Chiba participated in the 13th Asian-Pacific Corrosion Control Conference in Osaka, Japan to present three oral papers.

The following foreign scientists visited this laboratory: Mr. Park, Mr. Jung, Mr. Lee and Mr. Jang (Ph.D. Students of Prof. S.–I. Pyun), Department of Materials Science and Engineering, Korea Advanced Institute of Science and Technology (KAIST), Korea, from January 14 to 16, Prof. P. Marcus, Laboratorie de Physico-Chimie des Surface, CNRS, Université Pierre et Marie Curie, Paris, France, January 30, Dr. Lars Grásjö, Danderyds Gymnasium, Stockholm, Sweden, July 25, Prof. Gunnar Hultquist, Division of Corrosion Science, Royal Institute of Technology, Stockholm, Sweden, October 10, Dr. A. W. Hassel and Prof. M. Stratmann, Max-Planck-Institut für Eisenforschung, Düsseldorf, Germany, from November 11 to 12 and from November 27 to 28, respectively.

Presentation

- T. Ueno, K. Azumi, and M. Seo: Effects of sulfate ions on cathodic dissolution of Al; The 2003 Joint Meeting of Hokkaido Section of Electrochem. Soc. Jpn., Surf. Finish. Soc. Jpn., and Jpn. Corrosion Eng., Sapporo, Jan., 2003.
- T. Kurihara, K. Azumi and M. Seo: Morphology and adhesion strength of Ni-P layer deposited on Al-alloys by direct plating; ibid.
- A. Kanada, K. Azumi and M. Seo: Elemental depth-profiling of metal surface using high-voltage discharge technique in solution; ibid.
- K. Iokibe, K. Azumi and M. Seo: Calculation of activation energy of surface diffusion of zinc ad-atom using semiempirical MO methods; ibid.
- T. Yamaya and M. Seo: Study on Selective Formation of Porous Layer on Scratched Area of n-type InP Surface; ibid.
- M. Yamazaki and M. Seo: Response of Surface Stress of Gold Electrode by a Potential Step during Pb-UPD; ibid.
- M. Chiba and M. Seo: Potential Dependence of Friction Coefficient Evaluated by *In-situ* Nano-Scratching to the Single Crystal Iron Surface; ibid.
- N. Kikuchi and M. Seo: Effect of Trace Amount of Pb on Polarization Curve of Ni Thin Film; ibid.
- M. Hagioi and M. Seo: Measurement of Changes in Stress during Electrodeposition of Cu / Cu₂O Multilayers; ibid.
- Y. Hoshino, K. Azumi and M. Seo: Characterization and evaluation of stability of oxide film on titanium in the electrolyte solutions containing sulfate ion; ibid.
- N. Munakata, K. Azumi and M. Seo: Dissolution and deposition

conditions of Cu for the micro-electroforming; ibid.

- T. Yamaya and M. Seo: Local Formation of Porous Layer on n-Type InP Surface by Scratching; The 107th Annual Meeting of Surface Finishing Society of Japan, Tokyo. Mar., 2003.
- M. Hagioi and M. Seo: EQCM Analysis and Stress Measurement of Electrodeposition Process of Cu / Cu₂O Multilayers; The 70 years Anniversary Meeting of The Electrochem. Soc. Jpn., Tokyo, April, 2003.
- M. Seo and N. Kikuchi: Effect of Trace Amount of Pb on Polarization Behavior of Ni Thin Film; ibid.
- M. Yamazaki and M. Seo: Structural Changes of Pb-UPD Phase Predicted from Changes in Surface Stress of Gold Electrode; ibid.
- K. Fushimi, A. W. Hassel, M. Stratmann: Anodic Oxide Film on Shape Memory Ni-Ti Alloy, 203rd Meeting of The Electrochemical Society, Paris, France, May, 2003.
- M. Seo: Study on Passive Metal Surfaces by *In-situ* Analyses on Nano-levels; The 2003 Annual Meeting of Jpn. Soc. Corrosion Eng., Tokyo, June, 2003.
- M. Chiba and M. Seo: Potential Dependence of Friction Coefficient Measured with Nano-Scratching in Solution for Iron Electrode Surfaces; ibid.
- M. Seo, Y. Kurata and M. Chiba: Frictional Coefficients of the Passive Titanium Surfaces Evaluated with *In-situ* and *Ex-situ* Nano-scratching Tests; Intern. Symp. on Corrosion Science in the 21st. Century, Manchester, U.K., July, 2003.
- M. Chiba and M. Seo: Potential Dependence of Frictional Coefficient Evaluated by *In-situ* Nano-scratching for the Passive Iron Surface; ibid.
- A. Kanada, K. Azumi and M. Seo: Elemental depth-profiling of metal surface using high-voltage discharge technique in aqueous solution; The

- 2003 Autumn Meeting of the Electrochem. Soc. Jpn., Sapporo, Sep., 2003.
- M. Yamazaki and M. Seo: Changes in Surface Stress of Gold Electrode during Pb-UPD Anion Effect -; ibid.
- K. Iokibe, K. Azumi, H. Tachikawa and M. Seo: Computational simulation of surface dissusion of zinc ad-atom using MO method; ibid.
- M. Chiba and M. Seo: Difference between Friction Coefficients Measured by Nano-Scratching in Solution and in Air for the Passive Iron Surface; ibid.
- M. Hagioi and M. Seo: Anodic and Cathodic Behaviors of the Cu / Cu₂O Multilayers; ibid.
- K. Fushimi, A. W. Hassel, M. Stratmann: Anodic Polarization Behavior of Shape Memory Ni-Ti Alloy in H₂SO₄ Aqueous Solution; ibid.
- T. Yamaya and M. Seo: Survey of Optimum Condition for Local Formation of Porous Layer on n-Type InP Surface by Scratching; ibid.
- K. Fushimi, A. W. Hassel, M. Stratmann: Study on Electropolishing Behavior of Shape Memory Ni-Ti Alloy, The 108th Annual Meeting of Surface Finishing Society of Japan, Utsunomiya, Sept., 2003.
- K. Fushimi: Electrochemical Micromachining of Shape Memory (Ni-Ti) Alloy Using Microelectrode, Corrosion Dream 2003 Seminar of Corrosion Division, The Electrochem. Soc. Jpn., Tokyo, Sept., 2003.
- M. Chiba and M. Seo: Evaluation of Friction Coefficients of Passive iron Surfaces by Nano-Scratching in Solution; The 2003 Fall Meeting of The Japan Institute of Metals, Sapporo, Oct., 2003.
- M. Seo, M. Hagioi: EQCM and Stress Analyses of Electrodeposition Process Accompanying Potential Oscillations, 204th Meeting of The Electrochemical Society, Orlando, Florida, USA, Oct., 2003.

- K. Azumi: Electroless Ni plating on Al films; The 20th ARS (Anodizing Research Society, SFJ) Conference, Kitayuzawa, Oct. 2003
- K. Fushimi, A. W. Hassel, M. Stratmann: Passive Film on Shape Memory Ni-Ti Alloy in Sulfuric Acid; 13th Asian-Pacific Corrosion Control Conference, Osaka, Nov., 2003.
- M. Seo and N. Kikuchi: An EQCM Study on Passivation Process of Nickel Thin Films in Acidic and Alkaline Sulfate Solutions; ibid.
- M. Chiba and M. Seo: Friction Coefficients of the Passive Single Crystal Iron Surface and Their Potential Dependences Evaluated by an In-Situ Nano-Scratching; ibid.

DISSIMILAR MATERIALS INTERFACE ENGINEERING LABORATORY

Prof. Dr. T. Narita

Tel.:+81-11-706-6355 Fax.:+81-11-706-7814 E-mail:narita@eng.hokudai.ac.jp
Assoc. Prof. Dr. K. Ohsasa

Tel.:+81-11-706-6356 Fax.:+81-11-706-7814 E-mail:sasa@eng.hokudai.ac.jp Res. Assoc. H. Taumi

Tel.:+81-11-706-6356 Fax.:+81-11-706-7814 E-mail:taumi@eng.hokudai.ac.jp Res. Assoc. S. Hayashi

Tel.:+81-11-706-6357 Fax.:+81-11-706-7814 E-mail: hayashi@eng.hokudai.ac.jp Tech. Staff J. Tanaka

Tel.:+81-11-706-6357 Fax.:+81-11-706-7814 E-mail: jtanaka@eng.hokudai.ac.jp

Foreign Researchers

Dr. Zhenyu Liu, Dr. Fenqgun Lang, Dr. Kemas Zaini Thosin

Researchers

M. Segawa and Y. Katsumata

Students

T. Izumi, Y. Natsume, T. Nishimoto
D. Iino, Y. Matsumura, N. Nishiguchi
N. Suzuki, D. Sumoyama, Y. Taguwa and K. Nakagawa
K. Saitou, H. Matsumaru, S. Mikuni, H. Mizuno and M. Yamazaki

The research activities of the laboratory are directed to an understanding of the mechanism of the high temperature corrosion in super alloys, inter-metallic compounds and iron-based alloys, and to the development of the corrosion resistant alloys and corrosion protection of materials with coating and surface modification. The research activity is also directed to an understanding of the solidification mechanism of metals and alloys and to develop the modeling of casting structure using phase-field, cellular automata, montecalro and molecular dynamics methods.

Current topics on research are in the following:

(1) High temperature sulfidation of alloys Sulfidation properties of stainless steels, nickel alloys, and Ti-Al intermetallic compounds were investigated at relatively low sulfur pressures in $H_2S\text{-}H_2$ atmospheres.

(2) High temperature oxidation resistance of sulfidation processed Ti-Al alloys. High temperature oxidation behavior of sulfidation processed Ti-Al intermetallic compound was investigated. Effect of the third element addition on the oxidation

behavior was extensively investigated.

(3) High temperature corrosion under the atmosphere containing water vapor.

Oxidation behavior in Fe-Al and Fe-Si alloys under the atmosphere containing water vapor was studied. Acceleration of the oxidation was observed and its mechanism was investigated.

(4) Effect of Re coating on high temperature oxidation of super alloy.

Re was coated on the surface of a super alloy, and the oxidation behavior of the alloy was examined. A new method for coating Re on the surface of alloys based on electric plating was also investigated.

(5) Characterization of thermal barrier coatings

Thermal barrier coatings of the NiCrAlY-Zirconia composite were prepared by using Plasma Splay Coating Method and their mechanical and physical properties were investigated.

(6) Galvanizing process of steels by two step hot dipping

Galvanizing of steels was carried out by using a Zn-Al and a Zn-Al-Mg-Si molten alloys, and the optimum condition was investigated to make the galvanized layer having high corrosion resistance.

(7) Pb-free solder

Change in microstructure of a Pb-free solder due to composition and cooling rate during solidification was investigated. Effect of heat treatment on elastic modulus, microstructure and hardness of the solder was studied.

(8) TLP Bonding

Dissolution and isothermal solidification behavior during transient liquid phase bonding process of Ni, Ni base alloys and Al were investigated based on both experiment and computer simulation.

(9) Prediction of solidification structure of casting

A method to simulate the macro structure of a casting was investigated by

combining thermodynamics analysis, heat transfer calculation, Monte-Calro Method and Cellular Automata Method.

(10) Simulation of microstructure development in solidifying alloy by Phase-field model.

The dendrite growth in the solidification process of an alloy was investigated by using a Phase-Field Model. Change in dendrite morphology due to thermal, solutal and fluid flow conditions was examined.

Other Activities

Prof. Narita attended the International Symposium on Nb for high temperature application,

Araxia, Brazil 2003, Nov. 29~Dec. 10 as an invited speaker. Prof. Narita, Mr. Izumi and Mr. Nishimoto attended the Gordon Research Conference on High Temperature Corrosion, New London NH USA 2003, July 17~ July 27 and presented three papers. Prof. Narita attended the International Symposium on DIS'3 Wine, Austria, July 13~July 19 as an invited speaker. Prof. Narita attended the International Symposium on Corrosion Science in the 21st Century UMIST, Manchester UK 2003, July 5 ~July 12. Prof. Narita attended the International NEDO Joint Meeting, UNSW, Sydney Australia, 2003, April 19~April 26 as an invited speaker.

Presentations

Tensile Strength and fractured structure of Pb-free Sn-Ag--X(Cu, Al) Solder Alloy; N.Suzuki, J.Tanaka, T.Takashima and T.Narita: The Winter Joint Meeting of The Hokkaido Secs. of Jpn. Inst. Metals and Iron and Steel Inst. Jpn., Muroran, Jan 2003.

Application of αCr Diffusion Barrier to Ni-40Cr Alloy; Y.Taguwa, T.Izumi, T.Narita, Y.Shibata and S.Hayashi: ibid.

Analysis for Growth Direction of Cell and Dendrite Under Positive Temperature Gradient; Y.Natsume, K.Ohsasa, T.Narita and H.Esaka: ibid.

Simulation Technology for Solidification Structure Formation at the present time and Future Subjects; K.Ohsasa: Invited Lecture at Nagasaki University, Nagasaki, Jan. 2003.

Solidified Structure and Mechanical Properties of Sn-Ag-Al Solder Alloy; N.Suzuki, J.Tanaka, T.Takashima and T.Narita: MATE2003 9th Symposium on "Microjoining and Assembly Technology in Electronics", Yokohama, Feb 2003.

Solidified Structure of Sn-Ag Solder Alloy with Addition of Minute Amounts of Al; N.Suzuki, J.Tanaka, T.Takashima and T.Narita: The 132th Annual Meeting of Jpn. Inst. Metals; Chiba, Mar. 2003.

Evaluation of Tensile Properties of Pb-free Sn-Ag-X(Cu,A1) Solder Alloy; N.Suzuki, J.Tanaka, T.Takashima and T.Narita: ibid.

Application of σ Phase Diffusion Barrier to Ni Base Super Alloy; T.Izumi, S.hayashi, T.Nishimoto and T.Narita: ibid.

Hightemperature Oxidation Behavior of Pt-Si Alloy; T.Iino, T.Tanaka and T.Narita: ibid.

Application of αCr Diffusion Barrier to Ni-40Cr Alloy; Y.Taguwa, T.Izumi, T.Narita, Y.Shibata and S.Hayashi: ibid.

Analysis of Transient Liquid Phase Bonding Process Using Phase-field Model:

Y.Natsume, K.Ohsasa and T.Narita: ibid.

Evaluation of Probability Parameter for Nucleation to Predict Casting Structure; K.Ohsasa and H. Shirosawa: The 145th Annual Meeting of Iron and Steel Inst. Jpn., Chiba, Mar. 2003.

Heterogeneous Nucleation Behavior in Al and Al Base Alloys; K.Ohsasa: ibid.

Evaluation of Heterogeneous Nucleation Frequency to Predict Casting Structure; K.Ohsasa and M.Kudoh: Annual Meeting of 19 Committee of Jpn. Soc. Promotion of Science, Tokyo, May 2003.

Evaluation of Heterogeneous Nucleation Frequency to Predict the Casting Structure of Al Base Alloy; N.Nishiguchi, K.Ohsasa and T.Narita: Annual Meeting of the Hokkaido Sec. of Jpn. Foundry Engineering Soc. ,Otaru, June 2003. Simulation for Dendrite Growth by Using Front Tracking Method; M.Nakagawa, K.Ohsasa and T.Narita: ibid.

Heat Transfer Analysis for Multi-component Alloys by Computational Thermodynamics Using Thermo-Calc; K.Ohsasa and H.Shirosawa: Annual Meeting of 172 Committee of Jpn. Soc. Promotion of Science, Tokyo, June 2003.

Prediction of the Structure of Cast Steel with the Consideration of Peritectic Transformation; K.Ohsasa: Meeting of Solidification Forum in Iron and Steel Inst. Jpn., Chiba, June 2003.

Research and Development of Ultra-high Temperature Material:(Re-Cr-Ni)Alloy as Diffusion Barrier on Ni-based Superalloy; K. Zaini Thoshin, S.Ilyung, F.Lang and T.Narita: Joint Research Indonesian Institute of Science(LIPI) and Japan Society for Prpmotion of Science (JSPS), Workshop and Expose Result of Fundamental Research, Jakarta, July 2003.

Improving the Oxidation Resistance of TiAl by a Two-step Cr and Al Diffusion Treatment; T.Nishimoto, T.Izumi and T.Narita: Gordon Research Conference on High-temperature Corrosion, New London NH USA, July 2003.

Superior Long-term Oxidation Resistance of Ni-Al Coated TiAl Through Up-hill Diffusion; T.Izumi, T.Nishimoto and T.Narita: ibid.

Improvement in Oxidation Resistance of TiAl Alloy through Ni-AlCoating; T.Izumi and T.Narita: Innovation for Control of Nano Structure of Crystalline Material, Fukuoka, Sept. 2003.

Effect of Solidification Segregation on Diffusion Experiment in Liquid; K.Ohsasa, A.Hirata, M.Uchida and T.Itami: North Forum of The Hokkaido Sec. of Iron and Steel Inst. Jpn., Sapporo, Sept. 2003.

Structure and Thermal Fatigue properties of Sn-Ag-Al Solder Alloy Foil/Cu Joint; N.Suzuki, J.Tanaka, T.Takashima and T.Narita: MES2003 13th Micro-electronics Sinposium, Osaka, Oct. 2003.

Oxidation Resistance in long term oxidation experiment of TiAl with Up-hill Diffusion Treatment; T.Izumi, T.Nishimoto and T.Narita: The 133th Annual Meeting of Jpn. Inst. Metals, Sapporo, Oct. 2003.

Hightemperature Sulfidation Behavior of Fe-40AlFoil; F.Lang, T.Narita, Z.Yu, S.Gedevanishvili ans S.C.Deevi: ibid.

Application of Oxidation Resistant Coating to NbBase Composite Material; Y.Matsumura, S.Hayashi and T.Narita: ibid.

Effect of Film Construction on the Oxidation Resistance of TiAl Alloy with Cr,Al Vapor Diffusion Treatment; T.Nishimoto, T.Izumi and T.Narita: ibid.

Effect of the Addition of Ti and Si on Hightemperature Oxidation Behavior of Pt; T.Iino, T.Tanaka and T.Narita: ibid.

Numerical Modeling of the Transient Liquid Phase Diffusion Bonding Process of Al; Y.Natsume, K.Ohsasa, Y. Tayu T.Momono and T.Narita: ibid.

Heat Transfer Analysis for Iron Base Multi-component Alloys by Applying Computational Thermodynamics; K.Ohsasa and H.Shirosawa: The 146th Annual Meeting of Iron and Steel Inst. Jpn., Sapporo, Oct. 2003.

Prediction of the Structure of Cast Steel with the Consideration of Peritectic Transformation; K.Ohsasa: ibid.

Effect of Phosphorus on the Formation of Austenite Grain in Hyper Peritectic Carbon Steel; M.Kudoh, M.Saitou and K.Ohsasa: ibid.

Evaluation of Heterogeneous Nucleation Frequency for the Simulation of Casting Structure Formation of Alloys; N.Nishiguchi, K.Ohsasa and T.Narita: Poster Session for Students in the 146th Annual Meeting of Iron and Steel Inst. Jpn., Sapporo, Oct. 2003.

Long-term Oxidation Resistance of TiAl with Up-hill Diffusion Treatment; T.Izumi, T.Nishimoto and T.Narita: Young Scientist Forum, The 146th Annual Meeting of Iron and Steel Inst. Jpn., Sapporo, Oct. 2003.

Evaluation of Nucleation Rate to Predict the Macrostructure of Aluminum base Alloys during Unidirectional Solidification; K.Ohsasa and N.Nishiguchi: Eighth Asian Foundry Congress, Bangkok, Thailand, Oct. 2003.

Prediction of Casting Structure for Al Base Alloys Based on Heterogeneous Nucleation Parameter; N.Nishiguchi, K.Ohsasa and T.Narita: The 143th Annual Meeting of Jpn. Foundry Engineering Soc., Toyama, Oct. 2003.

Simulation for Dendrite Growth in Al Base Alloy Using Front Tracking Method; M.Nakagawa, K.Ohsasa and T.Narita: ibid.

Simulation for the Solidification Structure Formation of Al Base Alloy by Combining Phase-field and Cellular Automaton Methods; Y.Natsume, K.Ohsasa, N.Nishiguchi and T.Narita: ibid.

Effect of Nickel-Aluminide Coating Through up-hill Diffusion on Oxidation Properties of Tl-Al Alloy; T.Izumi, T.Nishimoto and T.Narita: 13th Asian Pacific Corrosion Control Conference, Osaka, Nov. 2003.

Effect of adding elements on the Oxidation Resistance of TiAl Alloy with Cr,Al Vapor Diffusion Treatment; T.Nishimoto, T.Izumi and T.Narita: ibid.

Hightemperature Corrosion Behavior of an Fe-40Al Sheet in Atmospheres Containing Air, SO₂ and H₂S; F.Lang, Z.Yu, S.Gedevanishvili, S.C.Deevi, S.Hayashi and T.Narita: ibid.

Two-Step Cr and Al Diffusion Coating on TiAl at High Temperatures; T.Nishimoto, T.Izumi and T.Narita: ibid.

Corrosion Behavior of Fe-40Al Foil in Air and in Mixed Pas Containing SO₂.; F.Lang, T.Narita, Z.Yu, S.Gedevanishvili ans S.C.Deevi: The 50th Annual Meeting of Jpn. Soc. Corro. Eng. Okinawa, Nov. 2003.

Effect of Alloy Composition on the formation of Oxidation Resistant Coating Film in Nb Base Alloy; Y.Matsumura, S.Hayashi and T.Narita: ibid.

Effect of Film Structure on the Oxidation Resistance of TiAl Alloy with Cr,Al Vapor Diffusion Treatment; T.Nishimoto, T.Izumi and T.Narita: ibid.

Long-term Oxidation Resistance of TiAl with Up-hill Diffusion Treatment; T.Izumi, T.Nishimoto and T.Narita: ibid.

Hightemperature Oxidation Behavior of Pt-Si-TiAlloy in Air; T.Iino, T.Tanaka and T.Narita: ibid.

Numerical Analysis of the Production Process of Composite Layer by Using Double Casting Method; K.Ohsasa and K.Matsuura: 15th Symposium on Functionally Graded Materials (FGM2003 in Sapporo), Sapporo, Nov. 2003.

Phase-field Simulation of TG-TLP Bonding; Y.Natsume, K.Ohsasa and T.Narita: ibid.

Production and Evaluation of Properties of Nb-Al-Si Ternary Alloy Having Fine Grain Structure: K.Taniguchi, K.Matsuura, M.Kudoh and K.Ohsasa: ibid.

INTERFACE MICRO-STRUCTURE ANALYSIS LABORATORY

Prof. Dr. H. Takahashi
Tel.:+81-11-706-7110 Fax.:+81-11-706-7881
E-mail: takahasi@elechem1-mc.eng.hokudai.ac.jp
Assoc. Prof. Dr. M. Sakairi
Tel.:+81-11-706-7111 Fax.:+81-11-706-7881
E-mail: msakairi@elechem1-mc.eng.hokudai.ac.jp

Resercher

Dr. T. Kikuchi

Students

Z. Kato, H. Matsuda E. Sakata, M. Yamada, M. Sunada, K. Nagahara, M. Yamada, Y. Akiyama, Y. Uchida, S. Kurokawa, Y. Shimoyama and S. Nishikawa

Equipments

Atomic force Microscope Confocal Scanning Laser Microscope Pulsed Nd-YAG Laser Patterning System

Research work at "Interface Micro-Structure Analysis Laboratory (LIMSA)" directs toward 1) the examination of structure and dielectric properties of anodic oxide films on aluminum and valve metals, 2) micro- and nano-patterning of aluminum using laser irradiation and AFM probe processing, 3) Localized corrosion of coated steels and aluminum alloys.

The topics of investigation are in the following:

(1) Fabrication of copper dot array on aluminum surface by AFM probe processing.

Aluminum specimens covered with thin barrier type anodic oxide films were scratched with a diamond-probe of atomic force microscope in CuSO₄ solutions to remove the oxide film locally. After scratching, the specimen was cathodically polarized, using the probe as a counter electrode. Copper dot array was fabricated by repeating scratching and copper deposition at different positions.

(2) Fabrication of micro three-dimensional structures by laser irradiation and metal deposition.

Local metal deposition by anodizing / laser irradiation / electroplating was applied on a columnar aluminum specimen with several mm diameter. During laser irradiation, the specimen was rotated and moved downwards and upwards. After metal deposition by electroplating, and electrophoretic deposition of acrylic resin, the specimen was immersed in NaOH solution to remove the oxide film and the metal substrate. Cylindrical Ni-, Pt- and acrylic resin-network structures were fabricated.

(3) Anodizing of aluminum coated with Ta₂O₅ and Nb₂O₅ films by MOCVD

Aluminum specimens were covered with Ta_2O_5 and Nb_2O_5 films by the metal organic chemical vapor deposition, and then anodized galvanostatically in a neutral borate solution. During anodizing, Al_2O_3 layer grew at the interface between Ta_2O_5 and Nb_2O_5 films and the metal substrate, and the Al_2O_3 / Ta_2O_5 (Nb_2O_5) layer interface became obscure. The electric capacitance of anodic oxide films formed after Nb_2O_5 coating was much higher than that formed on aluminum without Nb_2O_5 coating. The MOCVD coating of Ta_2O_5 and Nb_2O_5 films were attempted to etched aluminum foils before anodizing.

(4) Film breakdown of anodic oxide films on aluminum contacting with solid conductive phases.

Barrier type anodic oxide films formed on electropolished aluminum plates were attached with poly ethylenedioxy-thiophene (PEDT) and Pt and Au sputtered layers to examine breakdown of the oxide films. Film breakdown voltage of specimens attached to PEDT was much lower than that attached to Pt, and Au layers.

(5) Formation and dielectric properties of niobium anodic oxide films

Niobium specimens were anodized in H₃PO₄ solution galvanostatically up to 100 V, and then the potential of the specimens was kept at 100 V for 6 hrs. The structural change of the film surface during the potentiostatic anodizing was observed by SEM, CSLM, and AFM. During the potentiostatic anodizing, sub-µm imperfections formed at ridges of surface network structure grew to ten µm imperfections after 6 hrs. The structural change was correlated with bias dependency of the capacitance of anodic oxide films.

(6) Fabrication of micro electrochemical-reactors by anodizing, laser irradiation and electroplating

Aluminum specimen covered with porous anodic oxide films was irradiated with a pulsed Nd-YAG laser to produce through-holes with 300 μ m diameter, channels with 300 μ m width, and a chamber with 2 x 2 x 0.1 mm volume on the surface, and Au layer was deposited on the surface of the chamber. Electrochemical reactors were fabricated by attaching the surface-modified specimen to another one via a Teflon sheet, and evaluated on the electrochemical performance using a $[Fe(CN)_6]^{3-}$ / $[Fe(CN)_6]^{4-}$ solution system. A cyclic voltamogram showed redox peaks of $[Fe(CN)_6]^{3-}$ and $[Fe(CN)_6]^{4-}$ ions, indicating dependence of current on scanning rate and solution concentration.

(7) Study on initial stage of localized corrosion of Zn-Al alloy coated steel in zinc ion-containing solutions by photon rapture method.

Carbon steel coated with Zn, Zn / 5%Al and Zn / 55%Al layers were covered with a thin nitrocellulose film. The specimens were irradiated with a pulsed Nd-YAG laser in Cl⁻ containing solutions with and without zinc ions under potentiostaic conditions to remove the nitrocellulose film and air formed oxide film locally. Reformation of oxide film at the laser-irradiated area occurred at a low potential region in all the solutions, while localized corrosion occurred on Cl⁻ ion containing solutions at a high potential region. Zinc ions affected initial stage of localized corrosion of zinc-coated steels.

(8) Effect of anodic oxide film structure on galvanic corrosion of aluminum in Cl containing solutions

Aluminum specimens on which porous and barrier type oxide films were formed, were immersed in Cl ion containing solutions to study effects of film structure on galvanic corrosion, by monitoring rest-potential and corrosion current between sample and Pt-counter electrode. Oxide film microstructure affected the incubation time of localized corrosion. Corrosion impedance was also measured by FFT and decreased after localized corrosion started.

(9) Local deposition of electro-conductive organic film on aluminum by laser irradiation and electrolytic polymerization.

Aluminum specimens covered with porous type anodic oxide films were irradiated locally with a pulsed Nd-YAG laser to remove the oxide film at the laser-irradiated area.

Then, the specimen was anodically polarized in a pyrrole solution to deposit a poly-pyrrole film at the laser-irradiated area. The CV curve of the poly-pyrrole film deposited specimen showed a couple of redox peaks of poly-pyrrole.

(11) In situ AFM observation of aluminum covered with anodic oxide films during cathodic polarization in a neutral solution.

Aluminum specimens covered with barrier type anodic oxide films were cathodically polarized at a constant cathodic current to examine the change in the surface by in-situ AFM observation. Blisters formed at the initial stage of cathodic polarization grow with time, and eventually explode to allow local dissolution of metal substrate.

(12) Formation and dielectric properties of tantalum anodic oxide films

Tantalum specimens were anodized in H₃PO₄ solution galvanostatically up to 100 V, and then the potential of the specimens was kept at 100 V for 2 h. The structural changes in the film surface during the potentiostatic anodizing and heat treatment were observed by SEM and CSLM. The heat treatments were correlated with bias dependency of the capacitance of anodic oxide films.

(13) Anodizing of aluminum coated with SiO₂ films by sol-gel electro-phoretic method

Plain and DC-etched aluminum specimens were coated with SiO₂ films by the sol-gel electrophoretic method, and then anodized galvanostatically in a neutral borate solution. The SiO₂ film was deposited on both plain and DC-etched specimens uniformly, and anodizing of SiO₂ film-coated specimens lead to the formation of anodic oxide films consisting of an outer Al-Si composite oxide layer and an inner alumina layer. The parallel capacitance of the anodic oxide films was almost the same as that formed on non-coated specimens.

(14) Measurements of anodic oxide film thickness distribution by CSLM

Porous type anodic oxide films were formed on pure aluminum sheets in sulfuric acid and oxalic acid solutions, using two types of electrochemical cell. Oxide film thickness distribution on the specimen was examined with confocal scanning laser microscope. Five to ten % difference in the film thickness was found at the different positions of the specimen, depending on the configuration of electrodes in the electrochemical cell.

In March, Dr. T. Kikuchi received an engineering doctor degree, and joined again LIMSA as a researcher from Furuya Metal Co. Dr. K. Watanabe left for Okayama Univ. to continue his postdoctoral fellowship with Prof. K. Kondo, and Dr. A. Mozalev went back to Minsk, Belarus after finishing of mold fabrication project.

On the 1st of April, Associate Prof. K. Kurokawa was promoted to a professor of

Center for Advanced Research of Energy Technology, Hokkaido Univ., and moved out to a new laboratory with students, S. Matsushita, S. Nishizawa, N. Takada, and T. Nakagiri. The secretary of LIMS, Mrs. Y. Arihara, quitted her job at the end of April after much contribution for six years.

In May, a new secretary, Mrs. M. Murata joined LIMSA. Prof. Takahashi attended the 3rd International Symposium on Aluminum Surface Science and Technology (ASST) held in Bonn, Germany, and presented a paper entitled "Fabrication of Three-Dimensional Microstructures with Aluminum Anodizing, Laser Irradiation, and Metal Deposition." He visited Prof. K. Nisancioglu at Trondheim, Norway before ASST to discuss functions of anodic oxide films. He was a guest speaker on the 2003 International Conference on Advanced Capacitors held in Kyoto and presented a paper entitled "Formation and Breakdown of Anodic Oxide Films on Aluminum -For the Development of High Voltage Sustainable Capacitors-.

In July, Dr. Sakairi attended "Corrosion Science in the 21st Century" in Manchester to present a paper entitled "Initial Stage of Localized Corrosion on Zn - 5 mass% Al Alloy Coated Steels by Using Pulsed Photon Film Removal Technique". Before the symposium he visited Dr. Stratmann, Dr. Hassel and Dr. Fushimi at Maxplank Institute, Dusseldorf, to discuss corrosion and protection of steels.

In August, the 4th International Joint Symposium between Hokkaido Univ. and Chungnam National Univ. was held in Sapporo and Prof. Takahashi talked on "Electrochemical Micro-Technology of Aluminum Surface with Laser Irradiation and AFM Probe Processing".

In October, Research associate, Dr. M. Sakairi was promoted to an associate professor at LIMSA. Prof. Takahashi attended 204th ECS Meeting at Orlando, Florida and talked on "Fabrication of Metal Dot Array on Aluminum by AFM Probe Processing". Prof. Takahashi and Associate Prof. Sakairi were organizers of the Tarumae Conference (20th Annual Meeting of Anodizing Research Section, Surface Finishing Soc. Jpn.) held in Otaki-village, and invited Prof. K. Hebert, Iowa State Univ., as a guest speaker.

In November, Associate Prof. Sakairi attended 13th Asian-Pacific Corrosion Control Conference held in Osaka to present a paper entitled "Initial Stage of Localized Corrosion on Zinc Coated Steel with Photon Rupture Method in Chloride Ions Containing Solutions".

In December, Prof. Takahashi was invited in 2nd Changwon International Symposium on Advanced Science and Technology (CISAS 2003) held in Changwon, Korea and talked on "Anodizing of Aluminum Covered with SiO₂ and Nb₂O₅ Films by Sol-Gel Dip Coating -Innovation of New Type of Aluminum

Electrolytic Capacitors-". After the symposium, he visited Prof. J. -H. Yoon at Changwon Univ. to discuss on the coating technique.

The scientists visited LIMSA in 2003 were Prof. S. -G. Park, Chungbuk National Univ., Korea between July 3 - 31, Prof. G.-E. Jang, Chungbuk National Univ., Korea on July 28, Prof. W. Plieth, Dulesden Univ., Germany, on September 10, K. R. Hebeert, Iowa State Univ., U. S. A. on October 14, Dr. A. W. Hassel, Max Plank Institute, Germany, on November 13, and Dr. M. Stratmann, Max Plank Institute, Germany on November 28.

Presentations

Temperature Dependence on High Temperature Oxidation of $NbSi_2$ - ; S. Matsushita, K. Kurokawa, and H. Takahashi : The Winter Joint Meeting of the Hokkaido Secs. of Jpn. Inst. Metals and Iron and Steel Inst. Jpn., Muroran, Jan., 2003.

Initial Stage Localized Corrosion of Zn-Al alloy Coated Steels by Photon Rupture - Effect of NO₃²⁻ -; K. Itabashi, M. Sakairi, and H. Takahashi: The Joint Meeting of The Hokkaido Secs. of Electrochem. Soc. Jpn., Surf. Finish. Soc., and Jpn. Soc. Corros. Eng., Sapporo, Jan., 2003.

TEM Cross Sectional Observation of Zn Coated Steels by Ultra Microtomy; M. Sakairi, K. Itabashi, and H. Takahashi; ibid.

Structure Change of Aluminum Composite Oxide Films During Hot Water and Chemical Treatment and Void Reformation by Anodizing; T. Yasuda, N. Katayama, K. Watanabe, M. Sakairi, and H. Takahashi: The Hokkaido Secs. of Chem. Soc. Jpn. Soc. Anal. Chem., Sapporo, Feb., 2003.

Dielectric Properties of Aluminum Anodic Oxide Films Contacting with Organic Solid Electrolytes; M. Yamada, M. Sakairi, H. Takahashi, K. Nogami, and H. Uchi: ibid.

Formation of Al-Nb Composite Oxide Films by MOCVD / Anodizing; E. Sakata, M. Sakairi, and H. Takahashi: ibid.

Fabrication of Three-Dimensional Metal / Organic Microstructures by Laser Irradiation and Electrochemical Technique; T. Kikuchi, M. Sakairi, H. Takahashi, Y. Abe, and N. Katayama: The 107th Annual Meeting of Surf. Finish. Soc. Jpn., Tokyo, Mar., 2003.

Effect of Contacting Material on Potential Sustainability and Capacitance of Aluminum Anodic Oxide Films; M. Yamada, M. Sakairi, H. Takahashi, K. Nogami, and H. Uchi: ibid.

Change in Structure and Dielectric Properties of Al-Si Composite Oxide Films on Aluminum During Potentiostatic Anodizing; K. Watanabe, M. Sakairi, H. Takahashi, and S. Hirai: ibid.

Temperature Dependence on High Temperature Oxidation of NbSi₂; S. Matsushita, K. Kurokawa, and H. Takahashi: The 132nd Annual Meeting of Jpn. Inst. Metals, Chiba, Mar., 2003.

H₂O Distribution in Cr₂O₃ Scale Formed by High Temperature Oxidation in H₂O-Containing Atmosphere; A. Yamauchi, K. Kurokawa, and H. Takahashi: ibid.

Formation of Al-Nb Composite Oxide Films by MOCVD and Anodizing; E. Sakata, M. Sakairi, and H. Takahashi: The 70th Annual Meeting of the Electrochem. Soc. of Jpn., Tokyo, April, 2003.

Copper Plating on Aluminum Surfaces with AFM Probe; Z. Kato, M. Sakairi, and H. Takahashi: ibid.

Structure and Dielectric Properties of Niobium Anodic Oxide Films; K. Nagahara, M. Sakairi, H. Takahashi, K. Matsumoto, K. Takayama, and Y. Oda: Material for Charge Device Study Summit, Tokyo, April, 2003.

Structure and Dielectric Properties of Nb Anodic Oxide Films; M. Sakairi, K. Nagahara, H. Takahashi, T. Miyamoto, K. Matsumoto, K. Takayama, and Y. Oda: The 63rd ARS (Anodizig Research Society, SFJ) Meeting, Tokyo, April, 2003.

Novel Micro-Technologies Using Anodizing of Aluminum; H. Takahashi: Japan-Norwegian Mini-Seminar on Aluminum Surface and Technology, Trondheim, May, 2003.

Fabrication of Three-Dimensional Microstructures with Aluminum Anodizing, Laser Irradiation, and Metal Deposition; T. Kikuchi, M. Yamada, A. Mozalev, M. Sakairi, and H. Takahashi: International Conference on Aluminum Surface Science and Technology, Bonn, May, 2003.

Localized Corrosion of Zn Coated Steels by Photon Rupture Method - Effect of pH -; M. Sakairi, K. Itabashi, and H, Takahashi: The 4th Meeting of Surface Finishing Research for Coated Steel (ISIJ), Kitakyusyu, May, 2003.

Formation and Breakdown of Anodic Oxide Films on Aluminum - For the development of High Voltage Sustainable Capacitors; H. Takahashi, M. Sakairi,

and K. Watanabe: 2003 International Conference on Advanced Capacitors, Kyoto, May, 2003.

Initial Stage Localized Corrosion of Zn Alloy Coated Steels by Photon Rupture in pH=7.4 solutions; M. Sakairi, K. Itabashi, and H. Takahashi: 2003 Annual Meeting of Jpn. Soc. Corrs. Eng., Tokyo, June, 2003.

Micro Surface Patterning on Aluminum by Laser Irradiation and AFM Tip Processing; M. Sakairi: Seminar at Max-Planck Institute for Iron Research, Duesseldorf, July, 2003

Initial Stage of Localized Corrosion on Zn - 5 mass% Al Alloy Coated Steels by Using Pulsed Photon Film Removal Technique; M. Sakairi, K. Itabashi, and H. Takahashi: Corrosion Science in the 21st century, Manchester, July, 2003

New Development of Aluminum Surface Science and Technology; H. Takahashi: The 64th ARS (Anodizig Research Society, SFJ) Meeting, Tokyo, July, 2003.

Fabrication of Electrochemical Microcell on Aluminum by Laser Micro Processing; M. Yamada, M. Sakairi, and H. Takahashi: The Hokkaido Secs. of Chem. Soc. Jpn. and Jpn. Soc. Anal. Chem., Kitami, July, 2003

Change in Structure of Anodic Oxide Films on Niobium During Potentiostatic Anodizing; K. Nagahara, M. Sakairi, H. Takahashi, K. Matsumoto, K. Takayama, and Y. Oda: ibid.

Electrochemical Micro-Technology of Aluminum Surface with Laser Irradiation and AFM Probe Processing; T. Kikuchi, Z. Kato, M. Yamada, M. Sakairi, and H. Takahashi: The 4th Intern. Joint Symp. of Hokkaido Univ. and Chungnam National Univ., Sapporo, Aug., 2003

Problem Based Learning at Hokkaido University; H. Takahashi, T. Kishinami, K. Kudo, and T. Mikami: 2003 Meeting of Japanese Society for Engineering Education, Sapporo, Sep., 2003

Change in Structure and Dielectric Properties of Anodic Oxide Films on Niobium During Potentiostatic Anodizing; K. Nagahara, M. Sakairi, H. Takahashi, K. Matsumoto, K. Takayama, and Y. Oda: The Autumn Meeting of Electrochem. Soc. of Jpn., Sapporo, Sep., 2003

Fabrication of Micro Electrochemical Cell on Aluminum by Laser Processing; M. Yamada, M. Sakairi, and H. Takahashi: ibid.

Fabrication of Metal Dot Array with AFM-Probe Processing; Z. Kato, M. Sakairi, and H. Takahashi: ibid.

Anodizing of Etched-Aluminum Foil Coated with SiO₂; K. Watanabe, M. Sakairi, H. Takahashi, S. Hirai: ibid.

Hybrid Capacitance Properties of Conducting Polymer Thin Film Coated Aluminum; Y. Lee, T. Lee, S. Park, M. Sakairi, and H. Takahashi: ibid.

Formation of Al-Ta Composite Oxide Films on Etched Al Foil by MOCVD / Anodizing; E. Sakata, M. Sakairi, and H. Takahashi: The 108th Annual Meeting of Surf. Finish. Soc. Jpn., Utsunomiya, Sep., 2003

Behavior of Copper Deposition by Anodic Oxidation / AFM Processing / Cathodic Polarization; Z. Kato, M. Sakairi, and H. Takahashi: ibid.

Effect of the Structure of Interface between Contacting Material and Aluminum Anodic Oxide Films on Their Potential Sustainability; M. Yamada, M. Sakairi, H. Takahashi, K. Nogami, and H. Uchi: ibid.

Anodizing of Etched Al-Foil Coated with Nb₂O₅; K. Watanabe, M. Sakairi, H. Takahashi, S. Hirai, and S. Nagata: ibid.

Development of Fabrication Method of 3D-Microstructures by Laser Irradiation and Electrochemical Technique; T. Kikuchi, H. Takahashi, M. Sakairi, and T. Maruko: The 8th Young Scientist Forum (The Iron and Steel Inst. Jpn), Sapporo, Oct., 2003

Initial Stage of Localized Coroosion on Al-9mass%Si Alloy Coated Steels by Photon Rupture Method - Effect of Potential -; M. Sakairi, K. Itabashi, and H. Takahashi: The 146th Annual Meeting of the Iron and Steel Inst. Jpn., Sapporo, Oct., 2003

Localized Corrosion on Zn Coated Steels by Photon Rupture Method and Its Microstructure; M. Sakairi, K. Itabashi, and H. Takahashi: The 133rd Annual

Meeting of Jpn. Inst. Metals, Sapporo, Oct., 2003

3D-Microstructure Fabrication by Aluminum Anodizing and Laser Irradiation; T. Kikuchi, T. Maruko, M. Sakairi, and H. Takahashi: The 20th ARS (Anodizing Ressearch Society, SFJ), Otaki, Oct., 2003

Fabrication of Electrochemical Microcell on Aluminum by Laser Irradiation and Electrochemical Technique; M. Yamada, M. Sakairi, and H. Takahashi: ibid.

Formation of Sunflower-like defects formd on Anodic Oxide Films on Nb; K. Nagahara, M. Sakairi, H. Takahashi, K. Matsumoto, K. Takayama, and Y. Oda: ibid.

Fabrication of Metal Dot Array on Aluminum by AFM Probe Processing; Z. Kato, M. Sakairi, and H. Takahashi: The 204th Meeting of the Electrochem. Soc., Orlando, Oct., 2003

Initial Stage of Localized Corrosion on Zn-Al Alloy Coated Steels by Photon Rupture Method in Neutral Solutions; M. Sakairi, K. Itabashi, and H. Takahashi: The 50th Jpn. Conf. on Materials and Environments, Naha, Nov., 2003

Initial Stage of Localized Corrosion on Zinc Coated Steels with Photon Rupture Method in Chloride Ions Containing Solutions; M. Sakairi, K. Itabashi, and H. Takahashi: 13th Asian-Pacific Corrosion Control Conference, Osaka, Nov., 2003

Anodizing of Aluminum Covered with SiO2 and Nb2O5 Films by Sol-Gel Dip Coating - Innovation of New Type of Aluminum Electrolytic Capacitors -; K. Watanabe, M. Sakairi, H. Takahashi, S. Hirai, S. Nagata, and K. Takahiro: 2nd Changwon International Symposium on Advanced Science and Technology, Changwon, Dec., 2003

3D-Microstructure Fabrication by Laser Irradiation and Electrochemical Technique; H. Takahashi: Materials Engineering and Molecular Chemistry Group Forum, Tokyo, Dec., 2003

LABORATORY OF ADVANCED MATERIALS CHEMISTRY

Prof. Dr. Hidetaka Konno
Tel.&Fax:+81-11-706-7114
E-mail:ko@eng.hokudai.ac.jp
Assoc. Prof. Dr. Hiroki Habazaki
Tel.&Fax:+81-11-706-6575
E-mail:habazaki@eng.hokudai.ac.jp
Instructor Mr. Akira Shimizu
Tel.:+81-11-706-6577
akira@eng.hokudai.ac.jp

Students

S. Sato, A. Sudo, T. Matsuo, H. Tachibana, S. Sato, Y. Takahashi, D. Abe, A. Tamura, T. Onodera, K. Kimura, T. Kuranishi

Facilities and Capabilities

Dc and rf magnetron sputtering: Shimadzu SP-2C, suitable for preparation of various metallic thin film materials as well as oxide and nitride films.

X-ray diffractometer: Rigaku RINT2000, capacble of θ -2 θ and α -2 θ modes measurements using Cu α radiation.

Gas adsorption: Bel Japan Belsorp-Mini, capable of Specific surface area / pore size distribution measurements at high precision.

Laser Raman Spectrometer: Jasco TRS-401 and Jobin Yvon T64000, triple type spectrometers with a Ar gas laser of 2W.

FT-IR spectrometer: Jasco FT-IR350, equipped with DR and RAS attachments.

Uv-vis spectrometer: Jasco V-550, equipped with DR attachment.

EPMA: JEOL JSM-5410 equipped with Oxford WDX-400.

TG/DTA: Seiko TG/DTA6300, temperature range room temp. to 1500°C.

TOC analyzer: Shimadzu TOC-5000A.

Capillary Electrophoresis analyzer: Ohtsuka Electronics CAPI-3100.

The research activities of the laboratory are directed toward (1) formation and characterization of nanocarbons, carbon-based composites and carbides, (2) formation of dielectric layers by anodizing of valve metal alloys and (3) electrochemical and biological water treatments utilizing oxide anodes and carbon

materials.

Current research topics are in the following:

(1) Formation and characterization of composite materials of carbon, ceramics and metals

Various carbon composites were formed by carbonization of 1) polyimide films containing metal complexes, 2) powder mixtures of organic polymer and ceramics and 3) chelate resins complexed with metal ions. Basic researches on the structure, composition, electric and magnetic properties of the composites are in progress by using XRD, TEM, SEM, Raman spectroscopy, SQUID, EIS and others.

- (2) Development of a new formation process of B/C composites and B₄C carbide New precursors were found for production of title materials. They were prepared by chemical processes using the combinations of (a) sugars, polyhydric alcohols or the compounds containing N-glucamine functional groups and (b) boric acid or organoboranes. Carbonization of these precursors provided the B/C composites with high boron concentration and B₄C.
- (3) Preparation of carbon nanofilaments using porous anodic alumina and etched aluminum foil templates

Porous anodic alumina and etched aluminum foils have been used as template materials to prepare carbon nanofilaments. Instead of usual CVD process we have prepared these nanocarbon materials simply by heating a mixture of the template and organic polymers, such as polyvinylalcohol and polyvinylchloride, which liquefy during carbonization process.

(4) Electrochemical wastewater treatment using oxide anodes

Various oxide anodes have been prepared by thermal decomposition of precursor salts on titanium substrate and anodic deposition. Using these anodes electrochemical decomposition of organic pollutants such as phenol, which are not easily decomposed by other methods, in wastewater has been examined to clarify the suitable electrochemical conditions and to develop effective anodes for their anodic decomposition.

(5) Formation of barrier-type amorphous anodic films on titanium and niobium alloys

Alloying of titanium with other valve metals is found to result in the formation of uniform amorphous anodic films to relatively high voltages in neutral and acid electrolytes, in contrast to an amorphous-to-crystalline transition of anodic films on titanium at low voltages. Such anodic films formed on the titanium alloys are possible candidates of new dielectric materials for electrolytic capacitors. The positive effects of nitrogen addition to niobium on the dielectric properties and thermal stability of its anodic film for capacitor applications has been found recently.

(6) Novel oxidation-resistant multilayer coatings using anodic alumina layer as diffusion barrier

Barrier-type anodic alumina layer has been applied as diffusion barrier between the oxidation-resistant Al-Nb-Cr alloy and TiAl alloy substrate to improve the oxidation resistance of TiAl at elevated temperatures. It has been found that the alumina layer suppresses effectively the diffusion of titanium from the substrate to the alloy coating, which depredates the performance of the coating.

Other activities

Professor Konno, Associate Professor Habazaki attended 3rd International Symposium on Aluminium Surface Science and Technology 2003 (ASST2003) held at Bonn, Germany in May. Just before the Symposium, he visited Tronheim, Norway and attended Japan-Norway Mini-Seminar. He also attended International Symposium on Corrosion Science in 21st Century held at Manchester, England in July, International Symposium on Advanced Capacitors held at Kyoto in May and Asian Pacific Corrosion Control Conference held at Osaka in November.

Presentations

Effect of alloying elements on structure of anodic titania; M. Uozumi, H. Habazaki, H. Konno, K. Shimizu, S. Nagata, K. Matsumoto, K. Takayama, Y. Oda: The joint Meeting of Hokkaido Secs. of ECSJ, SFSJ and JSCE, Sapporo, Jan, 2003.

Synthesis of β-SiC fine particles with high specific surface areas; T. Kinomura, H. Habazaki, H. Konno, M. Aramata: The Winter Joint Meeting of Hokkaido Secs. of Chem. Soc. Jpn. and Jpn. Soc. Anal. Chem., Sapporo, Feb., 2003.

Preparation of carbon nanorods using porous anodic alumina templates; S. Sato, H. Habazaki, H. Konno: The Winter Joint Meeting of Hokkaido Secs. of Chem. Soc. Jpn. and Jpn. Soc. Anal. Chem., Sapporo, Feb., 2003.

Observation of initial growth of chromate conversion coating on aluminium using low-voltage, high-resolution SEM; K. Shimizu, H. Fujitani, H. Habazaki, 107th Meeting of SFSJ, Tokyo, Mar., 2003.

Formation and dielectric properties of crystalline anodic films formed on Zr-Ti alloys; H. Habazaki, M. Uozumi, H. Konno, K. Shimizu, K. Asami, S. Nagata, K. Matsumoto, K. Takayama, Y. Oda: 107th Meeting of SFSJ, Tokyo, Mar., 2003.

Preparation of nanocarbons using porous anodic alumina templates; S. Sato, H. Habazaki, H. Konno: 107th Meeting of SFSJ, Tokyo, Mar., 2003.

Effect of alloying elements on dielectric properties of anodic films on niobium alloys; T. Matsuo, H. Habazaki, H. Konno, K. Shimizu, K. Asami, S. Nagata, K. Matsumoto, K. Takayama, Y. Oda: 107th Meeting of SFSJ, Tokyo, Mar., 2003.

Cross-sectional observation of anodic films on aluminium using low-voltage, high-resolution SEM; K. Shimizu, H. Fujitani, H. Habazaki, 107th Meeting of SFSJ, Tokyo, Mar., 2003.

Observation of initial growth of porous anodic alumina using low-voltage, high-resolution SEM; K. Shimizu, H. Fujitani, H. Habazaki, 107th Meeting of SFSJ, Tokyo, Mar., 2003.

Formation and dielectric properties of anodic films formed on Nb-Si alloys; H. Habazaki, T. Matsuo, H. Konno, K. Shimizu, K. Asami, S. Nagata, K. Matsumoto,

K. Takayama, Y. Oda: 70th Meeting of ECSJ, Tokyo, Apr., 2003.

Deposition of MnO₂ by microbiological oxidation of dissolved Mn(II) ions and effect of carbon fiber; H. Konno, M. Endoh, and K. Sasaki: 70th Meeting of ECSJ, Tokyo, Apr., 2003.

Influence of alloying elements on formation and dielectric properties of anodic oxide films on niobium; H. Habazaki, T. Matsuo, H. Konno, K. Shimizu, K. Asami, S. Nagata, K. Matsumoto, K. Takayama, Y. Oda: 62th ARS Meeting, Tokyo, April, 2003.

Formation of carbon nano-materials by liquid phase carbonization using Al porous anodic oxide films as templates; H. Konno, S. Sato, H. Habazaki, M. Inagaki: 265th Meeting of JSPS 117 Committee, Tokyo, Apr., 2003.

Mobilities of metallic foreign species in anodic alumina, H. Habazaki, H. Konno, K. Shimizu, P. Skeldon, G.E. Thompson and G.C. Wood, 3rd Int. Symp. Aluminium Surface Science and Technology, Bonn, May, 2003.

Plasma electrolytic oxidation of light metals; A. Berkani, P. Skeldon, G.E. Thompson, H. Habazaki, K. Shimizu, K. Stevens: 3rd Int. Symp. Aluminium Surface Science and Technology, Bonn, May, 2003.

Corrosion potentials of aluminium alloys: effects of alloying elements; S. Garcia-Vergara, F. Colin, Y. Liu, P. Skeldon, G.E. Thompson, H. Habazaki, K. Shimizu: 3rd Int. Symp. Aluminium Surface Science and Technology, Bonn, May, 2003.

Medium energy ion scattering studies of filmed aluminium alloys; P. Bailey, T.C.Q. Noakes, S. R. Garcia-Vergara, E.V. Koroleva, Y. Liu, P. Skeldon, G.E. Thompson, H. Habazaki, K. Shimizu: 3rd Int. Symp. Aluminium Surface Science and Technology, Bonn, May, 2003.

Influence of alloying elements on formation and electric properties of anodic oxide films on niobium; H. Habazaki, T. Matsuo, H. Konno, K. Shimizu, S. Nagata, K. Matsumoto, K. Takayama and Y. Oda: 2003 Int. Conf. Advanced Capacitors, Kyoto, May 2003.

Breakdown of Anodic Films on Titanium and its Suppression by Alloying;

H.Habazaki, M.Uozumi, H.Konno, K.Shimizu, P.Skeldon and G.E.Thompson: Int. Symp. Corrosion Science in the 21st Centry, Manchester, July 2003.

Promoting Effect of Carbon Fiber on the Biological Oxidation of Dissolved Mn(II) Ions in Water; H. Konno, M. Endoh, and K. Sasaki: CARBON2003, Oviedo, Spain, July 2003.

Exfoliated Graphite Utilized for Synthesizing Nanoparticles of Metal Carbides; H. Konno, T. Kinomura, D. Abe, H. Habazaki, M. Aramata: CARBON2003, Oviedo, Spain, July 2003.

Carbonization of Kenaf to Prepare Activated Carbon; M. Inagaki, T. Katakura, T. Nishikawa, H. Konno, E. Morozumi: CARBON2003, Oviedo, Spain, July 2003.

Synthesis of B_4C microcrystals: A. Sudo, H. Habazaki, H. Konno: The Summer Joint Meeting of Hokkaido Secs. of Chem. Soc. Jpn. and Jpn. Soc. Anal. Chem., Kitami, July, 2003.

Improvement of dielectric properties of anodic niobia by alloying of niobium; T. Matsuo, H. Habazaki, H. Konno, K. Shimizu, S. Nagata, K. Matsumoto, K. Takayama and Y. Oda: The Summer Joint Meeting of Hokkaido Secs. of Chem. Soc. Jpn. and Jpn. Soc. Anal. Chem., Kitami, July, 2003.

Synthesis of ZrC fine particles using zirconium alkoxide and exfoliated graphite; D. Abe, H. Habazaki, H. Konno: The Summer Joint Meeting of Hokkaido Secs. of Chem. Soc. Jpn. and Jpn. Soc. Anal. Chem., Kitami, July, 2003.

Synthesis of Fine Particles of Metal Carbides Utilizing Exfoliated Graphite; H. Konno, T. Kinomura, D. Abe, H. Habazaki, M. Aramata: 266th Meeting of JSPS 117 Committee, Tokyo, July, 2003.

Formation of anodic oxide films on Ti-W alloys, M. Uozumi, H. Habazaki, H. Konno, K. Shimizu, S. Nagata, K. Matsumoto, K. Takayama and Y. Oda: The Fall Meeting of ECSJ, Sapporo, Sep., 2003.

Synthesis of carbonaceous materials utilizing exfoliated graphite; H. Konno: CPC Association, Tokyo, Oct., 2003.

Preparation and characterization of carbon nano- and micro-fibers using porous

templates; S. Sato, H. Habazaki, H. Konno, M. Inagaki: 30th Ann. Meeting of the Carbon Soc. of Jpn, Chiba, Dec., 2003.

Synthesis of TiC, ZrC and (Ti,Zr)C particles from exfoliated graphite and metal alkoxides; D. Abe, H. Habazaki, H. Konno: 30th Ann. Meeting of the Carbon Soc. of Jpn., Chiba, Dec., 2003.

LABORATORY FOR CHARACTERIZATION AND ANALYTICAL CHEMISTRY OF CARBONACEOUS RESOURCES

Prof. Dr. K. Kurokawa
Tel +81-11-706-7572, Fax +81-11-706-7119
E-mail: kurokawa@eng.hokudai.ac.jp
Res. Assoc. Dr. M. Satou
Tel +81-11-706-6846, Fax +81-11-706-7119
E-mail: satou@carbon.caret.eng.hokudai.ac.jp

Researcher

Dr. Wu Yingna

Students

J. Kuchino, S. Matsushita, S. Nishizawa, N. Takada, T. Nakagiri, S. Abe, and S. Tsubouchi, S. Jinno

Equipments

Spark Plasma Sintering Equipment
Ultra-High Vacuum Furnace with Mass Spectrometer
Oxidation Test Equipment with Thermobalance and Ultra-High Temperature
Furnace
Optical Microscope with High Temperature Furnace

Research work at "Laboratory for Characterization and Analytical Chemistry of Carbonaceous Resources", which will be renamed "Laboratory of High Temperature Materials" in 2004, directs toward 1) high temperature oxidation of metals and intermetallics, 2) interface reactions between metals and silicides, 3) sintering and synthesis of composites, 4) .Silicide coating on metals.

Current topics on research are in the following:

(1) Sintering behavior of ZrO₂-based oxide composites

Sintering behavior and structures of ZrO₂-Al₂O₃, ZrO₂-Y₂O₃, and ZrO₂-La₂O₃ are being investigated. The aim is to explore optimum foreign oxide for suppression of densification of ZrO₂ coatings on metals. The results demonstrated

that the addition of La₂O₃ to ZrO₂ was most effective to suppress densification of ZrO₂ at high temperatures.

(2) Oxidation behavior of metal disilicides.

In order to clarify the oxidation process of metal disilicides, high-temperature oxidation tests are being done. In particular, the requisite vapor pressure of metal oxide for the formation of a SiO₂ scale was clarified from the observation of the oxide scales formed on Mo, V, Re and W disilicides.

(3) Effect of B-addition on oxidation of metal disilicides

The effect of B-addition on oxidation of CrSi₂ and NbSi₂ are being investigated. The results demonstrated that the addition of B was very effective for the improvement of the oxidation resistance of the metal disilicides.

(4) TEM observation of oxide scales formed on MoSi₂

Microstructures of oxide scales formed on MoSi₂ in the temperature range of 773 to 1773 K are being observed. Based on the results, the mechanism of accelerated oxidation of MoSi₂ was proposed. In addition, the transition process from accelerated oxidation to passive oxidation was clarified.

(5) Silicide coatings

CrSi₂ and NiSi₂ coatings on a carbon steel using air plasma spraying were performed. Oxidation resistance of the coatings was investigated. In addition, interfacial reaction between coatings and substrate during oxidation at high temperatures was also discussed.

(6) Evaporation behavior of Cr₂O₃ and SiO₂ in H₂O-containing atmospheres

To clarify the degradation mechanism of Cr_2O_3 and SiO_2 scales in H_2O -containing atmospheres, evaporation behavior of sintered Cr_2O_3 and fused SiO_2 in $(N_2-3\%O_2)-XH_2O$ atmospheres is being investigated. The evaporation rates and structural change were clarified.

(7) High temperature oxidation of steels in H₂O-containing atmospheres

In order to clarify the effect of H_2O vapor on oxidation behavior of steels in a hot rolling process, oxidation tests at 1473 K in $(N_2-3\%O_2)-XH_2O$ atmospheres are being done. The results showed that spalling of oxide scale during cooling is liabke to occur in the $(Fe_3O_4+FeO)/FeO$ interface.

Other activities:

Dr. Wu Yingna from China joined this laboratory as a post-doctral fellow in August. Her work in this laboratory is "Silicide coatings on steel".

In July, Prof. Kurokawa attended the International Workshop on Designing of Interfacial Structures in Advanced materials and Their Joints (DIS'03) in Wien, Austria, and presented a paper entitled "TEM observation of SiO₂ scales formed on MoSi₂", and he visited to Prof. Schuster at University of Wien to discuss about advanced materials.

Presentations

Degradation of Protective Oxide Scales in H₂O-Containing Atmospheres –Degradation Mechanism of Cr₂O₃ Scale-, K. Kurokawa, A. Yamauchi, and H. Takahashi: The 139th Symposium on Corrosion and Protection, Hachioji, Jan., 2003.

Temperature Dependence of High-Temperature Oxidation Behavior of NbSi₂, S. Matsushita, K. Kurokawa, H. Takahashi: The Winter Joint Meeting of The Hokkaido Secs. of Jpn. Inst. Metals and Iron and Steel Inst. Jpn., Muroran, Jan., 2003.

Concentration and Distribution of Hydrogen in Cr_2O_3 Scale Formed in H_2O -Containing Atmospheres, A. Yamauchi, K. Kurokawa, H. Takahashi, Y. Yamauchi, Y. Hirohata, and T. Hino: The 132th Annual Meeting of Jpn. Inst. Metals, Chiba, Mar., 2003.

High-Temperature Oxidation Behavior of NbSi₂, S. Matsushita, K. Kurokawa, H. Takahashi: ibid.

Structure and Growth Behavior of Oxide Scale Formed on CrSi₂, N. Takada and K. Kurokawa: The Summer Joint Meeting of The Hokkaido Secs. of Jpn. Inst. Metals and Iron and Steel Inst. Jpn., Muroran, July., 2003.

Evaporation and Crystallization of SiO₂ in H₂O-Containing Atmospheres, T. Nakagiri and K. Kurokawa: ibid.

TEM Observation of SiO₂ scales Formed on MoSi₂, J. Kuchino, D. Gotoh, K. Kurokawa, T. Shibayama, and H. Takahashi: International Workshop on Designing of Interfacial Structures in Advanced Materials and Their Joints, Wien, July, 2003.

Structure and Oxidation Resistance of MoSi₂ Synthesized by Spark Plasma Sintering, J. Kuchino, K. Kurokawa, T. Shibayama, and H. Takahashi: The 4th Inter'l Sympo. on Applied Plasma Science, Kyoto, Sep., 2003.

Evaporation Behavior of SiO₂ in N₂-O₂-H₂O Atmospheres, T. Nakagiri and K. Kurokawa: The 133th Annual Meeting of Jpn. Inst. Metals, Sapporo, Oct. 2003.

Current Activities and Presentations

Structures of Oxide Scales Formed on MoSi₂ at Various Temperatures: J. Kuchino, K. Kurokawa, T. Shibayama, and H. Takahashi: ibid.

High-Temperature Oxidation Behavior and Scale Structure of CrSi₂, N. Takada and K. Kurokawa: ibid.

Structure and Spalling of Oxide Scales Formed on Steels at 1473 K in H_2O -Containing Atmospheres, S. Nishizawa and K. Kurokawa: The 146th Annual Meeting of The Iron and Steel Inst. of Jpn., Sapporo, Oct. 2003.

High Temperature Oxidation Behavior of B-NbSi₂, S. Matsushita and K. Kurokawa: The 15th Domestic Sympo. on FGM, Sapporo, Nov., 2003.

DENTAL MATERIALS AND ENGINEERING LABORATORY

Prof. Dr. F. Watari

Tel&Fax:+81-11-706-4251 E-mail:watari@den.hokudai.ac.jp

Assoc. Prof. Dr. M.Uo

Tel&Fax:+81-11-706-4251 E-mail:uo@den.hokudai.ac.jp

Res. Assoc. Dr. S.Ohkawa

Tel&Fax:+81-11-706-4251 E-mail:ohkawa@den.hokudai.ac.jp

Res. Assoc. Dr. T.Akasaka

Tel&Fax:+81-11-706-4251 E-mail:akasaka@den.hokudai.ac.jp Technician Mr.T.Sugawara

Tel&Fax:+81-11-706-4251 E-mail:stoshi@den.hokudai.ac.jp

Foreign Researchers

Rosca Iosif Daniel, Liao Susan

Students

M.K. Yamada, S. Tanaka, K. Tani, Y. Iwasaki, K. Tamura, K. Kondo, N. Kamishima, W. Wang, N. Aoki, H. Sasaki, Y.H. Zhu

Facilities and Capabilities

XSAM: HORIBA XGT-2000V, Scanning X-ray analytical microscope for elemental mapping analysis

AFM: TopoMetrix TMX2000 Explorer, AFM for dry and wet specimens

NSOM: TopoMetrix Aurora, Near field Scanning Optical Microscope

Laser Raman Spectrometer: Dilor Labram, Laser Raman Spectrometer with mapping analysis

ICP: HITACHI P-4010, ICP emission spectrometer for analysis of elements in aquaous solution

FT/IR: Jasco FT/IR-300E, FT/IR spectrometer with microscopic IR measurement

Particle Size Analyzer: Shimadzu SALD-7000, Particle size distribution analysis with laser scattering

Surface Area Analyzer: Shumadzu, Surface area analysis with gas absorption/desorption

Universal Testing Machine: INSTRON MODEL 4204, Testing for mechanical properties of materials

Laser Welder: ATJ TLL7000, Nd-YAG pulse laser welder with computer controlled x-v stage

Cold Isostatic Press: Hiikari Koatsu Kiki (10000atm type and 20000atm

type):Kobelco, Large volume isostatic press (4000atm)

Vickers Hardness Tester: Shimadzu

Acoustic Emission: Physical Acoustic Corporation

Thermal Gravitometry and Differential Thermal Analysis(TG/DTA):

Rigaku Denki

Diamond Cutter: Buehler and Struers diamond cutter

The research activities cover (1)the development, evaluation and application of dental and biomedical materials, (2)the development of methods and equipments for fabrication of materials and prostheses and (3)the measurement of properties. These are concerned with mechanical, thermal properties, corrosion, surface treatment, biocompatibility, bioreactivity, estheticity and various methods of imaging and microanalyses. Many researches are related to dental, biological and engineering fields and performed in collaboration with clinical departments including Removable Prosthetic Dentistry(Prof.Takao KAWASAKI), Orthodontics(Prof.Junnichiro IIDA), Operative Dentistry (Prof.Hidehiko SANO), Oral and Maxillofacial Surgery(Prof.Yasunori TOTSUKA), Crown and Bridge Prosthodontics(Prof.Noboru OHATA) and Protective Dentistry(Prof.Manabu MORITA).

Current topics on research are as follows;

(1) Biocompatibility and biomedical application of carbon nanotubes(CNT) and other fine particles

Biocompatibility and cytotoxicity of carbon nanotubes(CNT), carbon nanofibers(CNF), fullerene and other nano materials were investigated. Various type of CNT including single and muti-wall CNTs(SWCNT, MWCNT) and CNF were used with the aim of the biomedical application and the pretreatment method of purification, solubilization, dispersion, surface modification were developed. Biochemical cell functional test of cell survival rate, LDH activity, emission of oxygen radicals and cytokines IL-1 β , IL-8, TNF- α , M-CSF and implantation test in soft tissue was done and bioreaction was evaluated. With the decrease of particle size the cytotoxicity originated from the physical size effect was pronounced especially below 10 μ m. Maany interesting properties advantageous to buomedical application such as affinity for adhesion of cells, proteins, saccharides;

precipitation of apatite in artificial salivary fluid and strong binding of psuedopodium grown into the agglomeration of CNTs as scaffold, Applications of the monotubes as delivery system of DNA, protein, saccharic tips and the sintered bulk as implant materials are also developed.

(2) Development of functionally graded dental implant

The dental implant with the structure of functionally graded materials (FGM) has been fabricated to satisfy different properties. The typical example is such that the composition changes from the biocompatible metal, Ti, at one end, increasing the content of ceramics, hydroxyapatite (HAP), principal component of bone and teeth, toward 100% HAP at the other end. This can control the functions of mechanical properties and biocompatibility, optimize them, depending on the necessity of each part of implant, without the abrupt change by the formation of discrete boundary. The effect of FGM structure Ti/HAP, Ti/Co on tissue response is investigated by the animal implantation test into rats and rabbits. The tissue reaction and new bone formation around the implant to the gradient composition is evaluated by both the conventional method using an optical microscope with stained specimens and by elemental mapping and other imaging methods using microprobe analysis(EPMA) and X-ray scanning analytical microscope(XSAM) with unstained specimens.

(3) Biological application of carbon nanotubes

Modification and immobilization of various functional molecules on carbon nanotubes (CNTs) by covalent and non-covalent methods were done. Multi-walled carbon nanotubes (MWNTs) coated with a carbohydrate-carrying polymer can be easily prepared by a non-covalent method via hydrophobic interactions. Fluorescence observation by confocal laser scanning microscopy showed that dense localization of the carbohydrate polymer was uniform along the needle shape of MWNT. The carbohydrate coated MWNT was found to acquire a selective binding affinity to the corresponding lectin without a nonspecific interaction. On the other hand, a bare MWNT interacted nonspecifically with lectins. These results showed that a MWNT coated with a carbohydrate-carrying polymer has the biological recognition signals. Modification of a CNT with various carbohydrate chains will be a useful protocol for molecular designs of biomaterials, nano-architecture, and biosensors.

(4) Development of FRP esthetic orthodontic wire

To realize the esthetic, transparent orthodontic wire the FRP wires of the diameter 0.5mm with the multiple fiber structure has been fabricated by either

drawing of fiber-polymer complex at 250C or photopolymerization method. Biocompatible CaO-P₂O₅-SiO₂-Al₂O₃ (CPSA) glass fibers of 8-20µm in diameter are oriented unidimensionally to the longitudinal direction in polymer matrix of PMMA, UDMA or bis-GMA. The improvement has been done to obtain the adequate flexural strength and higher torque. FRP wire shows the sufficient flexural strength and a very good elastic recovery. The dependence of Young's modulus and flexural stress on fiber fraction obeys very well the rule of mixture. This FRP wire can cover the range of the strength corresponding to the conventional metal orthodontic wires from Ni-Ti used in the initial stage of orthodontic treatments to Co-Cr used in the last stage by changing the volume ratio of glass fibers with the same external diameter. FRP wire can satisfy both mechanical properties and estheticity, which is not possible for the conventional metal wire.

(5) Cytotoxicity due to ions and fine particles of Ti and other metals in vivo and in vitro:

The removal of Ti plates for fixing jaw bone in 6 months after operation often reveals the slightly dark colored tissue in the circumferential soft tissue. The observation and analysis by optical microscopy, electron microscopy and XSAM revealed that the colored tissue contains the abraded fine particles of Ti, probably produced during plate fixation in operation.

The animal experiments to implant various sizes of Ti particles of 1-100 μ m and macroscopic cylindrical Ti implant in μ m order for 3 days to 8 months showed that the macroscopic size of Ti was encircled with fibrous connective tissue layer from early stage and there was no inflammation. As the size of particle becomes smaller, many phagocytic cells appear with fibrous connective tissue layer inside the particle inserted region and tissue showed inflammation. It takes more time to encircle the particle-contained tissue region and heal inflammation. For 1-3 μ m the inserted region is never encircled with fibrous connective tissue layer and inflammation continues.

The in vitro cell functional tests on cell survial rate, LDH(Lactate Hydrogenase CII) protein released at the breakdown of cell membrane and superoxided anion(O^2) sing human neutrophils showed that Ni solution has he cell disruption effect. The deformed and disrupted morphology of neutrophils was confirmed by SEM observation. Whilst Ti and V solution showed the increase of superoxide anion and negligible change in the others, which suggests the cell stimulation effect. SEM observation confirmed that neutrophis are inflated with more complicated polyacicular morphology. One of the marking cytokines released at phagocytization, TNF- α , was not detected in any solution of Ni, V, Ti, the

simulated body fluid(Hank's solution) mixed with 10mm paricles of Ti and with submicron size Ni particles. TNF- α was found only in the 1-3 μ m Ti particle mixed Hank's solution, which suggests that particles were phagocytized. SEM observation and EDS elemental analysis confirmed the phagocytosis of Ti particles by neutrophils.

The difference of cell reaction to 1-3 μ m and 10 μ m Ti particles suggests that the particles(1-3 μ m) smaller than cell size(about 5 μ m in neutrophils) induces cytotoxicity as a result of phagocytosis, while for particles larger than cell size(10 μ m) phagocytosis is not possible, resulting in the less clear cytotoxicity effect.

The study shows the cytotoxicity originating from physical size effect of particles other than biochemical toxicity effect, which is significant for the cases where the fine particles are produced during abrasion by long term usage of moving parts in the artificial bone joint.

(6) In situ observation of etching process of human teeth in acid agent by atomic force microscopy

Composite resin with fillers of ceramic powders in polymer matrix has estheticity similar to natural teeth color and is widely used for treatments of caries in incisal teeth. Physical-mechanical anchoring effect plays an important part in binding force between teeth and composite resin. The pretreatment to make etching of teeth is generally done using acid agents for enhancement of binding. SEM is usually used for the evaluation of etching effect. It can observe, however, only the result after a certain etching time. To observe the sequence of etching process it is necessary to prepare the series of specimens treated with different etching time. Atomic force microscope is applied for the in-situ observation of etching process of human enamel and dentin in acid agents. The chronological change of surface morphology can be successively observed and quantitative analysis is done for different etching conditions.

(7) Fabrication of composite resin prostheses by laser lithography:

Laser lithography, one of the CAD/CAM systems to fabricate the polymer models by piling up the thin slices, which are photo-polymerized by scanning laser beam originally on the shallow depth of liquid epoxy monomer, was applied for the fabrication of dental prosthoses of photo-curing composite resin composed of silica fillers in the matrix of high strength UDMA resin. The full dental crown could be fabricated using the shape data pre-designed by computer with high accuracy due to the smaller polymmerization shrinkage than by conventional methods. Then the functionally graded dental core and post with gradually changing filler content

from 70 to 0% from the head of core abutment toward the apex of post was successfully fabricated. The stress concentration at the pulp root inserted with the conventional dental post has often caused the fracture in the surrounding dentin by impact force on the tooth crown. The stress relaxation effect by application of the functionally graded dental post was confirmed by simulation using the photoelastic method and finite element method(FEM).

(8) Radiation effects on polymer resin:

Radiation effects by C+ion, γ -ray from Co₆₀ and electrons on one of the main matrix polymer UDMA(urethane dimethacrylate) for dental composite resin were investigated with various mechanical tests and spectroscopies. C⁺ion radiation induced the large change in the structure sensitive properties of mechanical properties, Vickers hardness, flexural strength, abrasion resistance and little change in the non-structure sensitive properties of spectroscopies, FT-IR, Raman scattering, Fluorescence, NMR and thermal expansion coefficient. The results suggest that the mechanism of radiation effect is mostly due to the physical structure change such as lattice defects of vacancies, interstitials, depleted zone rather than the chemical effect of cross-linking by further progress of polymmerization of residual monomers.

(9) Evaluation of biocompatibility of refractory metals and their application

Refractory metals of IVA group(Ti, Zr, Hf), VA group(V, Nb, Ta) and VIIA group(Re) are investigated in their biocompatibility and other bioreactivities. Animal implantation tests show that the fraction of direct contact of newly formed bone to implant material without intervening of fibrous connective tissue at the interface and the amount of new bone vary depending on materials. The composites of these refractory metals are also made and the comparison and the composite effect is investigated.

(10) Surface treatment of dental and biomedical materials with sol-gel method Biocompatibility and adhesivity to tissue is important for dental materials. Various dental metals were coated by amorphous silica gels with sol-gel method. In some cases, biocompatibility were improved.

(11) Tissues and dental materials observation by XSAM

The scanning X-ray analytical microscope (XSAM) was applied for the analysis of the soft tissue of rat in which various metals including Fe, Cu, SUS, V, Co, Ni were implanted. The dissolution of implanted metals and inflammation of tissues were observed by elemental mapping image obtained by XSAM.

(12) Bonding property and cytotoxicity of dental zirconia ceramics (YPSZ)

Yttria partially stabilized zirconia (YPSZ) ceramic is suitable for dental and medical use because of it's high fracture toughness and chemical durability. The bonding properties of dental zirconia with various luting cements and surface treatments are investigating. The cytotoxicity dental zirconia ceramics compared to other dental ceramics was also evaluated.

(13) Abrasion-resistant implant made of refractory metal nitrides and carbides

Surface-nitrided titanium(Ti(-N)) showed high corrosion resistance and nearly equivalent biocompatibility with Ti in soft and hard tissue in animal implantation test. Surface durability was evaluated by three static and dynamic mechanical tests; Vickers hardness test, Martens scratch test and for more practical viewpoint newly developed abrasion test using ultrasonic dental scaler which is used to remove calculus on teeth in dental clinics. Vickers hardness of Ti(-N) was 1300, ten times larger than Ti. Martens scratch test showed that the bonding of nitrided layer with 2^µm thickness is coherent to matrix Ti and enough strong. Abraded volume by ultrasonic scaler was increased with the load in Ti, while no trace was formed in Ti-(N), instead stainless tip of scaler was abraded. The test showed that abrasion would be negligibly small under the practical conditions of the load 50g in clinics. Ti-(N) with biocompatibility and surface abrasion resistance would be suitable as abrasion-resistant implant materials for the application to the artificial joint of implant and abuttment part of dental implant.

(14) Development of visible-light responsible photocatalysis and its application

The current photocatalysis of anatase TiO₂ mostly works only by ultraviolet light. To make applicable for medical use it is necessary to develop the visible-light reactive photocatalysis. Visible light sesitization was obtained by surface modification with caions of Au, Ag, Cu, Pt, Pd. Depigmentation with visible light around 470nm which is used for photopolymerization of composite resin restoration in dental clinics could be done with the Ag activated TiO₂ in contrast to very little effect in an untreated TiO₂. Antibacterial effect was also confirmed to streptococcus mutans, one of the most popular bacteria for caries. The application to bleaching of pigmented teeth was developed.

(15) Development of discrimination method of resin-restored teeth

In the health checkup in school mass of patients must be checked in the limited time. Due to the recent development of estheticity of composite resin it is now very difficult to recognize the resin-restored teeth and discern resin part from

natural teeth. Total reflection spectroscopy and fluorescence spectroscopy were measured and images were taken with reflected light and fluorescence light using the filters to select the appropriate wave length. In the long wave length region for more than 600nm the reflectivity of teeth is higher than that of composite resin. The image formed with filtered light, however, did not show the contrast enough to discern the resin part from tooth. For less than 400nm both teeth and resin showed the fluorescence emission with high and comparable intensity. For the light of 430-450nm teeth emitted higher fluorescence and the relative difference is larger. The images formed with fluorescence light for more than 500nm emitted by 430-450nm light excitation showed the easily recognized contrast to discriminate resin from tooth.

(16) Microparticles of biodegradable polymers with controlled structure for drug delivery system

Single and double emulsification solvent evaporation method is extensively used for more than two decades for the encapsulation of various substances form simple pharmaceutical products to proteins and DNA.

Particle formation mechanism is crucial for size distribution, and morphology, which in turn determine the delivery system behavior during encapsulation and release.

In order to identify and quantify the main influence parameters that determine the microparticle performance as drug delivery system, the mechanism of particle formation of biodegradable polyesters: poly(DL-lactide co glycolide) and poly(L-Lactide), was investigated in their single and double emulsion formulation.

In situ optical microscopic investigations showed that the microparticles are formed by accelerated solvent elimination due to the combined effects of high solvent volatility and polymer precipitation. The fast shrinkage that accompanies the solvent elimination has important influence on the particle morphology. Scanning electron microscopy and laser diffractometry evidenced the presence of a thin nanoparticulate layer on the microparticles surface. This layer is formed during the solvent elimination by the shrinkage-induced fragmentation of the precipitating polymer. It is reasonable to believe that the encapsulated substance will accumulate in this layer contributing to the initial burst release.

The inner aqueous phase in the double emulsion formulations has important influence on the mechanism of particle formation. In this case microparticles with different structures are generated. The proportions of microparticles with different structure are determined mainly by the stirring rate and the polymer concentration.

During solvent elimination the droplets of inner aqueous phase coalesce under the precipitating polymer pressure. Due to the incompressibility of the inner aqueous phase, the polymer wall often breaks resulting in holes through which the inner aqueous phase is partly expulsed. Furthermore, after particle hardening the holes will contribute to the encapsulated substances leakage through partitioning with the external aqueous phase, and to the initial burst release.

Other activities:

Prof.WATARI promoted the 15th Symposium of the Functionally Graded Materials (FGM2003 in Sapporo) at Hokusei Gakuen University on Nov.20-21. More than 70 presentations including 4 special lectures were performed in the field from space engineering to biotechnology on "functional materials and their variations" in the symposium. Proceedings will be published in 2004.

The three-year research project in nanomedicine under the subject of "Tissue Reaction and Biomedical Application of Nanotubes, Nanoparticles and Microparticles" has been continued for the second year as Research on Advanced Medical Technology under Health and Laybour Sciences Research Grants from the Ministry of Health, Laybour and Welfare of Japan. The project team is constitute of Leader: Prof.Fumio WATARI, Assigned Researchers: Associate Prof.Mamoru OMORI (Institute for Materials Research, Tohoku University), Prof.Kazuyuki Tohoku University). TOHJI(Department of Geoscience and Technology, Prof. Toshiyuki HASHIDA (Fracture Research Institute, Graduate School of Engineering, Tohoku University), Prof. Yasunori TOTSUKA(Graduate School of Dental Medicine, Hokkaido University), Prof. Takao KAWASAKI (Graduate School of Dental Medicine, Hokkaido University), Prof.Kohichi HANEDA(Department of Information Technology and Electronics, Ishinomaki Senshu University), Prof.Fumio NOGATA(Department of Human and Information Systems, Tohoku University) and other Collaborating Researchers. The second winter meeting was held at Gifu Kanko Hotel 18rou-bekkan and Gifu Shogai Gakushu Kaikan, Gifu, on Feb.17-18. The third summer meeting was held at Matsushima Taikanso, Matsushima, Miyagi Prefecture, on Sep.9-10. The annual report of the first year research project was published in March.

Prof.CUI Fu-Zhai, Director of Biomaterials Laboratory, Department of Materials Science and Engineering, Tsinghua University, Beijing, China, was invited for the collaboration research on nano-biomaterials and visited Tokyo and Sapporo on Feb.3-16.

Dr.SUSAN Liao of Tsinghua University, Beijing, China joined, in November as the postdoctoral researcher of the Japan Society for Promotion of Science (JSPS) and started the collaboration research on the development of nanohydroxyapatite-collagen composite as bone substitute biomaterials for two year period.

Dr.ROSCA Iosif Daniel of University Polytechnica Bucharest, Bucharest, Romania, has continued the research on the development of polymer biomaterials of two year period as the invited researcher of the Japan Society for Promotion of Science (JSPS).

Prof.WATARI attended and made presentation in the Honorary Meeting for Profs.VAN LANDUYT and S.AMELINCKX of Belgian Society of Electron Microscopy, held at University of Antwerp(RUCA), Antwerp, Belgium on May 23.

Prof.WATARI, Assoc.Prof.UO, Dr.OHKAWA, Mr.K.TAMURA and Mr.TANI attended and made presentations in the 81st General Session of Int.Assoc.Dental Research (IADR) held at Goteborg, Sweden, on June 25-28. Prof.WATARI and Assoc.Prof.UO visited Prof.Emerita Maud Bergman (Dental Materials, University of Umea, SWEDEN) and Prof.Emeritus Bo BERGMAN (Prosthodontics) at Sundsvall and discussed on side effects and progress of dental materials.

Prof.WATARI and Mr.K.TAMURA attended the 16th Int.Symp.on Ceramics in Medicine at Porto, Portugal on Nov.6-9 and gave prsentations.

The international collaborations are continued with Institute of Dental Materials Science, Umea University, SWEDEN (Emerita Prof. Maud BERGMAN) on application of Ti, ZrO2, amalgum for dentistry, and research on side effects, with Department of Dental Materials, Chonbuk National University, KOREA (Prof.Tae-Sung BAE) on evaluation of mechanical properties of laser-welded Ti, dental porcelain, with Institute for Materials Science, Dresden Institute of Technology, GERMANY (Prof.W.POMPE) on the biocompatibility evaluation and application of collagen-hydroxyapatite composites and with Biomaterials Laboratory, Department of Materials Science and Engineering, Tsinghua University, CHINA (Prof.FZ CUI) on the development and biomedical application of nanobiomaterials.

The collaboration with Laboratory for Advanced Materials, Institute for Materials Research, Tohoku University (Assoc.Prof.Mamoru OMORI) is undergoing on the fabrication of new biomaterials including bulk carbon nanotubes and functionally graded materials by applying a spark plasma system(SPS) as a method to enhance sintering. The development of FRP esthetic orthodontic wire has continuously been done with Department of Industrial Chemistry, Chiba Institute of Technology(Associate Prof.Masahiro KOBAYASHI).

Presentations

The application of X-ray scanning analytical microscope (XSAM) for the analysis of biological tissues; M.Uo, F.Watari, T.Kohgo; The 81st general Session of the International Association for Dental Research, Göteborg, Sweden, Jun., 2003

Elemental Mapping in the Soft Tissues using X-ray Scanning Analytical Microscope; M.Uo, T.Akasaka; Annual Meeting of the Japanese Society of Microscopy, Jun., Sapporo, 2003

Application of X-ray Scanning Analytical Microscope for the Analysis of Tissue Implanted Metals and Surrounding Tissues; M.Uo, T.Akasaka, R.I.Daniel, F.Watari; 15th Symposium on Functionally Graded Materials, Nov., Sapporo, 2003.

Preparation and application of fluorescent glass filler for composite resin; M.Uo, F.Watari, K.Tani, M.Morita; The 51st Annual Meeting of the Japanese Association for Dental Research (JADR), Osaka, Dec, 2003

Surface Modification of Carbon Nanotubes with Artificial Glycoconjugate Polymers; T. Akasaka, M. Uo, K. Tohji, F. Watari; XXIVth Japanese carbohydrate symposium, Jul., Yokohama, 2003.

Surface modification of dentin by adsorption of carbon nanotube; T.Akasaka, M.Uo, S.Ohkawa, T.Sugawara, F.Watari; The 42th General Session of the Japanese Society for Dental Materials and Devices, Sept. Morioka, 2003.

Carbohydrate Coating of Carbon Nanotubes; T. Akasaka, Y. Sato, K. Tohji, F. Watari; 15th Symposium on Functionally Graded Materials, Nov., Sapporo, 2003.

Surface modification of culture materials by adsorption of carbon nanotube; T. Akasaka, K. Tamura, F. Watari; The 25th annual meeting of the Japanese society for biomaterials, Osaka, Dec, 2003.

Morphological Observation and Spectroscopic Analysis of Teeth Irradiated by Nd:YAG, Er:YAG and CO2 Lasers; M.K. Yamada, M.Uo, S.Ohkawa, T.Akasaka, T.Sugawara and F.Watari; The 41th General Session of the Japanese Society for Dental Materials and Devices, Tokyo, Apr 18-19, 2003

Simultaneous Imaging and Surface Roughness Analysis of Laser-Irradiated Teeth by Using

SEM and CLSM, M.K.Yamada, M.Uo, S.Ohkawa, F.Watari, The 51st Annual Meeting of the Japanese Association for Dental Research (JADR), Osaka, Dec, 2003

Examination of factors affecting on the flexural rupture of FRP orthodontic wire under wet conditions

S.Tanaka, S.Yamagata, M.Uga, N.Suwa, J.Iida M.Uo, S.Ohkawa, T.Sugawara, F.Watari, M.Kibayashi, 41th The Japanese Society of Dental Materials and Devices, Tokyo, Apr. 2003

Application of laser welding for titanium and dental precious alloys; K. Iwasaki, S. Ohkawa, M. Uo, T. Akasaka, T. Sugawara, F. Watari, The Japanese Society of Dental Materials and Devices, Tokyo, Apr., 2003

Laser groove welding for titanium and dental precious alloys; K. Iwasaki, S. Ohkawa, M. Uo, T. Akasaka, T. Sugawara, F. Watari, The Japanese Society of Dental Materials and Devices, Morioka-Iwate, Sept., 2003

Laser welding of titanium with dental precious alloys; K. Iwasaki, S. Ohkawa, M. Uo, T. Akasaka, T. Sugawara, F. Watari, 15th Symposium on Functionally Graded Materials, Sapporo, Nov., 2003

Spectroscopic research for the visible differentiation of tooth from composite resin and porcelain; K. Tani, M. Morita, M. Uo, S. Ohkawa, T. Akasaka. T.Sugawara, F. Watari, The Japanese Society of Dental Materials and Devices, Tokyo, Apr., 2003

Spectroscopic research for the visual differentiation of aesthetic materials in restored tooth; K. Tani, M. Morita, M. Uo, S. Ohkawa, F. Watari, International Association for Dental Research, Goteborg Sweden, Jun., 2003

Evaluation of the injury of cells by nano/micro particles; K.Tamura, N.Takashi, R.I. Daniel, M.UO, F.WATARI, 15th Society for Organ Substitution, Sapporo, Mar., 2003

Pathobiological Response to Carbon-nanotubes and nano particles; K. TAMURA, N.TAKASHI, R.I.Daniel, M.Uo, T.Sugawara, S.Ohkawa, F.Watari, The 41th General Session of the Japanese Society for Dental Materials and Devices, Tokyo, Apr., 2003

Size effect of micro-nano particles on cell functions; K.Tamura, N.Takashi,

F.Watari, Y.Totsuka, The 44th Congress of the Korean Association of Oral and Maxillofacial Surgeons, Korea, Apr., 2003

Size effect of micro-nano particles on cell functions; K.Tamura, N.Takashi, F.Watari, Y. Totsuka, The 1st International Bionano Interface, Tokyo, May, 2003

Size effect of nano/micro particles on cytotoxicity in vivo and in vitro; K.Tamura, N.Takashi, M.Uo, F.Watari, Y.Totsuka, The 81st general Session of the International Association for Dental Research, Goteborg, Sweden, Jun., 2003

Pathobiological response to nano/micro particles; K.Tamura. N.Takashi, R.I.Daniel, M. Uo, F.Watari, The 45th Japanese Association for Oral Biology, Morioka, Sept., 2003

Effect of particles in periodontal ligament cells; K.Tamura, N.Takashi, T.Akasaka, M.Uo, S.Ohkawa, T.Sugawara, Y.Totsuka, F.Watari, The 41th General Session of the Japanese Society for Dental Materials and Devices, Morioka, Sept., 2003

Effects of Micro/ Nano Particle Size on Cell Function and Morphology; K. Tamura, N. Takashi, T. Akasaka, I.D. Rosca, M. Uo, Y. Totsuka, F Watari, The 16th edition of the International Symposium on Ceramics in Medicine, Portugal, Nov., 2003

Pathobiological Response of Carbon nano-tubes and Micro/nano particles; K. Tamura, N. Takashi, T. Akasaka, I.D. Rosca, M. Uo, Y. Totsuka, F Watari, 15th Symposium on Functionally Graded Materials, Sapporo, Nov., 2003

Size-Dependent Proinflammatory Effects of micro/nano Particles on Cells; K.Tamura, R.I.Daniel, Y.Totsuka, F.Watari, The 51th general Session of the Japanese Association for Dental Research, Osaka, Dec., 2003

Cytotoxicity mechanism of micro/nano biomaterial particles; K.Tamura, N.Takashi, T.Akasaka, M.Uo, R.I.Daniel, Y.Totsuka, F.Watari, The 25th Japanese Society for Biomaterials, Osaka, Dec., 2003

Manufacture and evaluation of Ti-HAP complex by dry synthetic method; H.Kondo, A.Yokoyama, T.Kawasaki, M.Uo, S.Ohkawa, T.Sugawara, T.Akasaka, F.Watari; The Japanese Society for Dental Materials and Devices, Sept., 2003

Evaluation of properties and biocompatibility of titanium nitride/apatite

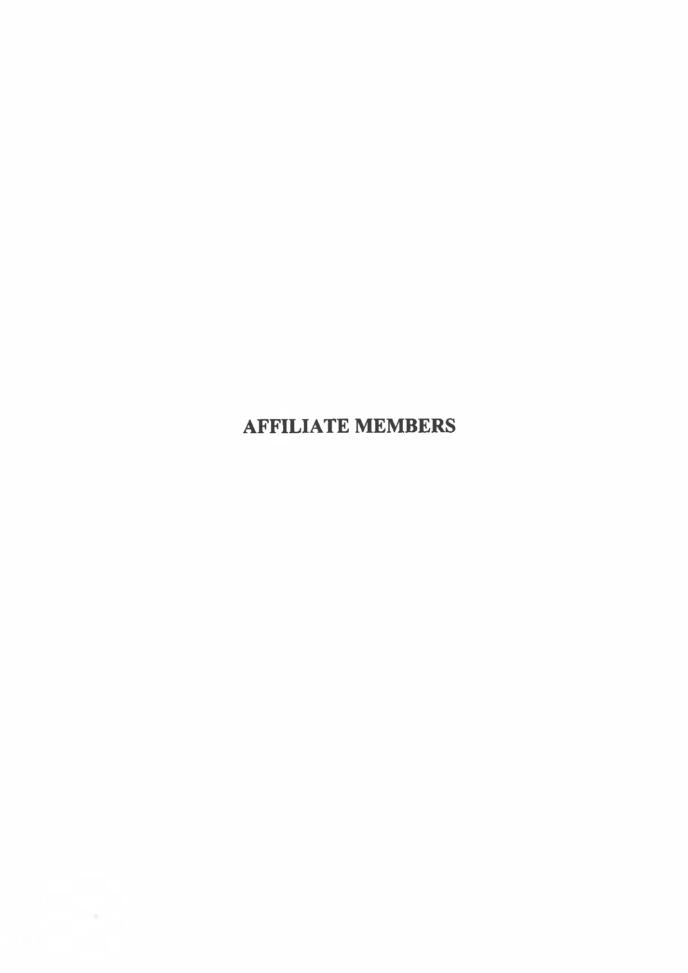
Current Activities and Presentations

functionally graded implants fabricated by spark plasma syntering; H.Kondo, A.Yokoyama, T.Kawasaki, M.Uo, F.Watari; 15th FGM 2003, Sapporo, Nov., 2003

Measurement of penetration of various resin monomers in teeth; N.Kamishima, N.Ohata, M.Uo, F.Watari; The Japan Institute of Metals, Jan., 2003

Measurement of penetration of various resin monomers in teeth; N.Kamishima, N.Sato, N.Ohata, M.Uo, S.Ohkawa, T.Akasaka, T.Sugawara, F.Watari; The Japanese Society for Dental Materials and Devices, Apr., 2003

Comparison of penetration of various resin monomers in dentin N.Kamishima, N.Sato, N.Ohata, M.Uo, S.Ohkawa, T.Akasaka, T.Sugawara, F.Watari; The Japanese Society for Dental Materials and Devices, Sept., 2003



AFFILIATE MEMBERS

Assoc. Prof. Dr. Hiroki Tamura

Tel.: +81-11-706-6741, Fax.: +81-11-706-6740 Email: h-tamura@eng.hokudai.ac.jp

Member of the committee for elucidation and control of corrosion protection of galvanized steels of the Iron and Steel Institute of Japan, and also of the organizing committee of the Ion Exchange Society. Research interests in the preparation and characterization of layered metal oxides and metal oxides in general as corrosion products from metals and as inorganic fine materials.

Presentations

Intercalation Reactions of Layered Manganese Oxide (Birnessite); K. Nakamura, H. Tamura, and S. Kikkawa: The 83rd Spring Meeting of the Japan Chemical Society, Tokyo, Mar., 2003.

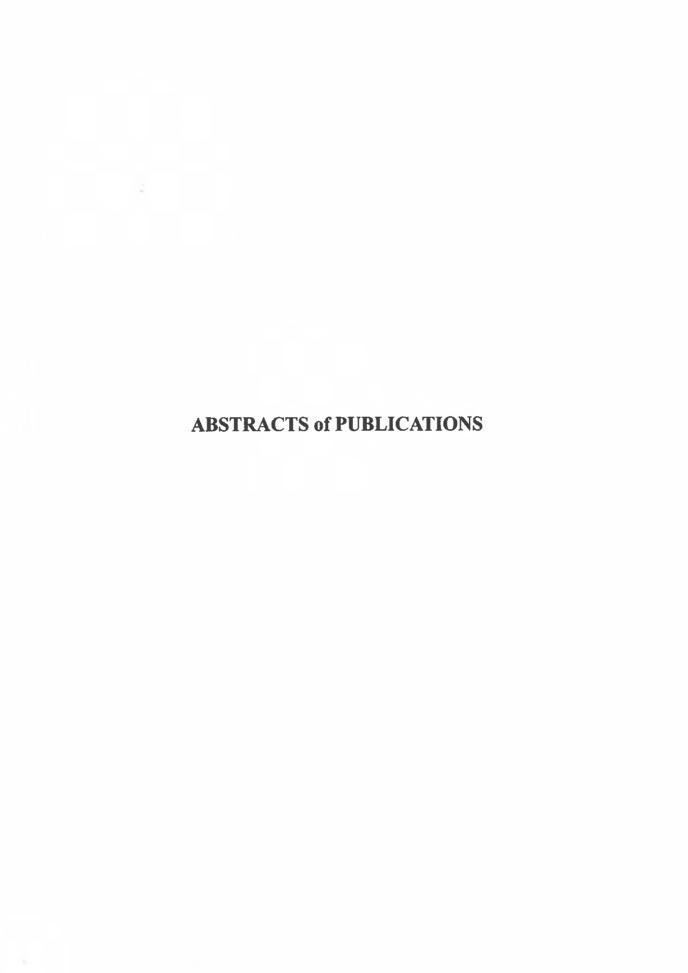
Preparation and Characterization of Layered Manganese Oxide (Birnessite) and Its Intercalation Reactions; Hiroki Tamura, Kyosuke Nakamura, Takashi Takeda, and Shinichi Kikkawa: The 3rd International Conference on Ion Exchange (ICIE'03), Kanazawa, July, 2003.

Synthesis of Hydrotalcite by a Coprecipitation Method and Its Nanohybridization with ATP; J. Chiba, T. Takeda, H. Tamura, and S. Kikkawa: '03 Tohoku and Hokkaido Branch Meeting of Ceramics Society of Japan, Sendai, Aug., 2003.

A Protective Film Component among Corrosion Products on Galvanized Steels Evaluated by Solubility Calculations; H. Tamura: The 146th Autumn Meeting of the Iron and Steel Institute of Japan, Sapporo, Oct., 2003.

Synthesis and Characterization of Hydrotalcite-ATP Intercalates; H. Tamura, J. Chiba, M. Ito, T. Takeda, and S. Kikkawa: The XVth International Symposium on the Reactivity of Solids (ISRS'03), Kyoto, Nov., 2003.

Synthesis of Hydrotalcite-Bio Nanohybrids; J. Chiba, T. Takeda, H. Tamura, and S. Kikkawa: The 15th Functional Gradient Materials Symposium, Sapporo, Nov., 2003.



Polypyrrole - Polymolybdate Composite Film for the Corrosion Protection of Steels

Takahiro Domyo, Mikito Ueda, and Toshiaki Ohtsuka

Zairyo-to-kankyo, 52. 421-427 (2003)

Conductive polymer film of polypyrrole (PPy) doped by polymolybdate (PMo) anions was prepared on mild steels by anodic polymerization for corrosion prevention of the steels. The PPy-PMo conductive film prepared exhibits good adherence to the steel substrate. The mass and thickness of the PPy-PMo film linearly increase with electricity during constant current polymerization at 5 mA cm⁻². The density of the PPy-PMo polymer film was evaluated to be 2.5 g cm⁻³ from the ratio of the mass to thickness. A corrosion test in neutral and acidic 3.5 wt% NaCl solutions was done for the steels covered by the PPy-PMo film. Corrosion of the steels is suppressed by the films: the corrosion rate in the neutral solution decreases by 1/3 compared with that of the bare steel and the rate in the acidic solution by 1/4. The film was gradually reduced during immersion in the solutions with progress of the corrosion reaction of Fe dissolution to Fe²⁺, which is accompanied with the dissolution from PMo in the film to MoO₄²⁻ in the neutral solution, or with pickup of protons and sodium ions in the acidic solution. (Japanese)

Corrosion Products and Adsorbed Water on Copper in Humid Air Containing SO₂

Yuuki Horiguchi, Takeshi Sasaki and Toshiaki Ohtsuka

Proceedings of the 13th Asian-Pacific Corrosion Control Conference, A-23 (2003)

To determine the amount of corrosion products and adsorbed water on copper in humid air containing SO₂, a series of in situ time-resolved IR-RAS spectra was measured. The components of the corrosion products were sulfite and sulfate, and the CuSO₃Cu₂SO₃·2H₂O was the main component of sulfite and CuSO₄ 5H₂O was that of sulfate. The amount of corrosion products slowly increased at the initial stage and next it steeply increased. That of adsorbed water showed nearly the same behavior. In the initial stage the corrosion rate was suppressed by cuprous oxide layer formed during the preparation of test specimens, and owing to the degradation of the layer with acidic layer dissolving SO₂, the corrosion rate became high. The amount of adsorbed water increased with the increase of amount of corrosion products and it is considered that most of adsorbed water existed of SO₂ and relative humidity, and the influence of concentration of SO₂ appeared remarkably in high relative humidity.

In-situ Raman Spectroscopy for Initial Corrosion Process of Zinc-coated Steel

Masaru Matsuda and Toashiaki Ohtsuka

Proceedings of the 13th Asian-Pacific Corrosion Control Conference, P-15 (2003)

It was investigated that the effect of Ni and Al contained in the coating layer on the formation sequence of the corrosion products. Three specimens of pure Zn, Zn-12% Ni and Zn-5% Al coated steels were employed for the zinc coating. The specimen was fixed in the corrosion cell for Raman spectroscopic measurement and the humidified air with RH 84% was introduced into the cell. Before the corrosion experiment, NaCl particles were precipitated by droping 10 ml 3 or 0.03 % NaCl aqueous solution on zinc-coated steel plates and drying in a vacuum desiccator. Surgface analysis by XPS and analysis of corrosion products by X-ray fluorescence spectroscopy were also done. During the exposure in humidified air, aq. ZnCl₂ solution layer was imitial formed and then ZnCl₂[Zn(OH)₂]₄ appeared for all zinc coatings at RH > 75 %. When the coating containing Ni and Al, however, the longer time period to observe the appreciable Raman peaks of aq. ZnCl₂ is required compared with the pure zinc coating. Ni and Al oxide and/or hydroxide on the initial surface may delay the appearance of aq. ZnCl₂ and ZnCl₂[Zn(OH)₂]₄. X-ray fluorescence spectroscopic analysis after 72 h exposure indicated that the corrosion products mainly consisted of Zn components, but Ni and Al components were detected by trace amount.

Corrosion Products of Tin in Humid Air Containing Sulfer Dioxide and Nitrogen Dioxide at Room Temperature

Tekeshi. Sasaki, Ryoji Kanagawa, Toshiaki Ohtsuka, and Kazuma Miura

Corrosion Science, 45, 847-854 (2003)

To obtain a fundamental understanding of the corrosion behavior of tin in corrosive gas environments, in situ infrared reflection absorption spectroscopy measurement were carried out on tin in humid air containing SO₂ and NO₂ at room temperature. A series of time-resolved in situ IR spectra in air of 90 % relative humidity (RH) containing 10-22 ppm SO₂ suggested that the oxide films on tin specimens had a protective effect and that no significant corrosion occurred. The corrosion products in air of 80-90 % RH containing 10-22 ppm NO₂ were SnO₂, SnO, nitrate and hydronitrite. The synergistic effect of SO₂ and 1.8 ppm NO₂ on corrosion of tim was not observed in humid air (RH of 90 %) containing 0.84 ppm SO₂ and 1.8 ppm NO₂.

In-situ Raman Spectroscopy for Corrosion Products Formed on Zinc in Humidified Atmosphere in the Presence of NaCl Precipitate

T. Ohtsuka and M. Matsuda

Corrosion, 59, 407-413 (2003)

The corrosion products of zinc in atmospheric environment in the presence of NaCl particles have been studied by in-situ detection using Raman spectroscopy. Zinc plate with the NaCl precipitate at a density of 0.4 mg cm⁻² was exposed for 3 d or longer in air with a controlled relative humidity (RH).

The corrosion products of zinc can be easily identified by comparison of the in-situ Raman spectra measured during the corrosion process with standard spectra of various zinc compounds. Zinc corrosion largely depends on the RH of the atmosphere in the presence of NaCl precipitate. When the RH is lower than 80 %, the main corrosion product is zinc oxide of ZnO. When the RH is higher than 80%, however, the corrosion products change to aqueous ZnCl2 in the initial stage, and Zn(Cl)₂[Zn(OH)₂]₄ (zinc hydroxy chloride or simonkollite) is formed in the latter stage. From the transient of the corrosion products measured by in-situ Raman spectroscopy, the corrosion process of zinc in the higher RH environment is assumed as the following. The water layer adsorbed from the humidified air with the relatively high RH dissolves NaCl precipitate on zinc surface. The water layer dissolving NaCl then corrodes zinc by electrochemically coupled reactions; Zn → $Zn^{2+} + 2e^-$ and $O_2 + 2H_2O + 4e^- \rightarrow 4OH^-$. As the concentration of ZnCl₂ thus formed in the water layer increases with the proceeding corrosion and reaches saturation, simonkollite begins to precipitate from the concentrated ZnCl₂ solution according to the reaction of $4Zn^{2+} + 4OH^{-} + ZnCl_{2}(aq) \rightarrow ZnCl_{2}[Zn(OH)_{2}]_{4}$.

Structure of Benzotriazole Film on Metals

Takenori Notoya, Toshiaki Ohtsuka, Genta Ando, Masatoshi Satake, Hitoshi Yashiro, and Miki Sato

J. Japan Research Institute for Advanced Copper-base Materials and Technologies, 42, 253-257 (2003)

Bebzotriazole (BTA) is one of the most effective and widely used corrosion inhibitors of copperand its alloys. It has been reported that the inhibitory action of BTA is due to the formation of Cu(I)-BTA polymeric complex filmon the surface of copper in a near-neutral solution. The molecular structure of the surface films formed by BTA on copper and six different metals (silver, zinc, nickel, iron, chromium and gold) were studied bu time-to-flight secondary ion mass spectroscopy (TOF SIMS). TOF SIMS spectra show that the surface film on BTA-treated copper is composed of relatively short Cn(I)-BTA polymers. For copper, positive ion fragments attributed to the Cn(I) complex were $[(Cu^{+})_{n}(C_{6}H_{4}N_{3}^{-})_{n-1}]^{-}$ (n<4) and negative ion fragments were $[(Cu^{+})_{m}(C_{6}H_{4}N_{3}^{-})_{m+1}]^{+}$ (n<3). For silver, positive ion fragments attributed to the silver-BTA complex were $[(Ag^{+})_{n}(C_{6}H_{4}N_{3}^{-})_{n-1}]^{-}$ (n<4) and negative ion fragments were $[(Ag^{+})_{m}(C_{6}H_{4}N_{3}^{-})_{m+1}]^{+}$ (m<2). For zinc, positive ion fragments attributed to zinc-BTA complex were $[(Z_n^{++})_n(C_6H_4N_3^-)_{2n-1}]^-$ (n=1 and 2) and negative ion fragments were $[(Zn^{++})_m(C_6H_4N_3)_{2m+1}]^-$ (m<2). For gold and nickel, positive and negative ion fragments attributed to these metal-BTA complexes were much shorter polymers than those of zinc. Neither positive nor negative ion fragments attributed to a metal-BTA complexes was detected for iron and chromium. The inhibitive actions of the surface films on metals were assessed by means of polarization resistance (R_p) measurements. The ratio of Rp (with BTA on 0.1 N NaCl) to Rp (without BTA) was in the decreasing order as follows: Cu>>Ag>>Zn>Ni, Fe. Thus, BTA is the most effective corrosion inhibitor for copper and the least effective inhibitor for nickel and iron.

(Japanese)

Structure of metal-benzotriazole Films on Copper and Other Metals

T. Notoya, M. Satake, T. Ohtsuka, H. Yashiro, M. sato, T. Yamaguchi, and D. P. Schweinberg

J. Corrosion Science and Engineering, 6, paper C076

The chemical states of benzotriazole (BTA) on copper and six other metals were investigated by measurements of time-of -flight secondary ion mass spectroscopy (ToF SIMS) of BTA-pretreated metals. The results were discussed in terms of the relationshipbetween the degree of polymerization BTA-metak compounds formed and corrosion inhibition efficiency determined by polarization resistance measurements for metaks in a mixed solution of BTA and NaCl. The order of inhibition efficiency corresponded of polarization; the higher degree of polarization, the higher the inhibition efficiency.

In situ IR-RAS investigation of corrosion of tin in air containing H₂O, NO₂ and SO₂ at room temperature

T. Sasaki, R. Kanagawa and T. Ohtsuka

J. Univ. Sci. Tech. Beijing, 10, 35-38(2003)

In order to obtain a fundamental understanding of the corrosion behavior of tin in atmosphere, in situ IR-RAS measurements were performed on tin in humid air containing SO₂ and NO₂ at room temperature. Time-resolved in situ IR spectra in air of 90% RH (relative humidity) containing 10 - 22 ppm SO₂ suggested that the tin oxide layers worked as a protective film and no significant corrosion occurred. The corrosion products in air of 80 - 90% RH containing 10 - 22 ppm NO₂ were SnO₂, SnO, nitrate and hyponitrite. The synergistic effect of SO₂ and NO₂ on corrosion of tin was not observed in air of 90% RH containing 0.84 ppm SO₂ and 1.8 ppm NO₂.

Corrosion Behavior of Titanium-clad Carbon Steel in Weakly Alkaline Solutions

K. Azumi and M. Seo

Corrosion Science, 45 (2003) 413-426

The electrochemical polarization curves and corrosion potentials during long-term immersion of Ti, carbon steel, carbon steel tightened-Ti and Ti clad carbon steel specimens were investigated in bentonite-contacting solution (mixture of sodium sulfate and sodium carbonate solutions), sodium sulfate solution and borate solution adjusted to pH = 9.0 - 9.84. Ti and carbon steel were passivated during immersion in borate solution, while carbon steel was corroded in the solutions containing SO_4^{2-} ions. The immersion potentials of Ti-clad steel and steel-tightened Ti specimens were controlled by the corrosion potential of carbon steel (about 0 V vs. R.H.E. at 298 K). The Ti side of the clad specimen was, therefore, polarized cathodically at this immersion potential, and this caused hydration of and/or hydrogen penetration into the oxide film, resulting in degradation of its barrier property. Furthermore, the cathodic current on the Ti side was partially coupled with the anodic current in the corrosion reaction on the carbon steel side, resulting in acceleration of the overall corrosion rate.

Application of Resistometry to the Study of Metal Corrosion

K. Azumi, K. Iokibe, T. Ueno, M. Seo

J. Surf. Fin. Soc. Jpn., 54 (2003) 224-229

Resistometry has been applied to the corrosion studies of Fe, Ti and Al electrodes in a thin wire form. Dissolution depth of Fe wire in the active potential range during potential sweep was estimated from resistance data and consistent with the value obtained from electric charge. In the passive potential range the dependences of resistance on growth of the passive film and change in space charge layer of the passive film were observed. For Ti and Al electrodes the resistance changes due to anodic oxide growth were observed. In the high voltage range, however, the temperature of specimen raised due to increase in electric energy loss in the oxide film and thus the resistivity increased apparently. For Ti electrodes the growth of hydride layer was monitored using resistometry under the condition of electrochemical hydrogen loading. For Al electrodes the cathodic dissolution under the condition of hydrogen evolution was measured. In the acidic solution the cathodic passivation phenomenon was observed in which deposition layer of Al hydroxide suppressed the cathodic reaction. (Japanese)

Corrosion Behavior of Iron Thin Film in Deaerated Phosphate Solutions by an Electrochemical Quartz Crystal Microbalance

M. Kurosaki and M. Seo

Corros. Sci., 45 (2003) 2597-2607

The corrosion rates of iron thin film in deaerated phosphate solutions were measured by an electrochemical quartz crystal microbalance (EQCM) as a function of solution pH or phosphorus concentration in solutions. The dependences of corrosion rate and corrosion potential on solution pH and phosphorus concentration have suggested that the corrosion mechanism changes in the vicinity of pH 5 and $H_2PO_4^-$ contributes to both anodic dissolution of iron and hydrogen evolution. The corrosion mechanism which contains iron-phosphate-hydroxide complex ion as an adsorbed intermediate was proposed to explain the experimental results.

Initial Stage of Localized Corrosion on Zn - 5 mass% Al Alloy Coated Steels by Pulsed Photon Film Removal Technique

M. Sakairi, K. Itabashi, and H. Takahashi

Proc. of Intern. Symp. on Corrosion Science in the 21st Century, C093 (2003)

A pulsed photon film removal technique, film removal by a focused one pulse of pulsed Nd- YAG laser beam irradiation, has been developed since it enables the oxide film stripping at extremely high rate without any contamination from film removal tools. In the present investigation, Zn, Zn - 5 mass% Al and Zn - 55 mass% Al alloy coated steel specimens covered with protective nitrocellulose film were irradiated with a focused one pulse of pulsed Nd - YAG laser beam at a constant potential in 0.1 kmol / m^3 Na₂B₄O₇ (pH = 9.4) solutions with / without chloride ions to monitor the current transient.

Irradiation with a pulsed laser in solutions causes abrupt removal of the nitrocellulose film on the specimens at the laser-irradiated area. Without chloride ions, oxide films were reformed in the solutions at 1 V. However, in chloride ion containing solutions, localized corrosion of coated layers occurs at high potentials, while film reformation occurs at low potentials. It was also found that chloride ions enhance dissolution of aluminum and zinc at the very initial period after laser irradiation. For long time polarization after laser irradiation in chloride ions containing solutions, corrosion products formed on nitrocellulose film removed area.

Initial Stage of Localized Corrosion of Al - 9 mass% Si Coated Steels After Removal with A Photon Rupture Method in Solutions

M. Sakairi, K. Itabashi, and H. Takahashi

Zairyo-to-Kankyo, 52, 524-528 (2003)

A photon rupture technique was used to investigate abrupt destruction and repair of passive oxide films on Al - 9 mass% Si coated steels. Specimens covered by anodic oxide films were irradiated with a focused pulse of a pulsed Nd - YAG laser beam at a constant potential in 0.1 kmol / m^3 Na₂B₄O₇, pH = 9.2, with and without Cl⁻ and SO₄²⁻ ions while monitoring the current transients.

Irradiation with a focused pulse of a pulsed laser beam in the solutions causes abrupt removal of the anodic oxide film at the irradiated area. Without aggressive anions and also with aggressive anions at low potential, oxide films were reformed after the laser irradiation.

With increasing the potential, the current increased in the solutions with aggressive anions. This behavior can be explained by a preferential dissolution of the metal substrate, which is enhanced at higher potentials. It may be concluded that localized corrosion of Al - Si coated layers occurs at high potentials while film repair occurs at low potentials in solutions with aggressive anions.

Initial Stage of Localized Corrosion on Zinc Coated Steel with Photon Rupture Method in Chloride Ions Containing Solutions

M. Sakairi, K. Itabashi, and H. Takahashi

Proc. of 13rd Asian-Pacific Crrosion Control Conference, P09 (2003)

A photon rupture method, film removal by a focused pulse of pulsed Nd - YAG laser beam irradiation, has been attempted to study initial stage of localized corrosion of metals since it enables the oxide film stripping at extremely high rate without any contamination from film removal tools. Zinc coated steel specimens covered with nitrocellulose film were irradiated with focused pulse of pulsed Nd -YAG laser beam at a constant potential in 0.5 kmol m⁻³ H₃BO₃ - 0.05 kmol m⁻³ $Na_2B_4O_7$ (pH = 7.4) with chloride ions to monitor the current transient. Irradiation with a pulsed laser beam in solutions causes abrupt removal of the nitrocellulose film and air formed oxide films on the specimens at the laser-irradiated area. With chloride ions at low potential, oxide films were reformed after the laser irradiation. The charge of film reformation increased with increasing set potential. This behavior can be explained by a preferential dissolution of the metal substrate, which is enhanced at higher potentials. In chloride ion containing solutions, localized corrosion of coated layers occurs at high potentials. It was also found that chloride ions enhance dissolution of zinc at the very initial period after removal of the nitrocellulose layer.

Photoluminescence of Ti Oxide Film in Phosphate, Sulfate, and Chloride Solution

Mikito Ueda and Toshiaki Ohtsuka

Proceedings of the 13th Asian-Pacific Corrosion Control Conference, F-07 (2003)

Luminescence light from the anodic thin oxide films which formed on titanium in neutral phosphate, sulfate, and chloride solution were measured by photo-excitation of ultra-violet irradiation with 325 nm. Maximum luminescence intensity was observed at bias of -0.6 V in neutral 0.1 M NaCl solution. The potential corresponds to the flat-band potential of TiO₂. A peak in the luminescence spectra was observed at 420 nm wavelength in every solution. This peak corresponds to the band-gap energy of TiO₂ at 3.1eV. The small peak of 660 nm was also observed in phosphate buffer and sulfate solution, this may suggest that impurity levels in the film are relatively high.

The Aging of the Anodic Oxide of Titanium during Potentiostatic Condition by Ellipsometry

T. Ohtsuka and T. Otsuki

Corrosion Science, 45, 1793-1801 (2003)

The aging effect of the anodic oxide film on titanium under constant potential oxidation was investigated by 3-parameter (3-P) ellipsometry in 0.1 mol dm⁻³ sulfuric scid solution. The oxide film was initially formed by a potential sweep oxidation, where the film with a low refractive index grew at relatively high rate. From the low value of the refractive index, the oxide film is assumed to be a hydrated structure. After the sweep oxidation to 4.26 V vs. reversible hydrogen electrode, the constant potential oxidation was performed at a potential of 4.26 V to examine the aging effect of the hydrated oxide film by 3-P ellipsometry It was found that the refractive index of the oxide film increased from 2.39 to 3.59 during the aging of the constant potential oxidation, and thickness decreased. The increase of the refractive index abd the decrease of thickness may be explained by conversion from the hydrated oxide to a dehydrated oxide during the aging.

Difference between Passivation Film and Rust Layer

Toshiaki Ohtsuka

Kinzoku (Material Science & Technology); Special Issue on Corrosion and Rust Layer on Iron, 2003, No.8, 21-26 (2003)

The passivation layer and rust layer on iron and steels were reviewed in a view point of ionic transport and potential distribution on the film. Although the both passive film and rust consists of Fe(III) oxide or oxyhydroxide, the film growth of passivation layer is limited to nm order, however, the rust layer can grow to μ m order. For the growth of the iron rust layer, the wet- and-dry cycle plays a large role: during the wet-and -dry cycle, the iron oxyhydroxide undergoes reduction-and-oxidation cycle. When the passivated iron electrode was applied to a cycle between a low potential and a high potential, the hydrated layer analogous to the rust can be grown. From the impedance diagram, the potential distribution and ionic transport in the layers was discussed. (Japanese)

Nano-Indentation in Solution to Passive Metal Surfaces

M. Seo, M. Chiba and Y. Kurata

Zairyo-to-Kankyo, 52 (2003) 5-11

This article reviewed the recent results of nano-indentation tests in solution for in-situ evaluation of the mechanical properties of passive iron and titanium surfaces electrochemically controlled in pH 8.4 borate solution. The hardness of passive metal surfaces in the solution could be determined from the load-depth curves measured with nano-indentation tests. In the absence of chromate treatment, the hardness of the passive iron (110) surface was larger by 10 % than that of the passive iron (100) surface which was ascribed to the difference in surface atomic density of the substrate. The chromate treatment increased the hardness of the passive iron (100) surface. The effect of chromate treatment on hardness was explained in terms of high repassivation rate at the ruptured sites of passive film during nano-indentation in solution.

The hardness of the titanium surface obtained with nano-indentation under the electrochemical control at 5 V(RHE) after anodic oxidation at 5 V for 1 h in the solution was 3-4 times as large as that of the titanium surface obtained with nano-indentation in air after anodic oxidation at the same condition.

This large difference in hardness was attributed to high repassivation rate at the ruptured sites of anodic oxide film under the electrochemical control at 5 V in the solution as well as the effect of the chromate treatment on hardness for the passive iron surface. (Japanese)

Effect of Hydrogen on Stresses in Anodic Oxide Film on Titanium

J.-D. Kim, S.-I. Pyun and M. Seo

Electrochim. Acta, 48 (2003) 1123-1130

Stresses in anodic oxide film on titanium thin film/glass electrode in pH 8.4 borate solution were investigated by a bending beam method. The increases in compressive stress observed with cathodic potential sweeps after formation of anodic oxide film were attributed to the volume expansion due to the compositional change of anodic oxide film from TiO_2 to $\text{TiO}_{2-x}(\text{OH})_x$. The instantaneous responses of changes in stress, $\Delta \sigma$, in the anodic oxide film to potential steps demonstrated the reversible characteristic of the $\text{TiO}_{2-x}(\text{OH})_x$ formation reaction. In contrast, the transient feature of $\Delta \sigma$ for the titanium without anodic oxide film represented the irreversible formation of TiH_x at the metal/oxide interphase.

The large difference in stress between with and without the oxide film, has generated during the hydrogen that most of stresses absorption/desorption reside in the anodic oxide film. A linear relationship between changes in stress, $\Delta(\Delta\sigma)_{des}$, and electric charge, ΔQ_{des} , during hydrogen desorption was found from the current and stress transients, manifesting that the stress changes were crucially determined by the amount of hydrogen desorbed from the oxide film. The increasing tendency of $-\Delta(\Delta\sigma)_{des}$ with increasing number of potential steps and film formation potential were discussed in connection with the increase in desorption amount of hydrogen in the oxide film with increasing absorption/desorption cycles and oxide film thickness.

Effect of Applied Potential Steps on Stresses of Anodic Oxide Film on Nickel

J. -D. Kim and M. Seo

J. Electrochem. Soc., **150** (2003) B193-B198

Stresses in anodic oxide film on nickel thin film/glass electrode in pH 8.4 borate solution were investigated by a bending beam method. Tensile stresses were always measured during the formation of the oxide film, representing the significant contribution of cation transport to the growth of the oxide film. The downward and upward potential steps in the passive and hydrogen evolution potential ranges after passive film formation produced instantaneous changes in stress to the compressive and tensile direction, respectively. It was attributed to the changes of cation valence and ratio of OH^{+}/O^{2-} in the hydrated passive film, $NiO_{1+x} \cdot yH_2O$.

The large difference in stress between with and without the oxide film has suggested that most of the stresses generated during the application of potential steps reside in the oxide film. A linear relationship between step changes in stress and relative concentration of absorbed hydrogen was found from the current and stress transients. The similarity of the magnitude of stress with potential steps between the oxide films formed in the passive and transpassive potential ranges, respectively, were discussed in terms of the structural characteristic of transpassive film consisting of a porous and a thick layer.

Nano-mechano-electrochemical Properties of Passive Titanium Surface Evaluated by *In-situ* Nano-indentation and Nano-scratching

M. Seo and Y. Kurata

Electrochim. Acta, 48 (2003) 3221-3228

In-situ nano-indentation and scratching tests using a pyramidal Berkovich diamond indenter were performed to examine the nano-mechano-electrochemical properties of the passivated polycrystalline titanium surfaces. There were significant differences in the load-depth curves obtained between in-situ (kept at 5 V(RHE) in solution) and ex-situ (in air) nano-indentation tests at a maximum load of $L_{max} = 300 \,\mu\text{N}$ for the titanium surfaces passivated at 5 V (RHE) for 1 h in pH 8.4 borate solution. The hardness (9 GPa) of the passive titanium surface obtained from the in-situ load-depth curve was three or four times as large as that obtained from the ex-situ load-depth curve. The coefficient of friction for the passive titanium surface obtained from the in-situ nano-scratching was also significantly larger than from that obtained from the ex-situ nano-scratching. The large differences in hardness and coefficient of friction between in-situ and ex-situ tests were discussed from the mechano-chemical viewpoint such as the differences in repassivation rate at the film rupture sites near edge of contact area during indentation or near the front area of scratching between under potential control in solution and in air.

Mechanoelectrochemical Properties of Passive Iron Surfaces Evaluated by an *In-Situ* Nanoscratching Test

M. Chiba and M. Seo

J. Electrochem. Soc., **150** (2003) B525-529

In-situ (as kept at 0.25 V vs. SHE in solution) and ex-situ (in air) nano-scratching tests were performed to the iron single crystal (110) and (100) surfaces passivated at 0.25 V (SHE) in pH 8.4 borate solution to evaluate the mechanical and electrochemical properties, i.e., correlated 'mechano-electrochemical properties' of the passive surfaces. The friction coefficient of the passive iron (100) surface was larger than that of the passive iron (110) surface, irrespective of in-situ or ex-situ nano-scratching. The friction coefficient obtained with *in-situ* nano-scratching for both the passive iron (110) and (100) surfaces were significantly larger than that obtained with ex-situ nano-scratching. The increase in friction coefficient due to in-situ nano-scratching was explained in terms of a series of mechano-electrochemical reaction taking place at the moving front of the indenter such as active dissolution from the film rupture sites followed by repassivation.

Frictional Coefficients of the Passive Titanium Surfaces Evaluated with *In-situ* and *Ex-situ* Nano-scratching Tests

M. Seo, Y. Kurata and M. Chiba

Proc. Intern. Symp. on Corrosion Science in the 21st. Century, CD-C097 (2003)

In-situ (kept at 5 V or 0 V in solution) and ex-situ (in air after anodic oxidation) nano-scratching tests by using the Berkovich pyramidal diamond indenter were performed to evaluate the friction coefficient of the polycrystalline titanium surface anodically oxidized at 5 V (RHE) for 1 h in pH 8.4 borate solution. The friction coefficients of the titanium surfaces obtained with in-situ nano-scratching were significantly larger than those obtained with ex-situ nano-scratching. Moreover, the in-situ friction coefficient of the titanium surface kept at 5 V (RHE) was larger than that of the titanium surface kept at 0 V (RHE).

Based on the large difference in AFM images of the scratched area after *in-situ* and *ex-situ* nano-scratching and on the stick-slip like a phenomenon observed only during *in-situ* nano-scratching, it has been proposed that a series of mechano-electrochemical reaction such as the film rupture, anodic dissolution from the rupture sites and the repassivation, takes place at the moving front of the indenter tip during *in-situ* nano-scratching, and the promotion of the repassivation gives the high impedance against the movement of the indenter tip. The large friction coefficient obtained with *in-situ* nano-scratching was explained in terms of the promotion of the repassivation by the large potential difference between the titanium substrate and solution.

Potential Dependence of Frictional Coefficient Evaluated by *In-situ* Nano-scratching for the Passive Iron Surface

M. Chiba and M. Seo

Proc. Intern. Symp. on Corrosion Science in the 21st. Century, CD-C016 (2003)

In-situ (kept potentiostatically in the passive state) and ex-situ (in air after passivation) nano-scratching tests were performed to the iron single crystal (100) surfaces passivated at 0.0 V - 1.0 V (SHE) in pH 8.4 borate solution to evaluate the friction coefficient of the passive surface and its potential dependence. The friction coefficient obtained with *in-situ* nano-scratching for the passive iron (100) surface was significantly larger than that obtained with ex-situ nano-scratching.

The friction coefficient obtained with ex-situ nano-scratching was almost independent of potential in the passive region. On the other hand, the friction coefficient obtained with in-situ nano-scratching increased with increasing potential in the passive region. These results were explained in terms of a series of mechano-electrochemical reaction such as the film rupture, active dissolution and repassivation taking place at the moving front of the indenter during in-situ nano-scratching.

Passive Film Formed on Shape Memory NiTi Ailoy in Sulfuric Acid

Koji Fushimi, Achim W. Hassel and Martin Stratmann

Proceedings of 13th Asian-Pacific Corrosion Control Conference (CD-ROM), L-06 (2003)

Shape memory NiTi alloy was polarized anodically in methanolic or aqueous H_2SO_4 solution to remove or to form oxide films on the surface. Anodic polarization of NiTi at potentials higher than 2 V in methanolic 3 mol dm⁻³ H_2SO_4 solution at 263 K gave a limiting current and produced a smooth surface. These conditions showed the best electropolishing results for 0.1 mol dm⁻³ $\leq C_{H2SO4} \leq 7$ mol dm⁻³. The passivity of NiTi was better than that of Ni but poorer than that of Ti in aqueous 0.1 mol dm⁻³ H_2SO_4 solution. XPS analysis revealed that TiO_2 -based oxide film formed on NiTi and its thickness and composition depended on film the formation potential. The semiconductive properties of the oxide film were investigated by EIS. The permittivity or donor density of the film was similar to that of anodic oxide film on pure Ti. The dependence of the inverse of capacitance, C^{-1} , on the potential was explained by using the band structure model.

An EQCM Study on Passivation Process of Nickel Thin Films in Acidic and Alkaline Sulfate Solutions

Masahiro Seo and Naoki Kikuchi

Proceedings of 13th Asian-Pacific Corrosion Control Conference (CD-ROM), F-04 (2003)

The passivation process of nickel thin films in acidic and alkaline sulfate solutions was analyzed by an electrochemical quartz crystal microbalance (EQCM) to separate the partial current density of nickel dissolution through the passive film, i_{Ni2+} , and the partial current density of film growth, i_{O2-} . The values of i_{Ni2+} and i_{O2-} during potentiodynamic polarization (20 mV s⁻¹) in the passive potential region could be separated by comparing the net mass change rate and polarization current as a function of electrode potential. The passivation mechanism was discussed from the dependences of i_{Ni2+} and i_{O2-} on sulfate concentration and solution pH.

Friction Coefficients of The Passive Single Crystal Iron Surfaces and Their Potential Dependences Evaluated by An *In-situ* Nano-Scratching

Makoto Chiba and Masahiro Seo

Proceedings of 13th Asian-Pacific Corrosion Control Conference (CD-ROM), F-05 (2003)

In-situ (kept potentiostatically in the passive state) and ex-situ (in air after passivation) nano-scratching tests were performed to the single crystal iron (100) surfaces passivated at 0.0 V - 1.0 V (SHE) in pH 8.4 borate solution to evaluate the friction coefficients of the passive surfaces and their potential dependences. The measured friction coefficients were normalized by taking into account the real geometry of the indenter tip. The normalized friction coefficient obtained with in-situ nano-scratching for the passive iron (100) surface was significantly larger than that obtained with ex-situ nano-scratching. The normalized friction coefficient obtained with ex-situ nano-scratching was almost independent of potential in the passive region. On the other hand, the normalized friction coefficient obtained with in-situ nano-scratching increased with increasing potential in the passive region. These results were explained in terms of a series of mechano-electrochemical reaction, such as film rupture, active dissolution and repassivation, taking place at the moving front of the indenter tip during in-situ nano-scratching.

Nucleation and Growth of the Nanostructured Anodic Oxides on Tantalum and Niobium under the Porous Alumina film

A. Mozalev, M. Sakairi, I. Saeki, and H. Takahashi

Electrochim. Acta, 48, 3155-3170 (2003)

Anodic oxidation of Ta-Al (aluminum deposited on tantalum) and Nb-Al (aluminum deposited on niobium) has been performed in organic and inorganic acid electrolytes for porous alumina formation. Arrays of tantalum nanoscale oxide hillocks and niobium oxide goblets derived from the anodised Ta-Al and Nb-Al bilayer samples have been investigated by scanning electron microscopy, transmission electron microscopy and X-ray photoelectron spectroscopy depth profiling. Anodising proceeds in the sequence of growth of porous anodic alumina and, when the aluminum layer is consumed up to the underlying metal results from metal ions migrating outward and oxygen ions transported through, and released from, the alumina barrier layer, which dissolves at the tantalum/alumina interface, i.e. without tantalum being in direct contact with the electrolyte. The shape and mutual arrangement of the anodic oxide nanostructures depend on the nature of the underlying metal, anodising solution, and are consistent with the difference between the resistivities of the tantalum (niobium) oxide formed and the barrier layer of the overlying alumina cells, which is influenced by incorporated electrolyte-derived species.

Local Removal of Thick Anodic Oxide Film on Aluminum with A Photon Rupture Technique and Local Metal Deposition

M. Sakairi, Z. Kato, S. Z. Chu, H. Takahashi, Y. Abe, and N. Katayama

Electrochemistry, 71, 920-926 (2003)

Aluminum specimens covered with thick porous type anodic oxide films, up to $100~\mu m$, were irradiated by a photon rupture technique, a focused pulsed Nd-YAG laser beam, in a Ni²⁺ solution. The thick anodic oxide films, which does not dyed, were ruptured with numerous cracks by laser ablation. However, dyed thick anodic oxide films were removed layer by layer without developing cracks, as the dyed oxide film absorbed the laser energy.

After laser irradiation, electroplating was attempted to form thick Ni layers at only the irradiated area. By this local electroplating, a Ni layer was found to deposit just at the irradiated area, as the pore sealed anodic oxide films acted as an insulating film.

Repairing of Oxide Films on Zn-55% Al Alloy Coated Steel after Removal with Photon Rupture in Solutions

M. Sakairi, K. Itabashi, and H. Takahashi

Electrochem. Soc. Proc., 2002-24, 399-410 (2003)

A photon rupture, focused one pulse of pulsed YAG-laser irradiation, technique was attempt to investigate abrupt destroyed and repair of passive oxide films on Zn - 55 mass% Al coated steels. The specimens were irradiated with a focused one pulse of pulsed Nd - YAG laser beam at a constant potential in borate solutions, pH = 9.2, with and without Cl⁻, NO₃⁻ and SO₄²⁻ ions monitoring current transients. The oxide films were reformed in the borate solution with NO₃⁻ and SO₄²⁻ ions after removal of the oxide film. As potential becomes nobler, current and peak current increase. These behavior can be explained by a preferential dissolution of the metal substrate, which is enhanced at nobler potential and anions. In Cl⁻ containing solutions, localized corrosion of coated layer occurs at high potential, while film reformation occurs at low potentials.

Nanocrystalline Heterogeneity Responsible for Localized Corrosion

K. Hashimoto, S. Meguro, H. Habazaki and K. Asami

Proc. Critical Factors in Localized Corrosion IV, Electrochemical Society, 318-327 (2003)

The critical size of less corrosion-resistant precipitates which is detrimental to the corrosion resistance of spontaneously passive amorphous alloys was examined. bulk Ni-10Cr-5Ta-16P-4B **Polarization** of amorphous and curves Ni-5Cr-5Ta-5Mo-16P-4B alloys measured in 6 M HCl at 30°C were not affected by precipitation of fcc Ni-Cr-Ta and Ni-Cr-Mo-Ta phases of 2 nm or less in diameter in the amorphous matrixes, while the anodic currents significantly increased by precipitation of these phases of 5 nm or more. The diameter of the less corrosion-resistant precipitates, which can be covered by the passive film originated from the corrosion-resistant matrix phase, is of the order of the thickness of the passive film.

Initial Stages of Plasma Electrolytic Oxidation of Titanium

T. H. Teh, A. Berkani, S. Mato, P. Skeldon, G. E. Thompson, H. Habazaki and K. Shimizu

Corrosion Science, 45, 2757-2768 (2003)

The initial stages of oxide growth on titanium are examined in a recently developed commercial alkaline pyrophosphate/aluminate electrolyte of interest for plasma electrolytic oxidation of light metal alloys. Constant current anodizing was employed, with resultant films examined by scanning and transmission electron microscopies and Rutherford backscattering spectroscopy. The initial film is relatively uniform and composed of TiO2, with low concentrations of aluminium and phosphorus species incorporated from the electrolyte. With increase in voltage the film breaks down locally, and regions of original and modified film develop simultaneously, with the latter occupying more of the surface as the voltage rises. Porous regions due to dielectric breakdown also become increasingly evident. At similar to 240 V, sparking commences, and the surface reveals extensive, relatively uniform porosity, with the coating now containing much enhanced concentrations of aluminium and phosphorus species compared with the coating at lower voltages. The films develop at low efficiency due to generation of oxygen. The oxygen is produced within the original film material and at sites of dielectric breakdown. The former type of film develops a two-layered morphology, with an outer layer of amorphous TiO2 and an inner layer with numerous fine and course cavities. The cavities are due to the generation of oxygen that may be associated with the formation of anatase in the inner layer.

Anodic Oxidation of Ta/Fe Alloys

S. Mato, G. Alcala, G. E. Thompson, P. Skeldon, K. Shimizu, H. Habazaki, T. Quance, M. J. Graham and D. Masheder

Corrosion Science, 45, 2881-2892 (2003)

The behaviour of iron during anodizing of sputter-deposited Ta/Fe alloys in ammonium pentaborate electrolyte has been examined by transmission electron microscopy, Rutherford backscattering spectroscopy, glow discharge optical emission spectroscopy and X-ray photoelectron spectroscopy. Anodic films on Ta/1.5 at.% Fe, Ta/3 at.% Fe and Ta/7 at.% Fe alloys are amorphous and featureless and develop at high current efficiency with respective formation ratios of 1.67, 1.60 and 1.55 nm V⁻¹. Anodic oxidation of the alloys proceeds without significant enrichment of iron in the alloy in the vicinity of the alloy/film interface and without oxygen generation during film growth, unlike the behaviour of Al/Fe alloys containing similar concentrations of iron. The higher migration rate of iron species relative to that of tantalum ions leads to the formation of an outer iron-rich layer at the film surface.

Influence of Current Density on Transport Numbers in Anodic Oxide Films on an Anodized Al-5.7at.%W Alloy

L. Iglesias-Rubianes, P. Skeldon, G. E. Thompson, H. Habazaki and K. Shimizu

Corrosion Science, 45, 2905-2913 (2003)

The ionic transport numbers in barrier anodic films, formed on an Al-5.7 at.% W alloy in 0.1 M sodium tungstate electrolyte at 293 K, have been measured for current densities from 0.1 to 1000 mA cm⁻². For this purpose, a xenon marker was ion implanted with a fluence of 1.5 x 10¹⁵ ions cm⁻² into a film formed to 10 V on the alloy, which was then further anodized to 150 V. The position of the marker layer in the final film was determined by transmission electron microscopy and Rutherford backscattering spectroscopy. The cation transport number was similar to 0.38, with no dependence upon current density to an accuracy of similar to 10%.

Influence of Oxidation Rate and Alloy Composition on Alloy Enrichments of Anodized Al-W Alloys

L. Iglesias-Rubianes, P. Skeldon, G. E. Thompson, P. Bailey, T. C. Q. Noakes, H. Habazaki and K. Shimizu

Corrosion Science, 45, 2915-2923 (2003)

The effect of oxidation rate on enrichment of tungsten in metastable, solid-solution Al-W alloys during anodizing has been investigated by Rutherford backscattering spectroscopy and medium energy ion scattering. The oxidation rate has negligible influence upon enrichment for current densities in the range 0.01-100 mA cm⁻², with levels between 1.3 x 10¹⁵ and 1.5 x 10¹⁵ W atoms cm⁻² for an Al-0.7at.% W alloy. Further, enrichment factors, expressing the ratio of the enrichment of tungsten in the alloy, in units of 10¹⁵ atoms cm⁻², to the bulk composition of the alloy, in units of at.%, for alloys of compositions in the range 0.1-30 at.% W, decrease progressively in the approximate range 2.5-0.2.

Impact of RF-GD-OES in Practical Surface Analysis

K. Shimizu, H. Habazaki, P. Skeldon and G. E. Thompson

Spectrochimica Acta Part B-Atomic Spectroscopy, 58, 1573-1583 (2003)

The capabilities of RF-GD-OES for depth profiling analysis are illustrated based on the recent results from the authors' laboratories. Through the analysis of a hard disk, a thin anodic alumina layer with a delta function marker layer, and a 5-nm thick air-formed oxide film on sputter deposited stainless steel, it is demonstrated that RF-GD-OES has enormous potential for depth profiling analysis of ultra-thin layers, less than 10-nm thick, as well as films of several tens of microns thickness. The remarkable features of RF-GD-OES arise from the nature of RF-GD sputtering where samples, conducting or non-conducting, are sputtered stably with Ar⁺ ions of very low energy (< 50 eV) and a current flux of the order of similar to100 mA cm⁻².

Influence of Silicon Species on the Electric Properties of Anodic Niobia

H. Habazaki, T. Matsuo, H. Konno, K. Shimizu, S. Nagata, K. Matsumoto, K. Takayama, Y. Oda, P. Skeldon and G. E. Thompson

Electrochimica Acta, 48, 3519-3526 (2003)

The influence of incorporation of silicon species on the electric properties of anodic niobia, formed in 0.1 mol dm⁻³ ammonium pentaborate electrolyte, has been examined using sputter-deposited Nb-Si alloys containing 5 and 17 at.% silicon. The potential dependence of the capacitance of anodic niobia, originating from its n-type semiconducting properties, becomes less significant by incorporation of silicon species. In addition, the leakage current decreases with increasing silicon content in the alloy. The thermal stability of the anodic niobia is also enhanced by silicon species; the capacitance and leakage current, which increase significantly for niobium, are little influenced by annealing up to 523 K. The silicon species are incorporated in the inner 72% of the film thickness, as a consequence of immobility of the species in growing anodic niobia. The immobility of silicon species is associated with a strong Si⁴⁺ -O bond, which may also contribute to the reduction of leakage current.

Radiofrequency GDOES: A Powerful Technique for Depth Profiling Analysis of Thin Films

K. Shimizu, H. Habazaki, P. Skeldon and G. E. Thompson

Surface and Interface Analysis, 35, 564-574 (2003)

Previously, glow discharge optical emission spectroscopy (GDOES), both d.c. and r.f. has been used for depth profiling analysis of thick films, several tens of microns thick, utilizing its high sputtering rates of >1 µm min⁻¹. Through selected examples, it is demonstrated here that r.f. GDOES also has enormous potential for depth profiling analysis of ultrathin films <10 nm thick, where AES and SIMS have dominant roles. The significant features of r.f. GDOES enabling such analysis arise from the nature of r.f. glow discharge sputtering where samples, both conducting and non-conducting, are sputtered very stably with Ar⁺ ions of low energies (<50 eV) and high current fluxes (of the order of 100 mA cm⁻²). The low Ar⁺ energy ensures that film sputtering proceeds without significant formation of altered layers, which is a prerequisite for successful depth profiling analysis of ultrathin films at high depth resolution. The high current fluxes allow sputtering to proceed at very high rates of >1 µm min⁻¹, thereby extending the limit of film thickness for analysis to $100 \ \mu m$. Thus r.f. GDOES, with its unique ability to accommodate depth profiling analysis of films of a very wide thickness range, is expected to play an important role in the field of practical surface analysis.

Radiofrequency GDOES, EPMA and AES Analysis of Zinc Die Casting Plated with Copper, Duplex Nickel and Microporous Chromium for Corrosion Protection

K. Shimizu, N. Kasahara, H. Habazaki, P. Skeldon and G. E. Thompson

Surface and Interface Analysis, 35, 611-617 (2003)

The distributions of the additive-derived carbon and sulphur impurities in electroplated metallic layers are of great concern in plating industries. The amounts of carbon and sulphur impurities in the layers are normally <1 wt.% but they influence significantly the structure and properties of the layers. By analysis of the duplex nickel layers for corrosion protection of exterior automotive zinc die casting, it is demonstrated that radiofrequency glow discharge optical emission spectroscopy is a powerful and reliable technique for this purpose, allowing rapid depth profiling analysis with excellent sensitivities for the detection of carbon and sulphur, along with other impurities such as hydrogen and iron, and depth resolution. A freshly generated and highly flat cross-section of the sample has been prepared using an ultramicrotome and a diamond knife and subsequently analysed by EPMA line-scan analysis and AES spot analysis. It appeared that EPMA and AES do not have sufficient sensitivities to detect small amounts of the additive-derived carbon and sulphur impurities, although they have distinct advantages for micro-area analysis.

Analysis of Anodic Films on Nb and NbNx by Glow Discharge Optical Emission Spectroscopy

H. Habazaki, T. Matsuo, H. Konno, K. Shimizu, K. Matsumoto, K. Takayama, Y. Oda, P. Skeldon and G. E. Thompson

Surface and Interface Analysis, 35, 618-622 (2003)

Sputter-deposited niobium layers containing nitrogen form anodic films with resultant capacitance and leakage current density little influenced by annealing up to 523 K. The nitrogen species incorporated into the anodic oxide films at the alloy/film interface are distributed in the inner 70-75% of the film thickness, with fine bubbles containing high-pressure N₂O gas being evident. Glow discharge optical emission spectroscopy (GDOES) analysis reveals their continued presence after annealing at 523 K. The insignificant changes in GDOES depth profiles also suggest that the formation of low-valent oxide at the metal/film interface as a result of annealing is not responsible for the behaviour. For thermal treatments above 400 K, capacitances and leakage currents increase significantly for niobium, with nitrogen additions diminishing the effects. Such behaviour is suggested to arise from suppression of mechanical damage to films through the presence of highly pressurized gas in the inner part of the films.

Mechanical Properties of Barrier-Type Anodic Alumina Films Using Nanoindentation

G. Alcala, S. Mato, P. Skeldon, G. E. Thompson, A. B. Mann, H. Habazaki and K. Shimizu

Surface & Coatings Technology, 173, 293-298 (2003)

This work uses nanoindentation to determine the mechanical properties of barrier-type anodic alumina films formed on aluminium in ammonium pentaborate electrolyte. Using indents to a depth of ~45 nm and a maximum load of 0.5 mN, with films of thicknesses 480 and 600 nm, values of similar to 140 and similar to 8.5 GPa were indicated for the elastic modulus and the hardness, respectively. Lower values were obtained for deeper indents, at higher loads, and for specimens with thinner films. The reduction of hardness was consistent with the commonly applied rule that the indent depth should not exceed 10% of the film thickness in order to avoid influences of the substrate. Although substrate properties can affect modulus measurement to shallower depths, the similarity of results for the two thickest films suggests a reasonable estimate of the film property.

Compositional Self-Organizing in the Anodic Film on a Mg-Ta Alloy

S. Mato, G. Alcala, P. Skeldon, G. E. Thompson, D. Masheder, H. Habazaki and K. Shimizu

Journal of the Electrochemical Society, 150, B439-B444 (2003)

Evidence is presented of compositional self-ordering in the amorphous anodic film that develops during anodizing of a Mg/40 atom % Ta alloy in sodium hydroxide electrolyte. This is manifested in an outer layer of film material, representing about 60% of the film thickness, that in cross section consists of bands, alternatively magnesium-rich and tantalum-rich, orientated normal to the film surface. Each band is typically about 10-20 nm wide. The remainder of the film is uniform in composition, comprising units of MgO and Ta₂O₅ in an amorphous network, similar to that of the tantalum-rich bands. The development of the bands is a consequence of the faster migration of Mg²⁺ ions relative to that of Ta⁵⁺ ions in the tantalum-rich oxide and the relatively high ionic resistance of the magnesium-rich material. Thus, ionic current flows preferentially through the tantalum-rich oxide, with compositional reorganization suggested to take place at the tips of the fingers close to the surface of the film.

Oxygen Generation in Anodized Ta-Cu Alloys

S. Mato, G. Alcala, P. Skeldon, G. E. Thompson, T. Quance, M. J. Graham, H. Habazaki, K. Shimizu and D. Masheder

Philosophical Magazine, 83, 2733-2746 (2003)

Comparison is made of the influences of copper in the development of amorphous anodic films on Ta-Cu alloys, containing up to 57at.%Cu, in ammonium pentaborate electrolyte at 293 K. The various films are based on tantala with low concentrations of copper, relative to those of the alloys, since copper species migrate through the films more rapidly than Ta⁵⁺ ions and are lost to the electrolyte on reaching the film Surface. Of particular interest, film growth on Ta-1.5at.% Cu alloy at 1, 0.1 and 0.01 mA cm⁻² proceeds with generation of oxygen, which is contained in nanoscale bubbles within the oxide. Bubbles are more numerous as the current density decreases. In the case of Ta-12 at.% Cu and Ta-57 at.% Cu alloys, the films are flawed extensively by more numerous oxygen bubbles, which are present mainly in the outer parts of the anodic films, oxygen production and film damage due to the bursting of bubbles limit the anodizing voltage to relatively low values. It is suggested that copper species modify the electron levels, and possibly structure, of the tantala-based films, thereby facilitating oxygen generation within the bulk film by oxidation of O2- ions of the oxide.

Crystallization of Anodic Titania on Titanium and Its Alloys

H. Habazaki, M. Uozumi, H. Konno, K. Shimizu, P. Skeldon and G. E. Thompson

Corrosion Science, 45, 2063-2073 (2003)

Crystallization of amorphous anodic films grown at constant current density on sputtering-deposited titanium, and Ti-Si and Ti-Al alloys, in ammonium pentaborate electrolyte, has been examined directly by transmission electron microscopy. In the case of titanium, anatase develops at relatively low voltage in the inner film region, formed by inward migration of oxygen species. In contrast, the outer film region, formed at the film/electrolyte interface, is composed of amorphous oxide only. Oxide crystals are particularly found near the plane, separating the two regions, which is located at a depth of 35-38% of the film thickness. Oxide zones, of size ~1 nm, with a relatively ordered structure, developed at the metal/film interface, are considered to lead to transformation of the inner region structure. The incorporation into the film of either aluminium or silicon species suppresses the formation of crystalline oxide to much increased voltages. However, eventually nanocrystals form at ~40% of the film thickness, probably originating from pre-cursor nuclei in the air-formed on the as-deposited alloy.

High Resistivity Magnesium-Rich Layers and Current Instability in Anodizing a Mg/Ta Alloy

S. Mato, G. Alcala, P. Skeldon, G. E. Thompson, D. Masheder, H. Habazaki and K. Shimizu

Corrosion Science, 45, 1779-1792 (2003)

Strikingly different morphologies of amorphous anodic films on a Mg/40 at.%Ta alloy are shown to result from single-stage and sequential anodizing procedures. The alloy, prepared by magnetron sputtering, was anodized galvanostatically in ammonium pentaborate (pH 8.3) and sodium silicate (pH 12.6) electrolytes at 293 K and studied by transmission electron microscopy, Rutherford backscattering spectroscopy, glow discharge optical emission spectroscopy and X-ray photoelectron spectroscopy. For one-step anodizing in the pentaborate electrolyte, a single-layered film, of approximate composition Ta₂O₅·MgO, forms at a ratio of ~1.8 nm V⁻¹. In the silicate electrolyte, an outer, magnesium-rich layer, containing silicon species, also forms, with a ratio of 0.8 nm V⁻¹. The outer layer can develop due to relatively fast migration of magnesium ions in the inner layer and the stabilization of the pH at the film surface, probably linked to generation of a silica gel that also limits loss of magnesium species to the electrolyte. Further thickening of the anodic film, in ammonium pentaborate electrolyte, produces fingers of low resistivity, inner oxide that penetrate the pre-existing, high resistivity outer layer, with a bi-modal distribution of finger sizes. When fingers reach the film surface, magnesium ions are ejected to the electrolyte. The absence of fingers in films grown in sodium silicate electrolyte is possibly due to prevention, by the silica gel, of their initiation.

Anodic Film Growth in the Al-Ta Alloy System

G. Alcala, S. Mato, P. Skeldon, G. E. Thompson, P. Bailey, T. C. Q. Noakes, H. Habazaki and K. Shimizu

Corrosion Science, 45, 1803-1813 (2003)

The ionic transport numbers, relative migration rates of cation species and formation ratios are reported for barrier anodic films formed on metastable, solid solution Al-Ta alloys, with compositions extending from the aluminium-rich to the tantalum-rich ends of the system. The data were obtained by marker experiments, using ion implanted xenon, transmission electron microscopy, Rutherford backscattering spectroscopy and medium energy ion scattering. The films are amorphous and form by migration of metal and oxygen species. The ionic transport numbers and the formation ratios depend approximately linearly upon the composition of the alloy, between the values for anodic alumina and anodic tantala. The migration rate of Al3+ ions exceeds that of Ta5+ ions, but reduces in relative magnitude as the tantalum content of film increases. The faster migration of Al³⁺ ions is consistent with the higher energy of the Ta⁵⁺-O bond compared with that of the Al³⁺-O bond. Due to the difference in mobilities of the cation species, the films comprise an outer layer of alumina and an inner layer containing units of both alumina and tantala. The two-layered films can develop fingers of inner layer oxide that penetrate the outer alumina layer due to the higher ionic resistivity of the alumina. Such channelling of current can lead to mixing of inner layer oxide and alumina and thereby hinder formation of an alumina layer, particularly in films on the more tantalum-rich alloys.

Interconversion between Rare-Earth Metal(III) Chromates(V) and Low-Crystalline Phases by Reduction with Methanol and Oxidation in Air

Y. Aoki, H. Habazaki and H. Konno

Chemistry of Materials, 15, 2419-2428 (2003)

Rare-earth metal(III) chromates(V), LaCrO₄, NdCrO₄, and Y_{0.9}CrO_{3.85}, were found to show reversible structural changes by reduction with methanol and oxidation in air. This anomalous behavior was investigated by X-ray diffraction, X-ray photoelectron spectroscopy, Fourier transform infrared, in situ Raman spectroscopy, and other methods. After less than 30 min of reduction at 543 K, zircon-type NdCrO₄ in the bulk scale changed to the low-crystalline II-KDP-type phase, which has the same arrangement of metal atoms as zircon. The reduced phase was quickly reverted to the zircon-type phase by air oxidation at 543 K for a few minutes. NdCrO₄ was reduced by hydrogen from methanol by forming hydrogen bonds between CrO₄ units, which caused the oxygen displacement and the formation of pseudo-octahedral CrO_{6-m}(OH)_m units, leading to the distorted II-YDP-type structure. Defect zircon-type Y_{0.9}CrO_{3.85} changed more quickly to the low-crystalline II-KDP-type phase than NdCrO4, and the structure was not completely restored by the oxidation at 543 K for 1 h, because of the formation of small amounts of YCrO3 and Cr2O3. Monazite-type LaCrO4 changed to an amorphous phase with the formation of the Schottky defects of oxide ions because of the structural differences between the monazite-type and II-KDP-type phases and was restored by air oxidation at 723 K.

Formation of Barrier-Type Amorphous Anodic Films on Ti-Mo Alloys

H. Habazaki, M. Uozumi, H. Konno, S. Nagata and K. Shimizu

Surface & Coatings Technology, 169, 151-154 (2003)

Barrier-type amorphous anodic films with uniform thickness grow at high current efficiency on sputter-deposited Ti-Mo alloys containing 11.5-37.0 at.% molybdenum to high voltages of more than 100 V in 0.1 mol dm(-3) ammonium pentaborate electrolyte, in contrast to an amorphous-to-crystalline transition of anodic film on titanium and subsequent oxygen formation at relatively low voltages of less than 20 V. During anodizing of the alloys at a constant voltage of 80 V, the currents decrease to the order of 10⁻² A m⁻² within 3 h, whereas the current for titanium decreases only to the order of 1 A m⁻², due to the presence of flaws in the film, associated with oxygen evolution. The capacitance of the anodic films formed on the Ti-11.5 at.% Mo alloy is almost comparable to that formed on tantalum at the same voltage. The increase in molybdenum content in the alloy results in a slight decrease in the capacitance of the films. From these results, the structure of anodic films on titanium can be modified by incorporation of molybdenum species from the substrate so that uniform amorphous anodic films with a relatively high capacitance and a low defect density have been obtained.

Formation of Black Anodic Films on Aluminum in Acid Electrolytes Containing Titanium Complex Anion

T. Takenaka, H. Habazaki and H. Konno

Surface & Coatings Technology, 169, 155-159 (2003)

Galvanostatic anodizing of aluminum in oxalic acid electrolytes containing sulfate and $[TiO(C_2O_4)_2]^{2-}$ complex anions results in the formation of black porous anodic film. The initial voltage-time response in the present electrolytes is similar to that in usual acid electrolytes: after showing a maximum voltage, anodizing voltage becomes almost constant, i.e. 40-50 V. Then, the anodizing voltage increases almost linearly with time, and black coloring of the films takes place. The films become darker with an increase in anodizing voltage. In contrast, the black films are not formed in the oxalic acid-titanium complex anion mixed solutions without sulfate anions, although the similar voltage increase has been observed in the sulfate-free electrolyte. From morphological examinations. it has been found that the presence of sulfate ions in the electrolytes reduces the cell size of the porous films formed before the voltage increase. After the voltage increase, the cell structure in the inner part of the film becomes rather irregular and cell size becomes larger. In addition, the metal/film interface is extremely rough, and particles of metallic aluminum are incorporated in the anodic films near the metal/film interface. Glow discharge optical emission spectroscopy analysis has revealed that a small amount of titanium species is present in the inner part of the film. From these results, the mechanism of the black coloring of the anodic films has been discussed.

Dielectric and Mechanical Properties of Anodic Films in the Ta-Ti System

S. Mato, G. Alcala, P. Skeldon, G. E. Thompson, A. B. Mann, D. Masheder, H. Habazaki and K. Shimizu

Surface and Interface Analysis, 35, 477-482 (2003)

Anodic oxidation at high efficiency of sputtering-deposited Ta-Ti alloys containing 0.6-40 at.% Ti is shown to result in amorphous films comprising a relatively thin outer layer of TiO₂-based material and an inner layer consisting of units of TiO₂ and Ta₂O₅. The two layers develop due to the faster migration of Ti⁴⁺ ions in the inner layer relative to that of Ta⁵⁺ ions. The formation ratios for the various films are in the approximate range 1.6-1.9 nm V⁻¹. The dielectric constants of the films are ~28, which is a similar value to that of anodic tantala. Nanoindentation revealed that the elastic modulus and hardness of the films are essentially independent of film composition, with average values of 134 and 5.3 GPa, respectively.

Formation of N₂O Gas Bubbles in Anodic Films on NbNx Alloys

H. Habazaki, T. Matsuo, H. Konno, K. Shimizu, S. Nagata, K. Takayama, Y. Oda, P. Skeldon and G. E. Thompson

Thin Solid Films, 429, 159-166 (2003)

Sputter-deposited niobium, and Nb₉₀N₁₀, Nb₈₃N₁₇ and Nb₆₀N₄₀ alloys, have been anodized at 50 A m⁻² in 0.1 mol dm⁻³ ammonium pentaborate electrolyte at 293 K and resultant amorphous anodic films have been characterized by transmission electron microscopy, glow discharge optical emission spectroscopy, Rutherford backscattering spectrometry and Fourier-transform, infra-red spectroscopy Except for the Nb₆₀N₄₀ alloy, which shows a breakdown at approximately 60 V, the deposited layers reveal a linear voltage increase to more than 150 V, with the rate decreasing with the niobium content. Additionally, anodic films, with flat and parallel metal/film and film/electrolyte interfaces, are formed on the specimens with the formation ratio decreasing with increasing nitrogen content in the deposited films. Nitrogen is incorporated into the inner similar to 70-75% of the film thickness as N₂O molecules, forming fine bubbles, with typical sizes up to 10 nm, in a Nb₂O₅-based matrix material. The remaining 25-30% of the film comprises a layer of Nb₂O₅ with the outer regions containing boron species derived from the electrolyte. Release of high pressure N₂O gas is associated with the relatively low breakdown voltage for the Nb₆₀N₄₀ alloy of highest nitrogen content. The two-layered nature of the anodic films arises from the film growth mechanism that involves outward migration of niobium species and inward migration of oxygen species; in contrast nitrogen species are immobile due either to the relatively high energy of the N-O bond or to their presence in bubbles.

Adsorption of Thiourea on Gold Electrode in Perchloric Acids Studied by in situ Surface-Enhanced Infrared Absorption Spectroscopy

Takeshi Sasaki, Mitsuo Kondoh, Hiroto Tachikawa, Masatoshi Osawa and Toshiaki Ohtsuka

Proc. the 7th international symposium on advances in electrochemical and science technology (ISAEST-VII A185-A187 (2003)

The behavior of adsorbed thiourea on gold electrode was investigated by the surface-enhanced infrared absorption spectroscopy (SEIRAS). Referring to the complementary ab initio calculation, the adsorbed molecules with potential changes were determined, and the reaction scheme was proposed.

Application of CSLM to the Surface Morphological Study of Al 5052 Alloy Anodized in Sulfuric Acid Solution

S.-M. Moon, M. Sakairi, and H. Takahashi

J. Electrochem. Soc., 150, B473-B480 (2003)

Confocal scanning laser microscopy (CSLM) was applied to the surface morphological study of the anodic oxide film-covered Al5052 alloy. Contrast and height images of the specimens were obtained by scanning the laser beam in the x, y, and z directions. The incident laser beam appeared to be reflected by either the outer oxide surface, imperfections in the oxide film, or the inner oxide/metal interface. Contrast images of the outer oxide surface and the metal/oxide interface were obtained separately by choosing different scanning ranges of the focused z point of the incident laser beam. Two different types of imperfections, bright and dark, were observed in the contrast images of CSLM. The bright imperfections may correspond to inclusions with high reflectivity, and the dark ones to inclusions with uneven surfaces. The z position of the bright imperfections in the oxide film was determined by analyzing the height images.

Stress Relaxation Effect of Functionally Graded Dental Post

F. Watari, S. Matsuo, N. Satoh, Y. Ueda, N. Ohata

Transaction of Functionally Graded Materials 2002 (FGM2002), 93-97 (2003)

Dental core and post, which is inserted in root canal after endodontic treatment to restore mastication function by setting a crown on the core part, often causes the fracture in dentin around the apex of post by imposition of impact force. To induce stress relaxation effect the composite resin with ceramic fillers in polymer matrix was used and FGM structure was formed by gradual change of filler content. Laser lithography, one of the photo-curing type CAD/CAM systems, was aplied for the fabrication of functionally graded post. The elastic modulus could be changed longitudinally from 10.6GPa in core part to 2.9GPa at the apex of post by decreasing the filler content of ceramic powders from 64% to 0% in polymer matrix. Stress analysis using finite element method showed the stress relaxation by further 30 % in FGM, compared with the uniform composite resin.

Fine Particles and Bioreaction

F. Watari

The Bulletin of the Society of Nano Science and Technology, 2, 33-37 (2003)

Biocompatibility of materials is generally dependent on the chemical dissolubility to ions, which is followed by absorption process to cells and tissue. Corrosion resistance is, therefore, prerequisite for biomaterials and Ti, highly corrosion-resistant, is one of the most biocompatible metals. However, the abraded fine particles often cause inflammation in the surounding tissue. *In vitro* biochemical study using human neutrophils as probe cell showed that the cytokine IL-1β, one of the markers of inflammation, increased as the particle size decreased from 150μm to 3μm. TNF-α was detected only in the 3μm particles, which is strongly correlated with phagocytosis. *In vivo* study showed that Ti fine particles less than 100μm caused the inflammation and as the particle size was smaller, the inflammation was pronounced. These lead to the conclusion that there is the physical size effect to affect on biocompatibility of fine particles, which is different from the toxicity due to the ionic dissolution effect.

Surface analysis of dental amalgams by X-ray photoelectron spectroscopy and X-ray diffraction

M.Uo, A.Berglund, J.Cardenas, L.Pohl, F.Watari, M.Bergman, S.Sjöberg

Dental Materials, 19, 639-644 (2003)

It is important to characterize the surface of dental amalgam in order to understand the process of mercury release from amalgam restorations in the oral. The mercury evaporation occurs not only from the newly made restoration but also from the set material. The surfaces of four different types of amalgams, which had been well set, were analyzed with X-ray photoelectron spectroscopy (XPS) and X-ray diffraction (XRD) and the relationship between surface compositions and mercury release was studied. Fresh amalgam surfaces as well as aged surfaces, which were stored for 30 days in air, were investigated using XPS and the chemical states of amalgam components and oxygen were studied. The aged surfaces were also characterized with XRD and grazing angle X-ray diffraction. With increased oxidation, the surface contents of tin and oxygen were increased in all amalgams. In contrast, the surface contents of copper and mercury were decreased. An increase of zinc or indium content were observed in zinc or indium containing amalgams, respectively. A surface layer enriched with indium and oxygen was clearly detected by XPS but not with grazing angle X-ray diffraction. The thickness of the enriched surface layer is estimated to be in the order of few nanometer, which is approximately equal to the analysis depth of XPS. In addition, the presence of metallic elements, like tin and zinc, that readily form a stable oxide layer at the surface suppress the release of mercury.

Cytotoxicity and bonding property of dental ceramics

M.Uo, G.Sjögren, A.Sundh, F.Watari, M.Bergman, U.Lerner

Dental Materials, 19, 487-492 (2003)

Yttria partially stabilized zirconia (YPSZ) ceramic is suitable for dental and medical use because of its high fracture toughness and chemical durability. The purpose of this study was to estimate the cytotoxicity and bonding property of dental zirconia ceramic compared to other dental ceramics. Eight commercial dental ceramics including Denzir (YPSZ) are used in this cytotoxicity test. The human gingival fibroblast cells were cultured using extraction solutions of ceramics. The cytotoxicity was estimated by two different methods. The bonding strength of Denzir was compared to Empress2 using zinc phosphate, glass ionomer and adhesive resin cements. A brass plate with drilled tapered holes was prepared and ceramic specimens were prepared to fit the holes and bonded. The bonding strength was estimated by the punching test. No significant cytotoxicity was observed in all ceramics extractions. The two evaluation methods showed no significant differences. The Denzir and Empress2 showed similar bonding strength with zinc phosphate or glass ionomer cement bonding. For both Empress2 and Denzir the glass ionomer cement showed significantly higher bonding strength compared to the zinc phosphate cement. All ceramics extractions did not show any evidence of cytotoxicity. Therefore, the low in vitro cytotoxicity of ceramic extractions including Denzir was confirmed. Denzir showed a similar bonding strength to Empress2 with zinc phosphate or glass ionomer cement bonding with this testing method and lower bonding strength with adhesive resin cement than that of Empress2.

Tissue Response to a Newly Developed Calcium Phosphate Cement containing Succinic Acid and Carboxymethyl-chitin

A. Yokoyama, H. Matsuno, S. Yamamoto, T. Kawasaki, T. Kohgo, M. Uo, F. Watari, and M. Nakasu

Journal of Biomedical Materials Research, Part-A, 64A, 491-501 (2003)

We developed a new calcium phosphate cement containing succinic acid and CM-chitin in the liquid component. In this study, the biocompatibility and osteoconductivity of this new cement were investigated. After mixing, cement in putty form was immediately implanted between the periosteum and parietal bone and in the subcutaneous tissues of rats. In control cement, distilled water was used instead of the liquid component. In addition to histological evaluations, analyses with XRD and FTIR were done for the subcutaneously implanted cements. Histological examination showed slight inflammation around the new cement on the bone and in the subcutaneous tissue at 1 week after surgery. At 2 weeks, the cement was partially bound to the parietal bone. The extent of the surface of the new cement directly in contact with the bone increased with time, and most of the undersurface of the new cement bound to the host parietal bone by 8 weeks. Analysis by XRD showed that the new cement in the subcutaneous tissue was transformed into hydroxyapatite by 8 weeks. These results indicate that this new calcium phosphate cement is useful as a bone substitute material.

Discrimination between Composite Resin and Teeth using Fluorescence Properties

K.Tani, F.Watari, M.Uo and M.Morita

Dental Materials Journal, 22, 569-580 (2003)

The differentiation of composite resin from teeth using fluorescence emission was investigated as basic research for the visual detection of resin filled teeth in mass dental health examinations. Fluorescence spectra were taken from extracted human maxillary central incisors and 12 types of light-cured composite resins with a maximum of 15 shades via excitation using light with wavelengths of 400~500nm. The fluorescence intensity ratio of resin to tooth was lowest around 500nm for all the resins. The fluorescent images were taken based on spectroscopic results, which confirmed discrimination between the resin part and the tooth in the resin filled tooth.

CLSM and SEM quantitative analysis of surface topography of human teeth irradiated by Nd:YAG, Er:YAG and CO₂ lasers

M.K.Yamada, M. Uo, S. Ohkawa, F. Watari

International Congress Series 1248, 135-137 (2003)

The quantitative analysis of surface roughness of cavities formed by three different lasers: Nd:YAG (wavelength 1.06µm), Er:YAG (2.94 µm) and CO2 laser (10.6 µm) on dentin and enamel surfaces was done and compared using confocal laser scanning microscope (CLSM) and scanning electron microscope (SEM). The three types of lasers were applied perpendicularly to the polished surface of human extracted caries-free molars. The highest value of surface roughness (Ra) was observed on enamel and dentin surfaces irradiated by Er:YAG laser. Cracks were observed on dentin after CO₂ laser irradiation. Er:YAG laser irradiation formed an imbricate-pattern while Nd:YAG laser had a flake-like surface. A layer of globules representing melted material was observed in the cross-sectional view of dentin irradiated by Nd:YAG laser. This area had a surface roughness of 0.88 μm, while a smooth area between the globules had Ra of 0.20 µm. Depth profile examination showed deeper cavities on surfaces irradiated by Er:YAG laser. Quantitative analysis of surface roughness by both CLSM and SEM provided Ra by non-contact method, which was effective to evaluate the structural change of tooth after laser irradiation.

Imaging and Non-Contact Profile Analysis of Nd:YAG Laser-Irradiated Teeth by Scanning Electron Microscopy and Confocal Laser Scanning Microscopy

M.K. Yamada and F. Watari

Dental Materials Journal, 22, 556-568 (2003)

Two types of non-contact optical profilometers, one performing scanning electron microscopy (SEM) installed with a 3D analyzer and another performing confocal laser scanning microscopy (CLSM) were applied to evaluate imaging and surface profiles simultaneously on enamel and dentin after Nd: YAG laser irradiation. The results were correlated with a stylus profilometer. Surface roughness (Ra) was also measured. Laser was applied perpendicularly to vertical sections of human extracted caries-free molars. Analysis was done on the same spot of the same specimen by both SEM and CLSM for comparison. After irradiation, enamel produced a flake-like surface and dentin resulted in a melted globule surface. SEM and CLSM gave similar surface profiles and different image contrast. The Ra obtained by CLSM was larger than that by SEM. Both SEM and CLSM provided a non-contact evaluation of tooth structural change by laser irradiation through surface analysis in selected micro areas, which was not possible using the stylus profilometer.

Change of Mechanical Properties of Esthetic Orthodontic Wire with Fiber Reinforced Plastic Structure in Wet Condition

S.Tanaka, F.Watari, J.Iida

The Journal of Japanese Society of Dental Materials and Devices, 23, 29-39, (2003)

FRP esthetic orthodontic wires are fabricated from CPSA glass fibers and Bis-GMA resin. The water absorption and change of mechanical properties were investigated in wet condition to simulate use in the oral cavity. As a result, the mechanical properties declined after water absorption for 3-6 hours. Decline of load and micro fracturing were found to be correlated by acoustic emission measurement during the stress relaxation test. In wet condition, AEs was 5-9 times higher than in dry condition. Silane-coupling suppressed the generation of micro fractures and decline of load. The modulus of longitudinal elasticity and load at 2mm deflection in the flexural test was reduced by half and the permanent deflection increased after 24 hours under 2mm fixed bending in wet condition. These changes were well represented using the energy required for 2mm deflection as a single evaluation index. Silane-coupling agent decreased the exfoliation of glass fiber/matrix interface and suppressed the decline of mechanical properties.

Static-Dynamic Friction Transition of FRP Esthetic Orthodontic Wires on Various Brackets by Suspension-Type Friction Test

N.Suwa, F.Watari, S.Yamagata, J.Iida, M.Kobayashi

Journal of Biomedical Material Research Part B: Applied Biomaterials 67B: 765-771, (2003)

A new testing apparatus for the measurement of friction properties was designed and the friction coefficients were obtained and compared with each other in various combinations of brackets and orthodontic wires, including esthetic fiber-reinforced plastic (FRP) wire that was especially designed and manufactured. Three kinds of wires (stainless steel, nickel-titanium, and FRP) and four brackets (single-crystal alumina, polycrystalline alumina, polycarbonate, and stainless steel) were used. The testing was done under dry and wet conditions. The friction testing equipment was designed to attach the bracket to a C-shaped bar suspended with a variable mass, and sliding along a fixed wire. The transition between static and dynamic friction was as a breakaway force, with the use of a universal test machine. In addition to material properties, this testing fixture eliminates geometrical factors, such as the rotational moment at the edge of the bracket slot, deflection of the orthodontic wire, and tension of the ligature wire. Nearly ideal frictional properties between materials are obtained. The frictional properties between materials are obtained. The frictional properties of FRP wire were similar to those of metal wires on all brackets, except the polycrystalline alumina bracket. The frictional coefficient between the polycrystalline ceramic bracket and FRP wire was larger than that of other combinations. There was little difference in frictional coefficients between dry and wet conditions.

Effects of Micro/Nano Particle Size on Cell Function and Morphology

K. Tamura, N. Takashi, T. Akasaka, I. D. Rosca, M. Uo, Y. Totsuka, F. Watari

Bioceramics 16, 909-913, (2003)

The cytotoxicity of micro/nano particles in Ti, TiO2 and carbon nanotube was investigated by in vitro biochemical analyses using human neutrophils. The particles smaller and larger than the neutrophils were used to determine the relationship between cell and particle size with respect to cytotoxicity. As the particle size decreased, the cell survival rate was decreased and, with the good corresponding relation to this, the value of lactate dehydrogenase (LDH), which is the indication of cell disruption, was increased. The release of superoxide anion showed the increasing tendency. Proinflammatory cytokines were detected distinctly for 3µm or smaller particles and very little in more than 10µm, which is closely related to the phagocytosis by neutrophils. ICP elemental analysis showed that the dissolution from Ti particles was below detection limit. Micro and nano particles stimulated the cell reactions according to the results of the human neutrophil functional tests. As the particle size was smaller, the inflammation was pronounced. The fine particles less than 3µm caused distinctly the inflammation in the surrounding tissue. All these results indicated that the cytotoxicity was induced due to the physical size effect of particles, which is different from the ionic dissolution effect. The clinical phenomenon confirmed the result obtained in vitro cell tests. The neutrophils stimulated by fine particles may cause the inflammatory cascade and harm the surrounding tissue.

Effect of Sphered Particles on the Firing Contraction of Porcelain Inlay Processed by Cold Isostatic Pressing

J.Konishi, F.Watari, C.Kawamoto, H.Sano

Journal of Biomedical Materials Research PartB, 66B, 553-558, (2003)

The effect of the sphered particles on the contraction ratio of porcelain inlay processed by the cold isostatic pressure (CIP)method was investigated. The conventional lathe-cut porcelain powder was crushed to ner particles and the secondary particles with spherical shape by adding binders of acrylic resin, wax, and polyvinyl alcohol, respectively. Porcelain powder was molded as a disc-shaped green body in a refractory model and compressed at 200 MPa by CIP. From this green compact, the sintered porcelain was obtained by only one step of ring. The porcelain discs were then used for the measurements of contraction ratio, scanning microscopic observation, biaxial exure strength, Vickers hardness, and density. Firing contraction was decreased to about 1% in the sphered particle groups, compared with 7% of the lathe-cut porcelain powder. Although biaxial exure strength was about 85 MPa, which is lower than the 120 MPa of the control group, and the density was signi cantly decreased by about 10% from the 2.4 g/cm 3 of the control substance, Vickers hardness, which ranged from 531 to 537, showed no signi cant differences among all of the groups. The CIP method could save labor in the process of making porcelain inlays, and sphered powders could contribute signi cantly to a decrease in the contraction ratio in the sintering process.

Influences of Structure and Composition on Growth of Anodic Oxide Films on Ti-Zr Alloys

H. Habazaki, M. Uozumi, H. Konno, K. Shimizu, S. Nagata, K. Asami, K. Matsumoto, K. Takayama, Y. Oda, P. Skeldon and G. E. Thompson

Electrochimica Acta, 48, 3257-3266 (2003)

Sputter-deposited Ti-Zr alloys of various compositions were anodized at a constant current density in 0.1 mol dm⁻³ ammonium pentaborate electrolyte at 298 K. The resultant anodic films were characterized using TEM, glow discharge optical emission spectroscopy (GD-OES), Rutherford backscattering spectroscopy and capacitance measurements to elucidate the influence of alloy composition on their structure, growth behavior and dielectric properties. The Ti-10.5 at.% Zr alloy reveals oxygen formation within the film .gtorsim.40 V, associated with crystallization of the anodic oxide to anatase. But amorphous anodic films, with a thin outer layer consisting of Zr-free TiO₂, grow up to ~250 V on Ti-23.0 at.% Zr and Ti-42.0 at. % Zr alloys at high current efficiency. Further increase in Zr content to 62.5 at.% gave a film containing nanocrystals of monoclinic ZrO₂ phase in an amorphous matrix. The crystalline oxide is formed predominantly in the inner region of the film that is developed by anion migration inward. An anodic film composed of monoclinic ZrO₂ throughout the film thickness is formed on the Zr. The influences of structure and composition of the anodic films on their growth behavior and dielectric properties are discussed and compared with findings for Al-Ta alloys, which form amorphous oxides over the entire composition range.

Grain Orientation Effects on Copper Enrichment and Oxygen Generation During Anodizing of an Al-Lat.%Cu Alloy

Y. Liu, E. A. Sultan, E. V. Koroleva, P. Skeldon, G. E. Thompson, X. Zhou, K. Shimizu and H. Habazaki

Corrosion Science, 45, 789-797 (2003)

Anodizing of solid-solution Al-lat.% Cu alloy in ammonium pentaborate electrolyte is shown to develop two distinct types of amorphous film. On alloy grains of {100} orientation, the alumina film is of uniform thickness and relatively featureless. For other grains, the film is of non-uniform thickness and contains oxygen bubbles. In both cases, copper species are distributed throughout the film. Copper is enriched in the alloy to similar to 5.8 x 10¹⁵ Cu atoms cm⁻² for bubble-free grains, with similar or slightly lower levels for other grains. Evidently, copper enrichment alone does not lead to generation of oxygen. Other factors suggested to be involved, each dependent upon grain orientation, are the structure of the enriched alloy layer, the cyclic nature of the oxidation of copper, and the generation of modulated film compositions.

Behavior of Hydrogen Impurity in Aluminum Alloys During Anodizing

L. Iglesias-Rubianes, P. Skeldon, G. E. Thompson, U. Kreissig, D. Grambole,
H. Habazaki and K. Shimizu

Thin Solid Films, 424, 201-207 (2003)

The present study examines the behavior of hydrogen impurity in an Al-6.5 at.% W alloy during anodizing, using elastic recoil detection and nuclear reaction analyses. Increased concentrations of hydrogen are found near the alloy/anodic film interface, amounting to approximately 2×10^{15} H atoms cm⁻² for the particular alloy, containing 0.1-0.3 at.% hydrogen in the bulk regions, and conditions of anodizing. The enrichment arises from hydrogen in the alloy (i) diffusing to the interface, which acts as a trap, or (ii) accumulating at the interface, due to the growth of the anodic film, or a combination of both processes. Diffusion is consistent with the known mobility of hydrogen in aluminum near ambient temperature Further, accumulation, and subsequent oxidation, of hydrogen are expected based on the general behavior of alloying elements in anodized aluminum. The anodic films contained approximately 0.1-0.3 at.% hydrogen, originating from either the electrolyte or the alloy.

Morphology of Enriched Alloy Layers in an Anodized Al-Cu Alloy

S. Garcia-Vergara, P. Skeldon, G. E. Thompson, P. Bailey, T. C. Q. Noakes, H. Habazaki and K. Shimizu

Applied Surface Science, 205, 121-127 (2003)

Using medium energy ion scattering, combined with Rutherford backscattering spectroscopy, transmission electron microscopy and atomic force microscopy, the development of the copper-enriched alloy layer during anodizing of a sputtering-deposited Al-0.4 at.% Cu alloy has been examined. The enriched layer is located just beneath the amorphous alumina film that is produced on the anodized alloy. Importantly for understanding the mechanism of formation of the enriched layer, the layer is revealed to be of thickness similar to2.1 nm from the start of the anodizing, when enrichment of copper is very low, with no significant increase in the thickness of the layer as the copper enriches to similar to3 x 10¹⁵ Cu atoms cm⁻², the maximum measured in the present experiments. The findings are consistent with a model of the layer in which the copper is present mainly in copper-rich clusters.

Preparation and Characterization of Layered Manganese Oxide (Birnessite) and Its Intercalation Reactions

Hiroki Tamura, Kyosuke Nakamura, Takashi Takeda and Shinichi Kikkawa

J. Ion Exchange, 14, 133-136 (2003)

Layered manganese oxide (birnessite) was prepared by oxidation of Mn(NO₃)₂ with H₂O₂ in NaOH solutions. The product had a composition of Na⁺_{0.44}(Mn^{III}_{0.44}Mn^{IV}_{0.56}O₂)^{0.44} • 0.5H₂O and the negative charge of the host MnO₂ layer due to Mn^{III} was counterbalanced by Na⁺ in the interlayer. This Na-birnessite was treated with a hydrochloric acid solution to exchange Na⁺ with H⁺. The H-birnessite obtained was further treated with an *n*-propylamine solution, and the interlayer distance nearly doubled to 1.41 nm by the incorporation of propylammnonium ions (PA). The PA-birnessite was suspended in a VCl₃ solution, and V ions were intercalated. The V-birnessite had a composition of V⁵⁺_{0.08}(H_{0.3}Mn^{III}_{0.7}Mn^{IV}_{0.3}O₂)^{0.4-} • 0.3H₂O, and it was found that the interlayer V ion was oxidized to 5+, possibly by Mn^{IV} in the host layer. This compound was expected to show better charge-discharge properties as a battery material than Na-birnessite, since multi-valent V⁵⁺ ions were likely to attract the layers more strongly and to support the layered structure more firmly.

A Protective Film Component among Corrosion Products on Galvanized Steels Estimated by Solubility Calculations

Hiroki Tamura

Tetsu-to-Hagane, 89, 1165-1169 (2003)

Galvanized steels are used extensively in atmospheric environments because of their high resistance to corrosion as well as their low cost of production. The corrosion resistance arises from the slow corrosion rate of the zinc layer that covers the steel (coating and shielding effect) and the low corrosion potential of zinc which keeps the steel under a reducing condition as long as zinc remains (sacrifice effect). However, detailed examination of the corrosion processes has shown that galvanized steels exhibit some corrosion resistance after the disappearance of metal zinc by corrosion. This effect has been ascribed to a protective nature of corrosion products from the zinc layer. It is important to establish the protective components of corrosion products for the elucidation of corrosion mechanisms and for the development and improvement of corrosion protection technologies. In this investigation, zinc oxide, zinc carbonate, basic zinc carbonate, and zinc ferrite were chosen as model corrosion products, it was noted that protective films must have very low solubilities and very low dissolution rates for them to persist, and their dissolution properties were examined by solubility calculations. The solubilities of zinc oxide, zinc carbonate, and basic zinc carbonate are similar and very large, indicating that these would be dissolved away in atmospheric environments. A further corrosion product, zinc ferrite, is not a major component, but can be formed as a thin layer by the corrosion of the zinc-steel alloy phase. The solubility product of zinc ferrite was estimated from thermodynamic data and its solubility was calculated. The solubility is very small and it can be concluded that zinc ferrite is the most likely protective film component among the zinc compounds described above. (Japanese)

Construction of Photosynthetic Antena Complex Using Light-harvesting Polypeptide-α from Photosynthetic Bacteria, R. rubrum with Zinc Substituted Bacteriachlorophyll a

M. Nagata, M. Nango, A. Kashiwada, S. Yamada, S. Ito, N. Sawa, M. Ogawa, K. iida, Y. Kurono, and T. Ohtsuka

Chemistry Lett., 32, 216-217 (2003)

The light-harvesting (LH)-α polypeptide isolated from *R-rubrum* only organized zinc bacteriochlorophyll a (Zn-Bchl a) complex in n-octyl-β-D-glucopyranoside (OG) miscelle, analogous to the LH 1-type complex of photosysnthetic bacteria.

Study of Cathodic Dissolution of an Aluminum Wire Electrode using AC Resistometry

T. Ueno, K. Azumi and M. Seo

J. Electroanal. Chem., 540 (2003) 97-104

Electric resistances of Al wire electrodes immersed in various electrolyte solutions were measured during potentiodynamic polarization. An increase in resistance due to Al dissolution was observed in the cathodic potential range. Al dissolution occurred due to a rise in pH in the electrolyte solution near the surface under hydrogen evolution. The amount of dissolution was estimated from the change in resistance and was found to be dependent on ionic species, pH and concentration of the electrolyte solution. In an acidic solution, a cathodic current peak appeared in the i-V curve. This peak was formed by suppression of cathodic reaction due to formation of a precipitation film of Al hydroxide covering the surface. Precipitation occurs when Al ions dissolved from the surface meet the neutral solution region formed between the alkalized solution near the surface and the acidic solution of bulk electrolyte solution. The precipitation film of Al hydroxide is transformed to the oxide in the following potential sweep and suppresses cathodic reaction in subsequent potential sweep cycles.

Experimental Simulation for Zincate Pretreatment of Al Pad Connected to LSI Circuit

K. Azumi, Y. Koyama and S. Kawashima

J. Surf. Fin. Soc. Jpn., 54 (2003) 422-427

Small Al electrodes connected to the pins of model IC was subjected to zincate pretreatment to simulate the plating process in LSI manufacturing line. From SEM observation deposition of Zn and dissolution of Al substrate depended on the potential of Al electrodes under the potentiostatic polarization in the zincate solution. Difference in electric impedance of IC pins affected the immersion potential of Al electrodes in the zincate solution and thus amount of Zn deposition. Visible light illumination to the separated p-Si electrode additionally connected to the power supply pin of IC generated photocurrent. This caused a shift in immersion potential of Al electrodes connected to the other pins of IC in a noble direction, resulting in suppression of Zn deposition in the zincate pretreatment. (Japanese)

Changes in Surface Stress of Platinum Electrode in Acidic and Alkaline Sulfate or Alkaline Fluoride Solutions

M. Seo and Y. Serizawa

J. Electrochem. Soc., 150 (2003) E472-E47

The changes in surface stress of platinum electrode in acidic and alkaline sulfate or alkaline fluoride solutions were measured by a bending beam method in connection with the surface oxygenation reaction of platinum. The surface stress took a maximum in the electric double layer potential region of platinum. The potential of surface stress maximum obtained in the anodic potential sweep showed the dependences of -40 mV / pH in acidic sulfate solution and of -90 mV / pH in alkaline sulfate and fluoride solutions, respectively, indicating the strong specific adsorption of OH ion on platinum in alkaline solutions.

It was found that the derivative of surface stress with electrode potential took a maximum in the potential range corresponding to the onset of surface oxygenation reaction for formation of PtOH_{ad} and deviated upward from the surface charge density estimated from the cyclic voltammogram. The potential at which the derivative of surface stress with electrode potential took a maximum, showed the dependence of -68 mV / pH in the wide pH range, irrespective of anion species (sulfate or fluoride ions). It has been pointed out that the difference between the derivative of surface stress with electrode potential and the surface charge density increases when the surface charge transfer reaction of adsorbed ion such as surface oxygenation reaction takes place on noble metal.

Study on Initiation of Localised Corrosion on Copper Thin Film Electrode by Combinational Use of an EQCM with a Liquid-phase Ion Gun

F. Falkenberg, K. Fushimi and M. Seo

Corros. Sci., 45 (2003) 2657-2670

A new method allowing simultaneous measurements of anodic currents and small mass changes during initiation and early growth of a single localised corrosion site was discussed. An electrochemical quartz crystal microbalance (EQCM) was combined with a liquid-phase ion gun consisting of an Ag/AgCl microelectrode which produces chloride ions, causing local breakdown of passive film and pit growth. The method was applied to copper thin films polarised anodically at 0.6 or 0.8 V (SHE) in pH 8.4 borate buffer solution. It was found from comparison between coulometry and gravimetry that copper dissolves as Cu^{2+} during the pit growth. The shape of the pit was almost circular and the average pit current density, $i_p = 25$ A cm⁻² was evaluated from the kinetics of 2D pit growth.

Effect of pre-oxidation on the corrosion behavior of Fe-40Al sheet in a N₂-11.2O₂-7.5CO₂-500ppmSO₂ Atmosphere at 1273K

F. Lang, Z. Yu, S. Gedevanishvili, S. C. Deevi and T. Narita

Intermetallics, 11 129-134 (2003)

A 200 μm thick Fe-40Al sheet, produced by powder metallurgy and hot extruding, was pre-oxidized at 1373K in air for different times and then the pre-oxidized specimens were corroded at 1273K for up to 360ks in a N₂ - 11.2vol%O₂-7.4vol%CO₂-500ppmSO₂ atmosphere. The pre-oxidation followed a parabolic rate law, forming continuous, adherent α-Al₂O₃ oxide scales, accompanied by the formation of valley-like flaws. The valley-like flaws originated from the inclusion of additives in the alloy substrate. The inclusion of additives as α-Al₂O₃ in the Fe-40Al sheet leads to some local exfoliation of the oxide scale in the SO₂ containing atmosphere. The Fe-40Al pre-oxidized for longer than 14.4ks showed very good corrosion resistance in the N₂-11.2vol%O₂-7.4vol%CO₂- 500 ppmSO₂ atmosphere, and there is little exfoliation of the oxide scale after 360ks oxidation at 1273K.

Corrosion Behavior of Fe-40Al Sheet in N₂-11.2O₂-7.5CO₂ Atmospheres with Various SO₂ Contents at 1273K

F. Lang, Z. Yu, S. Gedevanishvili, S. C. Deevi, S. Hayashi and T. Narita

Intermetallics, 11 135-141 (2003)

A 200 μ m thick Fe-40at%Al sheet, produced by powder metallurgy and hot extruding, was corroded at 1273K for up to 360ks in N₂ -11.2vol%O₂ -7.4vol%CO₂ atmospheres containing 100, 500, or 2000 ppmSO₂. The alloy oxidized rapidly at the very initial stage of corrosion, forming sulfides in addition to both θ - and α -Al₂O₃ scales, and it was suggested that sulfides may be formed by direct reaction of SO₂ gas molecules with the alloy. Sulfide or dissociated sulfur at the alloy-scale interface may promote exfoliation of the external scale. With further oxidation, the oxide scale consisted solely of α -Al₂O₃, and grows obeying a parabolic rate law. The parabolic rate constants are between 5.5x10⁻¹² and 7.2x10⁻¹² kg²m⁻⁴s⁻¹, independent of SO₂ concentration. After 360ks of corrosion the Al content in the alloy sheet remained at about 38at%Al, with an almost flat profile across the entire sheet.

Two-Step Cr and Al Diffusion Coating on TiAl at High Temperatures

T. Nishimoto, T. Izumi, S. Hayashi and T. Narita

Intermetallics, 11 225-235 (2003)

The formation of an oxidation resistive coating layer on a TiAl alloy was investigated with a two- step Cr (at 1573K for up to 72ks) and then Al (at temperatures between 1273 and 1573K for 36ks) pack diffusion process at high temperatures. The coated TiAl was oxidized in air at 1173K for up to 1,252.8ks under a thermal cycling condition. The Cr diffusion coating layer consisted of γ , β , and Laves phases, which were transformed during cooling from the β -phase formed at 1573K. The coating layer formed by the Al diffusion at 1473 and 1573K consisted of an outermost TiAl₂, outer Al-rich γ -TiAl, intermediate γ , β , and Laves phases, and a diffusion zone; there is little Al-diffusion at 1273 and 1373K. The TiAl coated by the two-step Cr and Al diffusion process at 1573K showed very good oxidation resistance in air at 1173K due to the formation of a protective α -Al₂O₃ scale. After oxidation for up to 1,252.8ks the coating layer maintained a structure with three phases γ , Laves, and β , which acts as a diffusion barrier to Al and Ti.

Effect of Coating Layer Structures and Surface Treatments on the Oxidation Behavior of a Ti-50at%Al Alloy

T. Nishimoto, T. Izumi, S. Hayashi and T. Narita

Intermetallics, 11 459-466 (2003)

A Ti-50at%Al alloy, coated by a two-step Cr (at 1573K for 7.2 and 18ks) and Al-diffusion (at 1573K for 36ks) process, was oxidized in air under thermal cycling between 1173K and room temperature for up to 3,600ks. The coated layer consisted of a three layer structure: an outermost TiAl₂ (τ phase), outer TiAl (Al-richy-phase), and intermediate γ , β , and Laves phase layers. The coated TiAl with an intermediate layer of a fine, three phase structure oxidized slowly due to a protective α -Al₂O₃ layer, while a coarse structured coating was oxidized catastrophically due to the formation of cracks. Vickers hardnesses of a β and Laves mixture as well as a γ and Laves one are around $700 \sim 800$ Hv, whereas the τ phase and a γ and τ mixture showed $300 \sim 400$ Hv. The Al content and its profile in the outermost and outer layers were almost unchanged before and after the 3,600ks oxidation, and it seems to arise from a slow diffusion of Al, Ti, and Cr through the three-phase intermediate layer. It was suggested that the fine, three-phase structured coating layer was very effective to suppress degradation due to both mutual diffusion and cracking.

Isothermal Oxidation Behavior of A Sheet Alloy of Fe-40at%Al at Temperatures between 1073 and 1473K

F. Lang, Z. Yu, S. Gedevanishvili, S. C. Deevi and T. Narita

Intermetallics, 11 697-705 (2003)

A sheet Fe-40at, %Al alloy with 200µm thickness was oxidized isothermally in air at temperatures between 1073 and 1473K for up to 608.4Ks. The oxidation behavior was classified into three temperature ranges. At temperatures below 1223K a mixture of α-and θ-Al₂O₃ grew fast, followed by slow oxidation with the formation of only α -Al₂O₃. The initial rapid oxidation is due to the formation of θ-Al₂O₃. Between 1273 and 1323K the oxidation obeyed a parabolic rate law over the whole oxidation time with the formation of α -Al₂O₃ scale, except for the very initial stage of oxidation up to 3.6ks. At temperatures above 1423K the parabolic rate constants tended to decrease with oxidation time, while the oxide grain size of the columnar structure increased by 3 to 4 times. The change in the parabolic rate constants with time at 1473K was reasonably well explained using the oxygen inward diffusion model along the grain boundary with a hypothetical width of 2 nm. The Fe-40Al showed the lowest oxidation rate and the activation energies for a parabolic Al₂O₃ growth are 422 kJ/mol above 1273K and 241 kJ/mol below 1223K. Oxide scale exfoliation was not observed for the Fe-40Al oxidized isothermally in air at the experimental temperatures here.

Formation of Nickel Aluminide Coating on γ -TiAl Alloy

T. Izumi, T. Nishimoto and T. Narita

Intermetallics, 11 841-848 (2003)

A nickel aluminide coating process was developed on y-TiAl alloy by electroplating a Ni film followed by a high Al activity pack cementation carried out in a vacuum with a mixture of fine Al, NH₄Cl, and Al₂O₃ powders at 1273K for 18ks. The coating has a duplex layer structure, an outer Ni₂Al₃ layer and an inner TiAl₃ / TiAl₂ / TiNiAl₂ layer. The coated TiAl was oxidized in air for up to 3,600ks under thermal cycling between room temperature and 1173K. A protective Al₂O₃ scale formed with little oxide exfoliation and the oxidation amount was 8 g/m² after the 3,600ks oxidation. During oxidation at 1173K the as-coated layer structure changed from an outer Ni₂Al₃ and inner TiAl₃ / TiAl₂ / TiNiAl₂ layers to an outer β-NiAl and inner TiAl₂ and TiNiAl₂ layers with voids in the outer layer. The voids appear to be formed by the phase change from the Ni₂Al₃ to β-NiAl during oxidation. A part of the Ti-Al-Ni phase diagram at 1173K was developed experimentally and it was shown that the solubility limits of Ti into both the Ni₂Al₃ and β-NiAl phases were less than 0.5at%. The coating with more Al in the inner layer that in the outer layer would be formed by inward diffusion of Al, caused by a so-called up-hill diffusion phenomenon. The higher Al content in the inner layer was retained after 3,600ks oxidation.

Coatings of Nb-based Alloy by Cr and/or Al Pack Cementations and Its Oxidation Behavior in Air at 1273-1473 K

M. Fukumoto, Y. Matsumura, S. Hayashi, T. Narita, K. Sakamoto, A. Kasama and R. Tanaka

Materials Transactions, 44 731-735 (2003)

An Nb-5Mo-15W alloy (mass%) was surface-treated in vacuum by Cr and/or Al pack cementations, and the oxidation behavior of the coated alloys was investigated in air at temperatures up to 1473 K for 32.4 ks. The Al packed alloy formed a coating layer with the outer NbAl₂ and the inner Nb₃Al, and showed poor oxidation resistance. The Cr packed alloy formed a coating with outer α -Cr and inner Cr₂Nb layer, and showed good oxidation resistance up to 1373 K. The alloy packed with Cr and then Al formed a coating layer with outermost α -Cr(Al), outer α -Cr(Nb), and inner Cr₂Nb layers, and this coated alloy showed good oxidation resistance up to 1473 K by forming an Al₂O₃ scale.

Evaporation of Cr₂O₃ in H₂O-Containing Atmospheres

A. Yamauchi, K. Kurokawa and H. Takahashi

Oxid. Met. 59, 517-527, (2003)

In oxidation of Type 430 at 1473 K in H₂O-containing atmospheres, there is an induction period in the early stage of oxidation, in which a Cr₂O₃ scale is formed. After the period, formation of a nodule-like scale is caused by degradation of the Cr₂O₃ scale. Then an external scale consisting of an iron oxides and an inner scale consisting of an Fe-Cr spinel oxide are formed, resulting in drastic increase in mass. In the present study, to discuss the degradation of a Cr₂O₃ scale by H₂O vapor, the evaporation behavior of Cr₂O₃ in H₂O-containing atmospheres was investigated. The sintered Cr₂O₃ was heated for up to 360 ks at 1473 K in N₂-3%O₂, N₂-2.4%O₂-19.7%H₂O, and N₂-19.7%H₂O, and the mass losses were measured by a micro balance. The mass losses in N₂-3%O₂ and N₂-19.7%H₂O were almost identical and the rates of the mass losses was about 8×10⁻⁹ kg/m²s. On the other hand, the rate of the mass loss in N₂-2.4%O₂-19.7%H₂O was 5×10⁻⁸ kg/m²s. Therefore, it can be concluded that the degradation of a Cr₂O₃ scale is likely to occur in mixed atmospheres of oxygen and H₂O vapor. Volatilization of Cr₂O₃ may be mainly based on the following reaction:

$$Cr_2O_3(s)+3/2O_2(g)+2H_2O(g)=2CrO_2(OH)_2(g)$$
.

The evaporation rate of Cr_2O_3 in N_2 -2.4% O_2 -19.7% H_2O is roughly comparable to the growth rate of the Cr_2O_3 scale in N_2 -3% O_2 . Therefore, the steady growth of a Cr_2O_3 scale could be prevented by the evaporation of Cr_2O_3 .

TEM Observation of SiO₂ Scales Formed on MoSi₂

J. Kuchino, D. Goto, K. Kurokawa, T. Shibayama, and H. Takahashi

Proc. of Inter'l Conf. on Designing of Interfacial Structures in Advanced Materials and their Joints, CD-ROM, .1-6, (2003)

The microstructures of scales formed on MoSi₂ at high temperatures in air were observed by TEM, and crystallization of amorphous SiO₂ scales was investigated. At 1273 K and 1373 K, the scales had a structure consisting of amorphous SiO₂ with small amounts of fine MoO₃ grains. The scales at 1573 K and 1773 K had a structure consisting of amorphous and crystalline SiO₂. Growth rate of the scale formed at 1773 K appreciably increased with increase in the crystallization of amorphous SiO₂. It was thought that the increase in the oxidation rate at 1773 K was caused by a change in the diffusion mechanism from O₂ diffusion to lattice diffusion of O² through SiO₂. In addition, the diffusion coefficient of oxygen was estimated from the growth rate of SiO₂ scale.

Structure and Oxidation Resistance of MoSi₂ Synthesized by Spark Plasma Sintering

J. Kuchino, K. Kurokawa, T. Shibayama, and H. Takahashi

Advances in Applied Plasma Science, 4, 451-454, (2003)

The mixed powders consisting of elemental Mo and Si were sintered at 1673 K with a spark plasma sintering method, and structure and oxidation resistance of the sintered MoSi₂ were studied. As the result, fully dense MoSi₂ which little contain SiO₂ inclusions was fabricated. Oxidation behavior in the accelerated oxidation temperature region for MoSi₂ showed that occurrence of simultaneous oxidation of Mo and Si was remarkably suppressed.

Fabrication and Oxidation Resistance of Metal Disilicides for Ultra-High Temperature Applications

K. Kurokawa

NSG Materials Science and Engineering Report, No. 21, 211-217, (2003)

Some of metal disilicides are receiving much attention as high-temperature materials having extremely-high oxidation resistance based on the formation of a protective silica scale. However, the mechanism of oxidation of the disilicides has not been clarified. In other words, it is not known that a protective silica scale is formed in what kind of disilicides. Therefore, this study focuses on the classification of oxidation mode in the disilicides.

A spark plasma sintering (SPS) method was applied for sintering of the disilicides such as MoSi₂, WSi₂, TaSi₂, NbSi₂, FeSi₂, CoSi₂, CrSi₂, VSi₂, and ReSi_{1.75}. The sintering behavior showed that the temperature of commencement of sintering was independent on the melting point of the disilicide. This suggests that spark between particles in the initiation of sintering assists the sintering. As a result, the application of the SPS method for the sintering of the disilicides enabled the fabrication of fully-dense sintered body.

High temperature oxidation tests of the sintered disilicides were carried out at the temperature range from 773 to 1773 K in air. The oxide scales were conveniently classified into three groups: (1) formation of a mixed oxide scale consisting of metal oxide and SiO₂ (TaSi₂, NbSi₂, CrSi₂) (2) formation of a SiO₂ scale by selective oxidation of Si (FeSi₂, CoSi₂,), and (3) formation of a SiO₂ scale by evaporation of metal oxide (MoSi₂, WSi₂, VSi₂, ReSi_{1.75}), though the scale structure depends on temperature. These results demonstrated that FeSi₂, CoSi₂, and CrSi₂ had high potential as high temperature materials having outstanding oxidation resistance at the temperatures below 1273 K, and MoSi₂, WSi₂, and VSi₂ at higher temperatures. (Japanese)

The Sulfidation and Oxidation Behavior of Sputter-Deposited Nb-Al-Cr Alloys at High Temperatures

H. Habazaki, K. Yokoyama and H. Konno

Corrosion Science and Technology, 2, 141-147 (2003)

Sputter-deposited Nb-Al-Cr alloys, 3-5 µm thick, have been prepared on quartz substrates as oxidation- and sulfidation-resistant materials at high temperatures. The oxidation of the alloys in the Ar-O₂ atmosphere of an oxygen partial pressure of 20 kPa follows approximately the parabolic rate law, thus being diffusion controlled. Their oxidation rates are almost the same as or even lower than those of the typical chromia-forming alloys. The multi-layered oxide scales are formed on the ternary alloys. The outermost layer is composed of Cr₂O₃, which is mainly responsible for the high oxidation resistance of these alloys. In contrast to sputter-deposited Cr-Nb binary alloys reported previously, the inner layer is not porous. TEM observation as well as EDX analysis indicates that the innermost layer is a mixture of Al₂O₃ and niobium oxide. The dispersion of Al₂O₃ in niobium oxide may be attributable to the prevention of the formation of the porous oxide layer. The sulfidation rates of the present ternary alloys are higher than those of the sputter-deposited Nb-Al binary alloys, but still several orders of magnitude lower than those of conventional high temperature alloys. Two-layered sulfide scales are formed, consisting of an outer Al₂S₃ layer containing chromium and an inner layer composed of NbS2 and a small amount of Cr2S3. The presence of Cr2S3 in the inner protective NbS₂ layer may be attributed to the increase in the sulfidation rates.

Anodic dissolution of TiAl surface as a pretreatment for Al-Anodic Dissolution of TiAl Surface as a Pretreatment for Al-Cr electroplating

Mikito Ueda, Daigo Susukida, Shoichi Konda, and Toshiaki Ohtsuka

J. The Surface Finishing Society of Japan 54, 363-366 (2003)

Anodic stripping of TiAl surface was carried out in AlCl₃-NaCl-KCl molten salt at 423K as a pretreatment of the deposit formation of Al-Cr alloy layer. The Al-Cr alloy deposit on the TiAl much improve the corrosion resistance of high temperature oxidation. In anodic stripping at 0.4 V vs. Al/Al³⁺, anodic dissolution of surface occurred ununiformly. On the other hand, oxide film on TiAl was completely removed by uniform anodic dissolution at 1.2 V with electricity of 1 C cm⁻². Al-Cr electroplating layer which was formed after the anodic stripping at 1.2 V, exhibited excellent oxidation resistance which was confirmed by an oxidation test at 1173 K for 24 h. (Japanese)

Direct Electroless Ni-P Plating to Sputter Deposited Al-Ni Alloy Films

K. Azumi, T. Yugiri, T. Kurihara, M. Seo, H. Habazaki, and S. Fujimoto

J. Elechtrochem. Soc., 150 (2003) C461-C464

Direct plating of electroless Ni-P layers on Al-Ni alloy films formed on glass substrates was performed using magnetron sputtered deposition and ion beam-assisted deposition methods. Dissolution of Al from the alloy films occurred in the initial stage of the plating process and resulted in enrichment of Ni on the surface. Since Ni acts as a catalyst for the Ni-P deposition reaction, Ni-P deposition occurs on the alloy surface without zincate pretreatment. In the case of an Al-10Ni alloy film, however, Ni clusters dropped from the Al-Ni alloy surface, and Ni-P particles grew in the plating bath, causing dissipation of chemicals in the bath. Such particles also re-adhered to the surface, resulting in a non-uniform plating layer. A lower concentration of Ni in an alloy such as an Al-3Ni or Al-1Ni alloy resulted in a rather smooth plating surface. In the case of a neutral plating bath containing a low concentration of P, cone structures were formed in the plating layer. Such structures seem to form at the nucleation sites of Ni deposition in the initial stage of the plating process.

Novel Micro-Patterning of Aluminum Surface by Anodizing and AFM-Processing

Z. Kato, M. Sakairi, and H. Takahashi

Zairyo-to-Kankyo, 52, 12-17 (2003)

Aluminum specimen covered with thin barrier type anodic oxide films was scratched with Si tip of AFM probe in a CuSO₄ solution, and then cathodically polarized in the solution, using the Si tip as a counter electrode. During AFM probe scratching, oscillation of current was observed and decreased with scratching time. Analysis of the current oscillation enable to examine the proceeding of the removal of anodic oxide films during AFM probe scratching. Silicon tip wore easily by scratching the oxide film-covered aluminum with a force. After AFM probe scratching, cathodic polarization of aluminum specimen caused the Cu deposition only at the film removed area, using a nitrocellulose film-coated Si tip as a counter electrode. (Japanese)

Fabrication of Micro-Printed Circuit Board by Aluminum Anodizing and Laser Irradiation - Influence of Thickness of Oxide Film on Formation of Pattern -

T. Kikuchi, M. Sakairi, H. Takahashi, Y. Abe, and N. Katayama

J. Surf. Fin. Soc. Jpn., 54, 137-144 (2003)

Aluminum specimen covered with porous type oxide films with 3 to 54 μm thickness was irradiated by a pulsed Nd-YAG laser through a convex lens with 20 mm focal length in a solution to examine the mode of oxide film removal by laser A prototype printed circuit board was fabricated using laser irradiation. Thin oxide films were removed irradiation and Au electroplating. instantaneously after laser irradiation onset by the laser ablation mechanism. Thick oxide films were destructed initially from the upper part of oxide films by the thermal shock mechanism, and then by the laser ablation mechanism. laser irradiation after the film removal caused the formation of many cracks in the oxide film surrounding irradiated area. By scanning laser beam on specimen covered with oxide films with 9 µm thickness, the oxide film was removed uniformly with 30 µm line width. Fine pattern coils of 30 µm wide Au lines were fabricated on the insulating board by consecutive processes of aluminum anodizing, laser irradiation, Au electroplating, resin attaching, and removal of aluminum substrate and oxide film. (Japanese)

Anodizing of Aluminum Coated with SiO₂ by Sol-Gel Coating - Formation of New Type Anodic Oxide Film with High Voltage Sustainability -

K. Watanabe, M. Sakairi, H. Takahashi, and S. Hirai

J. Surf. Fin. Soc. Jpn., 54, 235-240 (2003)

Aluminum specimens were covered with SiO₂ film by a sol-gel coating and then anodized galvanostatically in a boric acid solution. Time variations in the anode potential during anodizing were monitored, and the structure and dielectric properties of anodic oxide films were examined by TEM-EDS, and electrochemical impedance measurements. It was found that anodizing of aluminum coated with SiO₂ films leads to the formation of anodic oxide films that consist of an outer Al-Si composite oxide layer and an inner Al₂O₃ layer at the interface between the SiO₂ film and the metal substrate. The breakdown potential of anodic oxide films formed on specimens with SiO₂-coating was about 100V higher than that without SiO₂ coating. The capacitance of specimens after sol-gel coating and anodizing was slightly higher than that without sol-gel coating. In the film formation mechanism, the conversion of Al₂O₃ into Al-Si composite oxide at the interface between the inner and outer layers is discussed in term of inward transport of Si-bearing anions across the outer layer. (Japanese)

Electroless Ni-P Deposition through Imperfections in Anodic Oxide Films on Aluminum and Al5052 Alloy

S. Moon, M. Sakairi, H. Takahashi, and K. Shimamura

Electrochemistry, 71, 260-265 (2003)

The present investigation examined how to prevent Ni-P deposition through imperfections in anodic oxide films on aluminum and Al5052 alloy during electroless-plating. Pure aluminum and Al5052 alloy specimens were anodized in a sulfuric acid solution to form porous oxide films, and then immersed in boiling water to seal the pores. Confocal scanning laser microscopy was applied to examine the effect of pore-sealing on the Ni-P electroless deposition through imperfections. There were Ni-P domes deposited on both pure aluminum and Al5052 alloy covered with anodic oxide films through the imperfections in the oxide film. The number of Ni-P domes increased with electroless plating time on both kinds of specimens, and this change was more remarkable on Al5052 alloy, due to imperfections originating from second phase particles in the alloy substrate. Sealing treatment effectively prevented Ni-P dome deposition on both types of specimens, due to healing of the imperfections in the oxide films. Longer anodizing before the sealing treatment prevented the Ni-P deposition completely on the Al5052 alloy specimen even after 15h of electroless-plating.

Fabrication of Nickel Micro-pattern on Insulating Board by Anodizing / Laser Irradiation / Electrodeposition

T. Kikuchi, M. Sakairi, H. Takahashi, Y. Abe, and N. Katayama

Surface and Coatings Technology, 169-170, 199-202 (2003)

Nickel micro-pattern was fabricated on an insulating board via anodizing aluminum, laser irradiation, nickel electroplating, insulating board attachment, and aluminum substrate dissolution. Aluminum specimens covered with porous type oxide films were irradiated with a pulsed Nd-yttrium aluminum garnet laser through a convex lens with 10 mm focal length in a nickel electroplating solution to remove the anodic oxide film. The oxide film was destructed with minimum 6 μ m width at the focal position. After laser irradiation, nickel metal layer was electrodeposited at only the laser irradiated area. The specimen was attached on an epoxy resin before dissolving aluminum substrate. Nickel micro-pattern with a 9 μ m line width and 12 μ m intervals was obtained on the insulating board.

Nanopatterning on Aluminum Surfaces with AFM probe

Z. Kato, M. Sakairi, and H. Takahashi

Surface and Coatings Technology, 169-170, 195-198 (2003)

Aluminum specimens covered with anodic oxide films were scratched with a silicon probe tip of atomic force microscope in pure water, CuSO₄ solutions, Cu-electroless plating solutions and diluted NaOH solutions. The rate of groove development (R_{gd}) was in the order NaOH>CuSO₄>pure water>Cu-electroless solution, and increasing probe load and scratch number. Wear of the silicon probe tip was also examined by scratching many times in pure water and NaOH solution. It was greater in NaOH solution than in pure water. A silicon tip coated with polycrystalline diamond showed a high processing capability and wear resistance.

Purification of Carbon Nanofibers with Hydrogen Peroxide

W.-K. Choi, S.-G. Park, H. Takahashi, and T.-H. Cho

Synthetic Metals, 139, 39-42 (2003)

As-prepared carbon nanofibers (CNFs) contained some carbonaceous impurities of amorphous carbon and incompletely grown carbon nanofibers. Removal of those impurities using hydrogen peroxide as a reducing agent was carried out. Amorphous carbon synthesized in carbon nanofiber preparation and incompletely grown carbonaceous materials were distinctly removed in this purification process performed in hydrogen peroxide. The morphological changes of as-prepared and hydrogen peroxide treated carbon nanofibers were investigated by FE-SEM and TEM observations. After that purification, amorphous carbons were markedly removed by reduction and carbon nanofibers without carbonaceous impurities were obtained successfully. The X-ray diffraction results show that the purification method using hydrogen peroxide was very stable for carbon nanostructures.

Three-Dimensional Microstructure Fabrication with Aluminum Anodizing, Laser Irradiation, and Electrodeposition

- T. Kikuchi, M. Sakairi, and H. Takahashi
- J. Electrochem. Soc., 150, C567-C572 (2003)

Three-dimensional microstructures made of Ni metal or acrylic resin were fabricated by five sequential processes: porous anodic oxide film formation, pore sealing, laser irradiation, Ni electroplating or electrophoretic deposition of acrylic resin, and removal of the aluminum substrate and anodic oxide films. Cylindrical and prismatic aluminum rods were anodized in an oxalic acid solution to form porous type anodic oxide films, and then immersed in boiling distilled water for pore sealing. The anodized and pore-sealed specimens were irradiated with a pulsed neodymium-doped yttrium aluminum garnet (Nd-YAG) laser beam in a Ni plating solution or doubly distilled water to remove anodic oxide film locally by rotating and moving up / down with an XYZθ stage. Nickel or acrylic resin was deposited at the area where film had been removed by cathodic or anodic polarization in the solution before removing the aluminum substrate and anodic oxide films in NaOH solutions.

Cylindrical and prismatic network cages, rings, springs, and bellows made of Ni metal or acrylic acid resin were fabricated successfully.

Chromate Conversion Coatings on Aluminium: Influences of Alloying

Y. Liu, P. Skeldon, G. E. Thompson, H. Habazaki and K. Shimizu

Corrosion Science, 46, 297-312 (2003)

The growth kinetics of chromate/fluoride conversion coatings are examined for 99.99% aluminum, and Al-2.3at.%Cu, Al-1.9at.%Au and Al-20at.%Au alloys. The thickening of coatings and thinning of substrates, the latter deposited by magnetron sputtering, are detected by transmission electron microscopy. The results reveal consumption of substrates during the coating process, to the maximum immersion time of 24 min. Initial relatively rapid thinning in the period to 6 min is followed by slower, approximately constant thinning at about 9.3, 6.2, 6.0 and 5.4 nm min⁻¹ for the 99.99% Al, Al-2.3 at.% Cu, Al-1.9 at.% Au and Al-20 at.% Au alloys respectively. The ratio of the number of chromium atoms in the conversion coating. detected by Rutherford backscattering spectroscopy, to the number of oxidized substrate atoms is about 3, indicating a low efficiency of coating growth. Alloying decreases the coating thickness, as well as metal consumption. Alloying elements initially enrich beneath the coating, in alloy layers of a few nanometers thickness. Later, copper may be oxidized, and then enter the coating, whereas gold is occluded as nanoparticles. The gold nanoparticles act as markers to indicate formation of coating material at the metal/coating interface. Sudden loss of coating on the alloys, after about 6-9 min, occurs soon after entry of alloying element species into the coating. The loss may be related to the presence of nanoparticles of gold and copper near the alloy/coating interface, the latter possibly forming by reduction of copper species, that disrupt the bonding of the coating either directly though their presence or through their action as local cathodes.

Enrichment Factors for Copper in Aluminium Alloys Following Chemical and Electrochemical Surface Treatments

Y. Liu, F. Colin, P. Skeldon, G. E. Thompson, X. Zhou, H. Habazaki and K. Shimizu

Corrosion Science, 45, 1539-1544 (2003)

Surface treatments, including chemical polishing, alkaline etching, acid pickling, and electropolishing, of aluminium and copper-containing aluminium alloys lead to enrichment of solid solution copper in the metal just beneath the residual oxide films of the treatment processes. The paper presents the enrichment factor for copper as a function of the copper content of the bulk matrix material. The factor is defined as the ratio of the copper enrichment, measured in units of 10¹⁵ atoms cm⁻², to the copper content of the matrix in at.%. Although absolute levels of enrichment increase with increase in copper content of the alloy, the enrichment factor increases in the opposite sense.

Improving the Performance of Aerospace Alloys

G. E. Thompson, P. Skeldon, X. Zhou, K. Shimizu, H. Habazaki and C. F. E. Smith

Aircraft Engineering and Aerospace Technology, 75, 372-379 (2003)

This paper reviews the role of alloying elements in aluminium and alloy fabrication on performance during surface treatment and surface finishing. Such elements may be present in solid solution as fine segregates, strengthening phase and equilibrium phases. For surface treatment and finishes, which generally proceed in the presence of alumina film, knowledge of the processes proceeding at the alloy/film and film/electrolyte interfaces, and those within anodic alumina films, gives rise to the possibility of controlling features of nanoscale dimensions, for improved performance, arises. Its influence on nanotextures at treated surfaces and compositionally and morphologically modified films is explained briefly.

Mechanical Properties and Modifying Solidification of Sn-Ag-Al Solders Alloy

J. Tanaka, N. Suzuki, T. Takashima and T. Narita

Microjoining and Assembly Technology in Electronics, 213-218 (2003)

The precipitation of coarse β -Sn primary in solder deteriorates mechanical properties of the solders. It was found that the β -Sn primary phase precipitation in Sn-Ag alloys became fine by the addition of 0.1wt% Al. Sn-2wt%-0.1wt%Al alloys showed higher elongation with Sn-3.0wt%Ag-0.5wt%Cu eutectic alloys. It was presumed that fine sub-grain structures was formed in the β -Sn primary phase by the addition of Al, and the mechanical properties were improved due to the enrichment of Al and Ag in sub-grain boundaries. (Japanese)

Dissolution of Copper-plate and Growth of Reaction Layer with Lead-Free Solders

S. Saitou, T. Takashima, T. Yamamoto, T. Narita and J. Tanaka

Microjoining and Assembly Technology in Electronics, 271-276 (2003)

Copper plate were dipped in solder baths of Sn-3.5Ag,Sn-3Ag-0.5Cu and Sn-37Pb and the dissolution of the Cu plate and formation of the reaction layer were investigated. A reaction layer of up to 1µm thick formed on the Cu plate, and the activation energy for dissolution of the Cu plate in the temperature range 493-543K were determined as follows; 81KJ/mol with a Sn-Ag solder, 85KJ/mol with a Sn-Ag-Cu solder, and 141KJ/mol with a Sn-Pb solder.

Close examination of the interface after annealing at 423 and 448K revealed the formation of a Cu3Sn layer on the Cu-plate side, and a Cu6Sn5 layer on the outer solder side. The Vickers hardness of the Cu3Sn layer was found to be higher than that of the Cu6Sn5 layer. The activation energy for the growth of the total reaction layer at 398-448K was estimated to be 93KJ/mol with a Sn-Ag solder, 94KJ/mol with a Sn-Ag-Cu solder, and 84KJ/mol with a Sn-Pb solder. (Japanese)

Phase-field Simulation of Transient Liquid Phase Bonding Process of Ni Using Ni-P Binary Filler Metal

Y. Natsume, K. Ohsasa and T. Narita

Materials Transactions, 44 819-823 (2003)

The transient liquid phase (TLP) bonding process of Ni using a Ni-11mass%P binary filler metal was simulated by using both a phase-field model (PFM) and a moving boundary model (MBM). The dissolution of the base metal and isothermal solidification behavior during the TLP bonding process were simulated, and the results calculated by using the PFM were compared with those obtained by using the MBM. The results obtained during the isothermal solidification process in the two models were the same. The change in the concentration at the solid-liquid interface during the dissolution of the base metal was examined, and deviation from the local equilibrium concentration occurred in samples with a high heating rate in the phase-field simulation. On the other hand, the local equilibrium was always maintained in the MBM, but the calculation time of the simulation using the MBM was several hundred-times faster than that using the PFM.

Analysis of Growth Behavior of a Cellular and Dendritic Interface under a Constrained Growth Condition using a Phase-Field Model

Y. Natsume, K. Ohsasa, H. Esaka and T. Narita

Materials Transactions, 44 824-828 (2003)

A phase-field simulation was carried out to investigate the growth behavior of a cellular and dendritic interface of an Fe-C binary alloy in a constrained growth condition. The simulated results were in good agreement with the experimental results. The effect of the magnitude of anisotropy at solid/liquid interface energy was examined, and it was found that the magnitude of anisotropy affected the growth direction when the growth rate was low. Dimensionless growth direction, π' , was used to examine the obtained results, and it was found that π' increases from zero and approaches unity with increase in growth velocity. A good correlation was obtained between calculated growth velocity and growth direction by using dimensionless growth velocity (V/Vc), and this correlation was in agreement with the experimental results.

Numerical Analysis of Solidification Effect on Diffusion Measurement in Liquid using the Long Capillary Method

K. Ohsasa, A. Hirata, M. Uchida and T. Itami

Materials Transactions, 44 8241068-1074 (2003)

A numerical analysis was carried out to examine the solidification effect on the concentration distribution of a solute in an Ag/Ag-5at%Au diffusion couple in a liquid diffusion experiment using the long capillary method. Shrinkage-induced fluid flow in the solidifying sample was calculated, and the solute movement due to the fluid flow was evaluated. In the analysis, molten samples in a graphite crucible were cooled in air at three different cooling rates. Flat isoconcentration contours in the horizontal plane of the diffusion couple were formed in the sample with a low cooling rate, whereas concave isoconcentration contours were formed in the samples with high cooling rates. Those features in the simulation agreed with the experimental results. The optimum conditions to avoid the solidification effect in liquid diffusion experiments are discussed.

Numerical Modeling of the Transient Liquid-Phase Diffusion Bonding Process of Al Using Cu Filler Metal

Y. Natsume, K. Ohsasa, Y. Tayu, T. Momono and T. Narita

ISIJ International, 43, 1976-1982 (2002)

A numerical modeling of dissolution and isothermal solidification during the transient liquid-phase (TLP) diffusion bonding process of Al using pure Cu filler metal based on a diffusion-controlled model was carried out. In the modeling, both the changes in volume accompanying interdiffusion between the base metal (Al) and the filler metal (Cu) and the solid-liquid transformation were taken into account by using variable grids. The effect of a load applied to the base metal was also examined by considering simple force balance among the surface and interface energies of the base metal and liquid formed in the bonding region. The early dissolution process simulated by the developed model agreed with the experimental results, and the predicted isothermal solidification time of a sample with an applied load also agreed with the experimental results.

Heat Transfer Analysis for Aluminum Base and Ferrous Multi-component Alloys Using Computational Thermodynamics

H.Shirosawa and K.Ohsasa

Journal of Japan Foundry Engineering Society, 75 612-617 (2003)

Temperature-enthalpy curves of AC2A and AC8C aluminum base and FCD500 ferrous multi-component commercial alloys were calculated based on the thermodynamic calculation using the ThermoCalc for a nonequilibrium state with limited diffusion in solid. The phase transformation kinetics during eutectic solidification was also taken into account for calculating the temperature-enthalpy curve of the FCD500 cast iron. Heat transfer simulations during the solidification of the alloys based on the enthalpy method were carried out using the calculated temperature-enthalpy curves. Thermal analysis experiment of the alloys were carried out and measured cooling curves were compared with simulated ones. The simulated cooling curves obtained with the nonequilibrium state showed similar shape with those obtained in the experiments.

Prediction of the Solidification Structure of Casting and Heterogeneous Nucleation

K. Ohsasa, H.Shirosawa and T.Narita

Journal of University of Science and Technology Beijing, 10 43-46 (2003)

The frequency of heterogeneous nucleation during the solidification of Al-Si binary alloy was estimated by comparing experimentally obtained macrostructures of castings with numerically simulated ones. A molten alloy was unidirectionally solidified from a water-cooled copper chill in an adiabatic mold. The location of columnar to equiaxed transition (CET) in the solidified alloy ingot was measured. A numerical simulation for grain structure formation based on the Monte Carlo method was carried out, and the frequency of heterogeneous nucleation in the alloy was evaluated by producing similar structure with the experimental one. The frequency of heterogeneous nucleation was expressed as a probabilistic function with an exponential form of undercooling that determines the probability of nucleation event in the simulation. The value of the exponent is regarded as the nucleation parameter. The nucleation parameter of Al-Si binary alloy varied with initial Si content.

Macrostructure of Aluminum base Alloys during Unidirectional Solidification

K. Ohsasa and N. Nishiguchi

Proc. of the 8th Asian Foundry Congress (AFC-8) 599-606 (2003)

Heterogeneous nucleation rate during the solidification of aluminum base alloys were evaluated by comparing experimentally observed macrostructures of ingots with numerically simulated ones. Al-Si and Al-Cu binary alloys were used in the present study. Molten alloys were unidirectionally solidified in an adiabatic mold from a steel chill block located at the bottom of the mold. The top of the mold was heated with an electric furnace for preventing the alloys from the nucleation at the melt surface. In the experiment, columnar grains grew from the bottom chill and CET (columnar to equiaxed transition) occurred at the middle region of the ingots, then macrostructure changed to columnar morphology at the upper region of the sample due to the effect of the heating at the top of the mold. Numerical simulations for macrostructure formation of the samples were carried out using both Monte Carlo (MC) and cellular automata (CA) methods, and heterogeneous nucleation rate in solidifying alloys were evaluated by producing similar structures to experimental ones, i.e. (CECT) columnar-equiaxed-columnar transition. Heterogeneous nucleation rate was expressed as a probabilistic function with an exponential form of undercooling that determines the probability of nucleation event in the simulation, and the value of the exponent was regarded as a nucleation parameter. The nucleation parameters of Al-Si and Al-Cu binary alloys varied with initial solute content of the alloys. An attempt to predict the macrostructure of conventionally cast ingot was made using the evaluated nucleation parameters and the simulation predicted the macrostructure similar to experimentally observed one.